VOL. 22 NO. 2 AUGUST 1969
COMPLETING VOLUME 22
PUBLISHED MONTHLY

JOURNAL OF ELECTROANALYTICAL CHEMISTRY AND INTERFACIAL ELECTROCHEMISTRY

International Journal devoted to all Aspects of Electroanalytical Chemistry, Double Layer Studies, Electrokinetics, Colloid Stability, and Electrode Kinetics.

ELSEVIER

GENERAL INFORMATION

Types of contributions

(a) Original research work not previously published in other periodicals.
(b) Reviews on recent developments in various fields.
(c) Short communications.
(d) Preliminary notes.

Languages

Papers will be published in English, French or German.

Submission of papers

Papers should be sent to one of the following Editors:
Professor J. O'M. Bockris, John Harrison Laboratory of Chemistry, University of Pennsylvania, Philadelphia 4, Pa. 19104, U.S.A.
Dr. R. H. Ottewill, Department of Chemistry, The University, Bristol 8, England.
Dr. R. Parsons, Department of Chemistry, The University, Bristol 8, England.
Professor C. N. Reilley, Department of Chemistry, University of North Carolina, Chapel Hill, N.C. 27515, U.S.A.

Authors should preferably submit two copies in double-spaced typing on pages of uniform size. Legends for figures should be typed on a separate page. The figures should be in a form suitable for reproduction, drawn in Indian ink on drawing paper or tracing paper, with lettering etc. in thin pencil. The sheets of drawing or tracing paper should preferably be of the same dimensions as those on which the article is typed. Photographs should be submitted as clear black and white prints on glossy paper. Standard symbols should be used in line drawings, the following are available to the printers:

All references should be given at the end of the paper. They should be numbered and the numbers should appear in the text at the appropriate places.
A summary of 50 to 200 words should be included.

Reprints

Fifty reprints will be supplied free of charge. Additional reprints (minimum 100) can be ordered at quoted prices. They must be ordered on order forms which are sent together with the proofs.

Publication

The *Journal of Electroanalytical Chemistry and Interfacial Electrochemistry* appears monthly. For 1969, each volume has 3 issues and 4 volumes will appear.
Subscription price: Sfr. 316.— (U.S. $ 74.60) per year incl. postage. Additional cost for copies by air mail available on request. For subscribers in the U.S.A. and Canada, 2nd class postage paid at Jamaica, N.Y. For advertising rates apply to the publishers.

Subscriptions

Subscriptions should be sent to:

ELSEVIER SEQUOIA S.A., P.O. Box 851, 1001 Lausanne 1, Switzerland

ELECTROANALYTICAL CHEMISTRY AND INTERFACIAL ELECTROCHEMISTRY
Elsevier Sequoia S.A., Lausanne – Printed in The Netherlands

IMMERSION-ELECTRODE METHOD FOR THE DETERMINATION OF THE POINT OF ZERO CHARGE OF SOLID METALS

VOJISLAV JENDRAŠIĆ
Department of Chemistry, New York University, New York, N.Y. 10003 (U.S.A.)
(Received February 25th, 1969)

INTRODUCTION

An ideal polarized electrode exhibits a charging current when the electrode-interface area varies. If the electrode potential is constant, the charging current is simply proportional to the rate of change of the interface area, the proportionality constant being the charge density. The direction of the charging current, at constant potential, is reversed at the point of zero charge, E_z, which thus may be determined from current measurements. This idea, which goes back to the early days of polarography, was applied in the immersion-electrode method of Jakuszewski and Kozlowski[1]. The present paper deals with a further study of this method. Reference is made to a review[2] and some more recent papers[3–7] for other methods of determining E_z.

A spurious faradaic current would interfere with the E_z-determination in the immersion-electrode method. This interference must be eliminated either by separation of the faradaic and non-faradaic currents or by selection of conditions in which the faradaic current is negligible. The former approach was applied to dropping metal electrodes[8,9] in cases in which the time-dependence is known. Such a procedure would be uncertain at best with solid electrodes, and one is left with the alternative of minimizing the faradaic current in relation to the charging current. This can be achieved by immersing the electrode as rapidly as possible. The non-faradaic current then increases with the immersion rate whereas the faradaic current, in the absence of time-dependent complications (*e.g.*, diffusion), is independent of the immersion rate.

CURRENT–TIME VARIATIONS

We shall derive the current–time relationship for somewhat idealized conditions which nevertheless are approximated in actuality. We assume:

(a) The area of the electrode–solution interface is proportional to the time elapsed since the beginning of immersion. The assumption is justified under the following conditions: no meniscus complication, constant rate of immersion, constant electrode cross section, and negligible contribution of the area at the tip of the electrode.

(b) The cell composed of the immersion electrode and a reference electrode, in series with a standard resistance, is connected to a potentiometer, *i.e.*, the total applied voltage is constant. A potentiostat was not available and could be dispensed with at the cost of a rather minor drawback as we shall see. It is assumed that the resistance of the circuit connected to the potentiometer is $R + (r/t)$ where the last term (r constant)

represents the effect of immersion, and R is a constant corresponding to the standard resistance and the contribution of the cell resistance not included in r/t. The cell resistance for a long, fine wire-electrode in an electrolyte is mostly in a thin sleeve around the electrode provided the resistance of the reference electrode is negligible. The resistance for this model is inversely proportional to the electrode area which itself is supposed to be proportional to time. The inductance of the circuit is supposed to be zero.

One has during dt for an ideal polarized electrode:

$$dq = i\,dt = V\,dC + C\,dV \tag{1}$$

where C is the integral capacity of the double layer, that is

$$C = ct \tag{2}$$

c being a constant (interface area proportional to t). Moreover

$$V = E - E_z - i(R + (r/t)) \tag{3}$$

where E is the electrode potential and i the current. The latter is positive when a positive charge is supplied to the electrode by the potentiometer. By evaluating dC and dV from (2) and (3), one deduces from (1)

$$di/dt + [(1 + Rc)/c(r + Rt)]i = (E - E_z)/(r + Rt) \tag{4}$$

At $t = 0$, the cell resistance is infinite, and $i = 0$. Thus

$$i = [(E - E_z)c/(1 + Rc)]\{1 - [1/(1 + (Rt/r))]^{(1 + (1/Rc))}\} \tag{5}$$

The limiting current for $t \to \infty$ is:

$$i_\infty = (E - E_z)c/(1 + Rc) \tag{6}$$

This value corresponds to the case of an infinitely long wire with a continuously rising solution. Note that i_∞ is proportional, through the factor c, to the rate of change of the interface area. For $R = 0$, the limiting value is $(E - E_z)c$ as follows directly from the assumption of proportionality between time and the interface area. This limiting value of the current would be obtained with an ideal potentiostat at any time during immersion since the potential is then rigorously constant. The more complicated expression (5) results from the variable circuit resistance and, consequently, the variable potential and time constant of the circuit.

Typically one has $200 < R < 500\ \Omega$ and $2 \cdot 10^{-4} < c < 10^{-3}$ F sec^{-1}. Hence $Rc \gg 1$, and eqn. (5) then becomes

$$i = [(E - E_z)/R]\{1 - [1/(1 + (R/r)t)]^{1/Rc}\} \tag{7}$$

If $Rc \gg 1$, the term with the exponent $1/RC$ soon vanishes, and the limiting value, $(E - E_z)/R$, is approached rapidly.

It is obvious that the limiting value, $(E - E_z)/R$ for $Rc \gg 1$, must always be lower than the current calculated for $R = 0$, *i.e.*, $(E - E_z)c$.

We now assume that immersion is stopped at time $t = \tau$, and we derive the current–time relationship. Both the capacity, $C = c\tau$, and the circuit resistance, $R + r/\tau$, are constant. Hence

$$i = i_\tau \exp[-(t - \tau)/(R\tau + r)c] \tag{8}$$

where i_τ is the current given by eqn. (5). If $Rc \gg 1$, $i_\tau = (E - E_z)/R$ for all practical purposes. The current simply decays exponentially with time for $t > \tau$. With an ideal potentiostat, the current would drop to zero as soon as immersion is stopped.

EXPERIMENTAL

Cell and electrical equipment

The cell of Fig. 1 provided for immersion of a *dry* electrode in a rising solution under controlled conditions. The solution was initially at the same level in compartments A and B and did not make contact with the electrode in B. Nitrogen, at constant pressure, was then admitted in A through inlet, M, for a known time by means of a

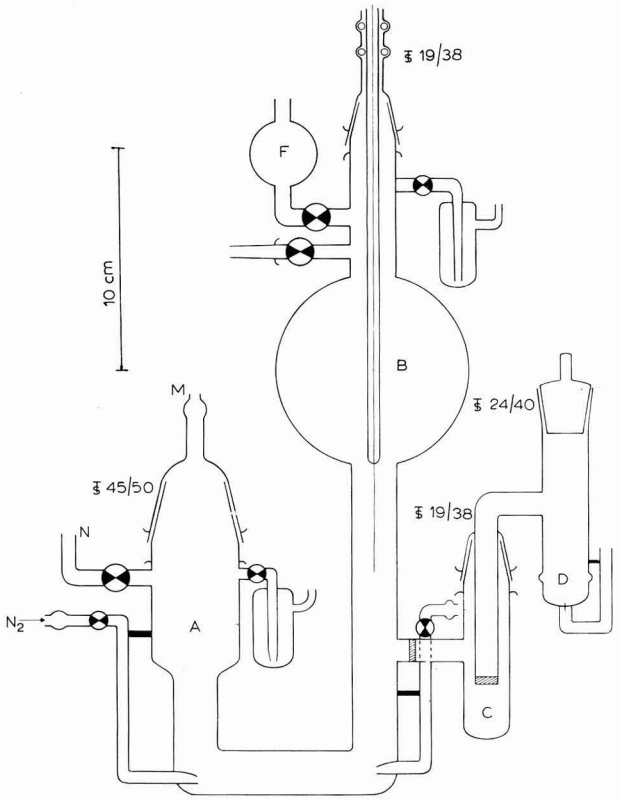

Fig. 1. Cell.

solenoid-operated microvalve (model 316 F 4 with spring return and aluminum body, 3/32-in. orifice, In-Val-Co, P.O. Box 556, 3102 Charles Page Road, Tulsa, Oklahoma). The current pulse of adjustable length was applied to the solenoid by means of a Tektronix waveform generator, type 162. The nitrogen pressure was measured with a mercury manometer and was adjusted between 100 and 350 mm. Details of the whole operation are given below.

The electrode in B was polarized against the reference in D by means of a Leeds and Northrup student potentiometer, a standard resistance (generally 150 Ω) being in series with the cell. Current–time curves were recorded with a Tektronix oscilloscope 547 with plug-in unit 1A7 at a sensitivity of 2–10 mV/division. The error on potential resulting from the ohmic drop was negligible at and near E_z since the total current is equal to, or near zero, in the absence of a faradaic current.

Chemicals and electrode material

Chemicals were of analytical reagent-grade (Baker), and water was distilled twice. The platinum electrode was obtained from Englehard, Baker Platinum Division, Newark, New Jersey (99.95% pure, 0.5 mm diameter), and the gold electrode from Sigmund Cohn Co., Mount Vernon, New York (99.99% pure, 0.025 in. diameter).

Electrode treatment

The platinum electrode was treated with *aqua regia* for 15 sec. It was then rinsed in distilled water and dried in nitrogen at approximately 100°C. Alternate cathodic and anodic treatment was also applied, but the electrode treated in this fashion exhibited a rather high spurious faradaic current.

In initial work with the gold electrode, the *aqua regia* treatment was used. The electrochemical treatment of Green and Dahms[10] was adopted in subsequent work.

Immediately after each recording of a current–time curve, the electrode was washed with water and dried with nitrogen. The electrode was treated anew, as described above, before each recording.

Pre-electrolysis

Pre-electrolysis was used for the gold electrode but not with platinum. The immersion electrode in B was replaced by a 1-cm^2 platinum electrode (cathode). Compartment D was also removed and a 1-cm^2 platinum electrode was inserted in C. This electrode (not shown in Fig. 1) was fitted in a ground-glass cap with a bubbler to allow escape of oxygen during pre-electrolysis. The cell was then cleaned and washed: concentrated sulfuric acid (no chromic acid!), distilled water and solution. A and B were filled with 65 ml of solution, and C with a sufficient volume to equalize the levels. The solution was de-aerated by bubbling nitrogen through the inlets in A and B for a period of up to 12 h. The solution was then pre-electrolyzed for at least 12 h at 2–3 mA cm^{-2}. Mixing of solution between A and B was achieved by nitrogen bubbling. The pre-electrolyzed solution was used only for one series of measurements with one type of electrode.

Recording of current–time curves

If the solution had been pre-electrolyzed, the platinum electrode in C was replaced at this stage by the reference electrode, D. The latter was a normal calomel electrode prepared with NaCl (investigation of 1 *M* $HClO_4$). Contamination was greatly minimized by the intermediate compartment, C, and the use of fritted disks of medium porosity.

The pre-electrolysis electrode in B was also replaced by the immersion electrode. The latter was slipped (sleeve with O-rings) in the top of B near the inlet of hot nitrogen. The electrode was dried for 30 min in a stream of nitrogen which was heated

($T \simeq 100°C$) by passing it through a 150-mm long tube surrounded by heating tape. The electrode was then lowered in B with its end within 5 mm of the solution level.

The pressure in the nitrogen reservoir (1500 ml) connected to the solenoid-operated microvalve was adjusted, and a current–time curve was recorded as described under Cell and Electrical Equipment. The stopcock, Q, between B and F was open during the recording to avoid splashing in the top bubbler of B. The level of the solution at the end of the pressure surge was along the glass sleeve of the immersion electrode. Oscillations of the level thus did not change the electrode–solution interface area. Nitrogen, at room temperature, was passed through P when F was connected to B to avoid contamination, but the nitrogen flow was stopped in A and B. The levels of solution in A and B were equalized by opening stopcock, N, after the recording. The temperature was that of the room.

RESULTS

Pt in 0.1 M NaF

Examples of current–time curves are shown in Fig. 2. The curves have very approximately the shape predicted by eqns. (5) and (8), namely, a more or less constant current that is rapidly reached at the beginning of immersion, and an exponentially-looking decay after interruption of immersion. There is no sharp break between the two parts of the curve at the time the solenoid-operated valve was closed. Thus, solution transfer gradually slowed down afterwards (expansion of nitrogen in chamber A, inertia of the solution). This is one reason why the decay is not truly exponential, as was found by analysis of some of the *i vs. t* curves.

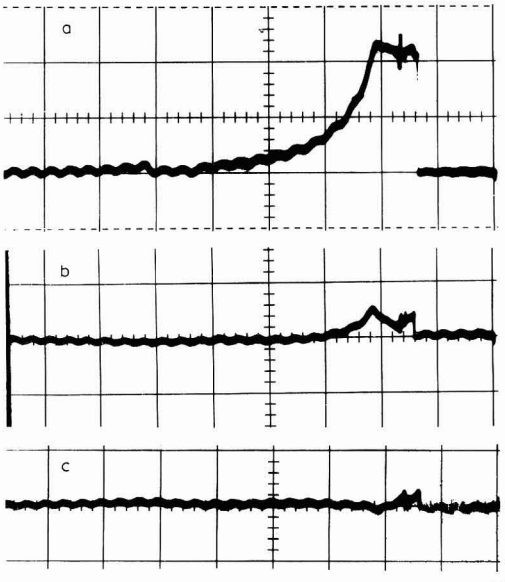

Fig. 2. Current–time curves for Pt in 0.1 *M* NaF at: (a), −0.1; (b), +0.1; (c), +0.12 V *vs.* NCE (NaCl). Nitrogen pressure: 100 mm Hg. Vertical scale, 13.3 μA/main division; horizontal scale, 50 msec/main division. Read from right to left.

Current–time curves were analyzed in two ways: (a) measurement of the maximum current, i_{max}, and (b) determination of the quantity of electricity, Q, supplied to, or removed from the electrode. The latter quantity was obtained by graphic integration (an operational amplifier integrating current would be useful in systematic application). Results are compared in Fig. 3 for two pressures of nitrogen. The two methods

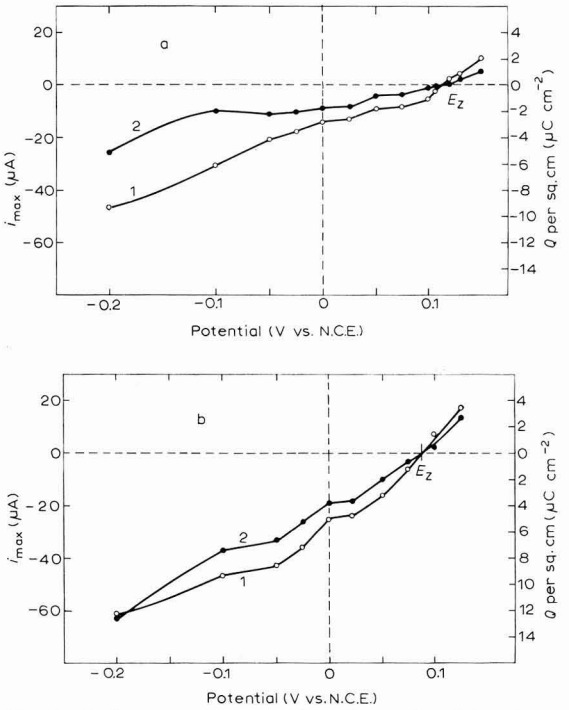

Fig. 3. Maximum current, i_{max}, (1) and quantity of electricity, Q, (2) *vs.* potential for Pt in 0.1 *M* NaF for nitrogen pressures: (a), 100; (b), 340 mm Hg.

of analysis give nearly the same E_z, but our general experience is that scattering of data is lower with Q *vs.* E plots than i_{max} *vs.* E plots. Figure 3 also shows that i_{max} or Q, at a given E, are very roughly proportional to the pressure, *i.e.*, to the rate of change of the interface area. Note also the shift in E_z for the two pressures—undoubtedly an effect caused by a difference in surface conditions.

Pt in 0.1 M $HClO_4$

Plots of i_{max} and Q *vs.* E (Fig. 4) were less smooth than in the previous case although the i *vs.* t curves were quite satisfactory (Fig. 5). The value $E_z = 0.23 \pm 0.04$ V *vs.* NCE (with NaCl) is *tentatively* reported. This value would be quite close to the extrapolated value from the data of Gileadi *et al.*[11], namely, +0.53 V *vs.* NHE (the lowest pH in this work is 2.5). Our E_z-value is approximately 0.51 V *vs* NHE. This comparison is very tentative since E_z would depend on the nature of the electrolyte. Frumkin[2] quotes 0.11–0.17 V *vs.* NHE for 0.5 *M* $Na_2SO_4 + 0.005$ *M* H_2SO_4. Differences in the preparation of the electrode surface may account for the difference.

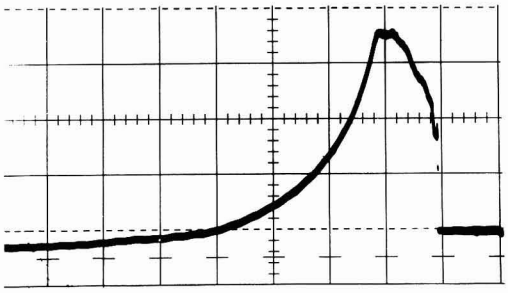

Fig. 4. Current–time curve for Pt in 1 M $HClO_4$ at -0.15 V *vs.* NCE (NaCl). Nitrogen pressure: 100 mm Hg. Vertical scale, 66.6 μA/main division; horizontal scale, 50 msec. Read from right to left.

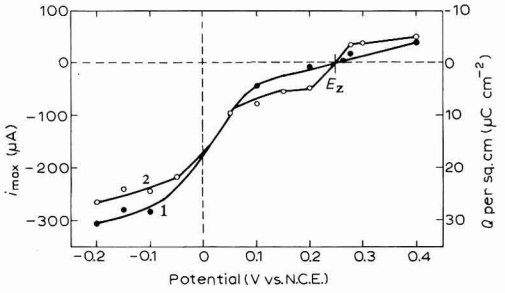

Fig. 5. i_{max} (1) and Q (2) *vs.* E for Pt in 1 M $HClO_4$ at 100 mm Hg.

Au in 0.1 M $HClO_4$

Some effort was spent on this electrode, but results are not well understood; i *vs.* t curves were somewhat distorted, and Q *vs.* E plots were quite erratic. A marked difference in i_{max} and Q, at a given E, was observed depending on previous values of E_z. Interference by some faradaic process could account, at least in part, for these seemingly abnormal results but it is not clear what this process might be. Values of E_z were more positive than those reported for 1 M $HClO_4$ and other solutions[5,7,10,12–14], by a few tenths of a volt. A faradaic cathodic process would account for a shift of the apparent E_z toward more positive values. Electrode contamination seems not to be the primary source of trouble as care was taken to minimize it. The method clearly failed in this instance, possibly because of the non-equilibrium between the solution and the electrode surface.

CONCLUSION

The immersion-electrode method for determining E_z has been shown to be workable in some instances. Adaptation of the technique to single crystals seems feasible. Contamination by traces of impurities in solution is minimized because contact of the electrode with solution is less than 0.1–0.5 sec. Contact of short duration, however, has its drawback in as much as results correspond to an electrode whose condition is possibly quite different from that of an identical electrode after prolonged contact with the solution (ionic adsorption, hydrogen or oxygen coverage, etc.). The ne-

cessity of drying the electrode, even in an inert gas, probably effects its surface condition in most cases and thus influences experimental E_z-values, yet it does not seem practical to apply the technique reliably with a wet electrode. However, one should remember that most, if not all, methods for determining E_z with solid electrodes leave something to be desired, in addition to having the common feature of being affected by the uncertain and rather empirical art of surface preparation.

ACKNOWLEDGEMENT

This work was supported by the National Science Foundation. The author is indebted to Professor Paul Delahay for his interest and detailed discussion of this work.

SUMMARY

A method is described whereby the area of a solid metal–electrolyte interface is varied, and the point of zero charge of the metal is determined from the variations of the charging current with time during immersion. A simple treatment is given for current–time curves obtained at constant total applied voltage. Examples are given.

REFERENCES

1 B. JAKUSZEWSKI AND Z. KOZLOWSKI, *Roczniki Chem.*, 36 (1962) 1873.
2 A. N. FRUMKIN, *Svensk Kem. Tidskr.*, 77 (1965) 300.
3 T. N. ANDERSEN, R. S. PERKINS AND H. EYRING, *J. Am. Chem. Soc.*, 86 (1964) 4496.
4 R. S. PERKINS, R. C. LIVINGSTON, T. N. ANDERSEN AND H. EYRING, *J. Phys. Chem.*, 69 (1965) 3329.
5 D. D. BODE, JR., T. N. ANDERSEN AND H. EYRING, *J. Phys. Chem.*, 71 (1967) 792.
6 I. MORCOS AND H. FISCHER, *J. Electroanal. Chem.*, 17 (1968) 7.
7 T. R. BECK, paper presented at the 19th meeting of CITCE, Detroit, September, 1968.
8 J. N. BUTLER AND M. L. MEEHAN, *J. Phys. Chem.*, 69 (1965) 4051.
9 G. TESSARI, J. MURPHY, R. DE LEVIE AND P. DELAHAY, unpublished work.
10 M. GREEN AND H. DAHMS, *J. Electrochem. Soc.*, 110 (1963) 466, 1075.
11 E. GILEADI, S.D.ARGADE AND J. O'M. BOCKRIS, *J. Phys. Chem.*, 70 (1966) 2044.
12 G. M. SCHMID AND N. HACKERMAN, *J. Electrochem. Soc.*, 109 (1962) 243.
13 S. D. ARGADE AND E. GILEADI, in *Electrosorption*, edited by E. GILEADI, Plenum Press, New York, 1967, p. 95.
14 M. PETIT AND J. CLAVILIER, *Compt. Rend.*, 265 (1967) 145.

ELECTROANALYTICAL CHEMISTRY AND INTERFACIAL ELECTROCHEMISTRY
Elsevier Sequoia S.A., Lausanne – Printed in The Netherlands

STUDY OF THE KINETICS OF ELECTROCHEMICAL REACTIONS BY THIN-LAYER VOLTAMMETRY

I. THEORY

A. T. HUBBARD
Department of Chemistry, University of Hawaii, Honolulu, Hawaii 96822 (U.S.A.)
(Received February 8th, 1969)

INTRODUCTION

The advantages of thin layer electrodes for the study of systems marked by adsorption of reactants at the electrode surface[1-3], complex stoichiometry[4,5], or coupled, chemical and electrochemical reactions[6-10], has been the subject of a number of recent papers.

Linear potential sweep voltammetry in thin layers of solution appears well-suited to the study of irreversible systems involving multiple reactants or reaction steps or interfering background reactions[4]. When systems having simple stoichiometry are being studied, the experimental equations may be solved directly for the apparent electrochemical rate parameters in terms of the measured peak currents and potentials, provided that the rates are rather small. Equations are readily obtained for systems exhibiting complex stoichiometry, although the use of numerical methods to obtain k^0 and αn_0 from the measured quantities is sometimes necessary.

Equations describing thin layer voltammetry with irreversible[4,5,11] systems are derived here and will be exploited in subsequent communications[12-14].

1. *Thin layer current–potential curve for a reversible reaction involving single soluble product and reactant species: $ox + ne^- = red$*

The equations describing thin layer current–potential curves obtained with reversible couples have already been reported[4,11], and are briefly summarized here to facilitate their comparison with the results obtained for irreversible couples.

If the solution layer thickness (l) and the rate of potential sweep (r) are made sufficiently small (typically, $l = 4 \cdot 10^{-3}$ cm and $r = 2$ mV sec^{-1}) the reactant concentration at the electrode surface will differ to a negligible extent from that in the bulk solution. During a cathodic potential sweep the concentration ratio appearing in the Nernst equation:

$$E = E^0 + (RT/nF) \ln (C_{ox}/C_{red}) \quad (1)$$

varies continuously from $C_{ox}/C_{red} \rightarrow \infty$ to $C_{ox}/C_{red} \rightarrow 0$. Thus, the current–potential curve, obtained by combining eqn. (1) with Faradays's law written in differential form

$$i = -nFV(dC_{ox}/dt) \quad (2)$$

is symmetrical. The current approaches asymptotically to zero at positive and negative extremes of potential (Fig. 1A). The peak current and potential are:

$$i_p = n^2F^2V(-r)C^0/4RT \tag{3}$$

$$E_p = E^0 \tag{4}$$

V is the thin layer volume and r is the rate of potential sweep (dE/dt) taken with regard to its sign. Equations (3) and (4) are applicable without change for any number of cycles. They are also valid for mixtures of reactants so long as the peak potentials differ by more than $4RT/nF$ (typically $240/n$ mV); otherwise, the peak currents must be corrected for overlap with the use of eqn. (6) of ref. 4.

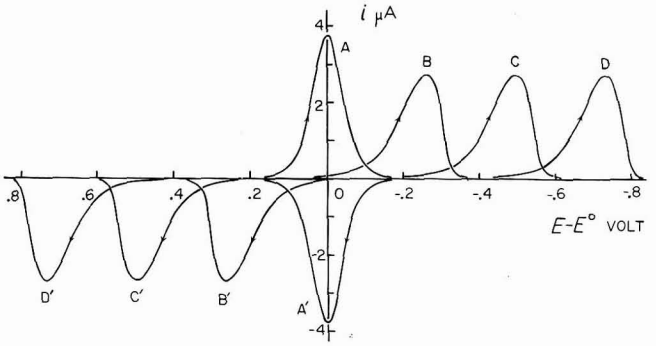

Fig. 1. Theoretical cyclic current–potential curves for reversible and totally irreversible reactions in thin layers of solution. Graph of eqn. (10) for various values of k^0. (A), Reversible reaction: $k^0 \geqq 4 \cdot 10^{-3}$ cm sec^{-1}; (B–D), totally irreversible reactions; k^0: B. 10^{-6}, C. 10^{-8}, D. 10^{-10} cm sec^{-1}.
The following values were assumed in making the plots: $\alpha n_0 = 0.5$; $V = 2 \cdot 10^{-3}$ cm^3; $|r| = 2 \cdot 10^{-3}$ V sec^{-1}; $n = 1$; $A = 0.5$ cm^2; $C^0 = 10^{-6}$ mole cm^{-3}; $T = 298°$K.

2. *Thin layer current–potential curve for a totally irreversible reaction involving single, soluble product and reactant species*: $ox + ne^- \rightarrow red$

The current–potential curve obtained with an irreversible couple is unsymmetrical and the peak potentials are related through a simple equation to the electrochemical rate parameters, k^0 and αn_0. The Nernst equation does not apply; instead, the potential and concentration are related by eqn. (5).

$$i = nFAk^0 \left\{ C_{ox} \exp\left[\frac{-\alpha n_0 F}{RT}(E - E^0)\right] - C_{red} \exp\left[\frac{(1-\alpha)n_0 F}{RT}(E - E^0)\right]\right\} \tag{5}$$

If the reaction proceeds totally irreversibly under the experimental conditions—that is, the observed peak current is about one hundred times larger than the exchange current—the back reaction contributes insignificantly to the observed current–potential curve and eqn. (5) may be replaced by eqn. (6).

$$i = nFAk^0 C_{ox} \exp\left[(-\alpha n_0 F/RT)(E - E^0)\right] \tag{6}$$

The conditions under which this simplification is permissible are derived in the Appendix (k^0 less than about 10^{-5} cm sec^{-1}, or $|E_p - E^0|$ greater than about 0.1 V).

Combining eqns. (2) and (6) gives

$$\frac{dC_{ox}}{dt} = -\frac{Ak^0 C_{ox}}{V} \exp\left[\frac{-\alpha n_0 F}{RT}(E-E^0)\right] \tag{7}$$

Integrating eqn. (7) and combining the result with eqn. (6) gives an expression for the (cathodic) current–potential curve.

$$i = nFAk^0 C_{ox}^0 \exp\left\{\frac{-\alpha n_0 F}{RT}(E-E^0) - \frac{ARTk^0}{\alpha n_0 FV(-r)} \exp\left[\frac{-\alpha n_0 F}{RT}(E-E^0)\right]\right\} \tag{8}$$

Graphs of eqn. (8) for various values of k^0 with one particular value of αn_0 appear in Fig. 1.

The shape of the curves is not affected by k^0 in the range for which eqn. (8) applies (Fig. 1); the curves are merely shifted along the axis of potentials. However, the breadth of the curves increases substantially and hence the peak current decreases, with decreasing values of αn_0; this trend is illustrated in Fig. 2.

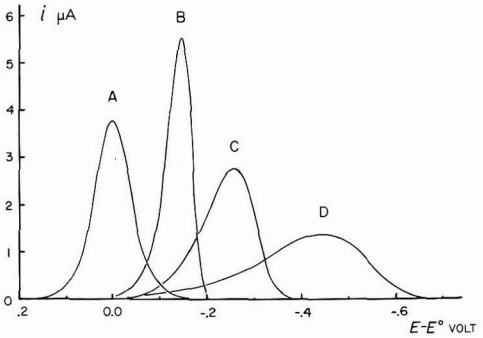

Fig. 2. Theoretical cyclic current–potential curves for reversible and totally irreversible reactions in thin layers of solution. Graph of eqn. (10) for various values of αn_0. (A) Reversible reaction: $k^0 \geqq 4 \cdot 10^{-3}$ cm sec^{-1}; (B–D) irreversible reactions, αn_0: B. 0.75; C. 0.50; D. 0.25. The following values were assumed in making the plots: $k^0 = 10^{-6}$ cm sec^{-1} (except Curve A); V, $|r|$, n, A, C^0 and T as in Fig. 1.

The peak potential depends upon αn_0 and k^0 according to eqn. (9)

$$_cE_p = E^0 - (2.3RT/\alpha n_0 F) \log [\alpha n_0 F(-r)V/ARTk^0] \tag{9}$$

whereas the peak current depends only on αn_0 according to eqn. (10)

$$_ci_p = \alpha n_0 nF^2 V(-r)C_{ox}^0/2.718\ RT \tag{10}$$

αn_0 can be obtained from a single value of the peak current:

$$\alpha n_0 = 2.718RT\ _ci_p/nF^2V(-r)C_{ox}^0 \tag{11}$$

k^0 can be obtained from $_ci_p$ and $_cE_p$ provided that E^0 is known. Combining eqns. (9) and (11) gives

$$k^0 = (2.718\ _ci_p/nFAC_{ox}^0) \exp [2.718\ _ci_p(_cE_p - E^0)/nFV(-r)C_{ox}^0] \tag{12}$$

A similar set of equations is obtained for anodic reactions when α is replaced by $(1-\alpha)$

and C_{ox}^0 by C_{red}^0:

$$ {}_{a}i_p = -(1-\alpha)n_0 nF^2 VrC_{red}^0/2.718\ RT \tag{13} $$

$$ {}_{a}E_p = E^0 + \{2.3RT/(1-\alpha)n_0 F\} \log [(1-\alpha)n_0 FrV/ART\ k^0] \tag{14} $$

$$ k^0 = (-2.718\ {}_{a}i_p/nFAC_{red}^0) \exp [2.718\ {}_{a}i_p({}_{a}E_p - E^0)/nFVrC_{red}^0] \tag{15} $$

The necessity of knowing the standard potential, E^0, for calculation of k^0 can be avoided in the event that it is possible to obtain a cyclic current–potential curve. Solving eqn. (15) for E^0 and substituting this expression for E^0 in eqn. (12) gives:

$$ k^0 = \left\{ \frac{2.718\ {}_{c}i_p}{nFAC^0} \left(\frac{-2.718\ {}_{a}i_p}{nFAC^0} \right)^{-{}_{c}i_p/{}_{a}i_p} \exp \left[\frac{-2.718\ {}_{c}i_p}{nFV|r|C^0} ({}_{a}E_p - {}_{c}E_p) \right] \right\}^{{}_{a}i_p/({}_{a}i_p - {}_{c}i_p)} \tag{16} $$

If it is arbitrarily assumed that $\alpha n_0 = 0.5$, then ${}_{c}i_p = {}_{a}i_p$ and eqn. (16) achieves a simple logarithmic form:

$$ \log k^0 = -(1260/T)({}_{a}E_p - {}_{c}E_p) + \log (VF|r|/2ART) $$

which betrays the approximately logarithmic relationship existing in the general case between peak separation $({}_{a}E_p - {}_{c}E_p)$ and k^0. Solving eqn. (11) for n_0 and substituting this value for n_0 in eqn. (13) gives

$$ \alpha = {}_{c}i_p/({}_{c}i_p - {}_{a}i_p) \tag{17} $$

In addition to its simplicity, eqn. (17) indicates a possible advantage of cyclic thin layer voltammetry—that α and n_0 are formally separable, provided it is assumed that n_0 is the same for the anodic and cathodic reactions.

The simplicity of the above equations and the fact that they allow αn_0 and k^0 to be calculated directly from the result of a single experiment performed with a single starting reactant suggest the usefulness of thin layer voltammetry for characterization of the rates of irreversible electrode reactions, and explains the convenience of the technique as a measure of electrochemical reversibility.

The above equations were obtained without regard for the potential difference across the diffuse double layer, the outer Helmholtz potential, ϕ_2. The expression analogous to eqn. (6) which takes into account the alteration in effective electrode potential and surface concentration of reactant resulting from ϕ_2[15] is given by eqn. (18).

$$ i = nFAk^0\ C_{ox} Z(\phi_2) \exp [(-\alpha n_0 F/RT)(E - E^0)] \tag{18} $$

where $Z(\phi_2) \equiv \exp [(\alpha n_0 - Z_{ox})(F/RT)\phi_2]$ and Z_{ox} is the ionic charge of the reactant particle. An expression for the cathodic current–potential curve is obtained from eqns. (7) and (18). The result is:

$$ i = nFAk^0 C_{ox}^0 Z(\phi_2) \exp \left\{ \frac{-\alpha n_0 F}{RT} (E - E^0) + \right. $$
$$ \left. + \frac{Ak^0}{V(-r)} \int_{E_i}^{E} Z(\phi_2) \exp \left[-\frac{\alpha n_0 F}{RT} (E - E^0) \right] dE \right\} \tag{19} $$

where E_i is the initial potential of the potential sweep.

If the electrode potential is considered to be distributed across a series combi-

nation (C) of capacitances due to compact (C_c) and diffuse (C_d) regions of the double layer, and these capacitances are regarded as approximately constant over the narrow range of potentials for which the current is appreciable (about $200/n$ mV), then the outer Helmholtz potential may be estimated by means of eqn. (20),

$$\phi_2 \approx (C/C_d)(E-E_z) \tag{20}$$

in which E_z is the zero charge potential.
Combining eqns. (19) and (20) gives:

$$i = nFAK^0 C_{ox}^0 Z(\phi_2) \exp\left\{\frac{-\alpha n_0 F}{RT}(E-E^0) + \right.$$
$$\left. - \frac{ARTk^0}{FV(-r)} \frac{Z(\phi_2)\exp\left[\frac{-\alpha n_0 F}{RT}(E-E^0)\right]}{[\alpha n_0 + (Z_{ox}-\alpha n_0)C/C_d]}\right\} \tag{21}$$

The peak potential is found from eqn. (22).

$${}_cE_p = \frac{\alpha n_0 E^0 + (Z_{ox}-\alpha n_0)\frac{C}{C_d}E_z - \frac{RT}{F}\ln\left\{\frac{FV(-r)}{ARTk^0}\left[\alpha n_0 + (Z_{ox}-\alpha n_0)\frac{C}{C_d}\right]\right\}}{\alpha n_0 + (Z_{ox}-\alpha n_0)C/C_d} \tag{22}$$

Equation (22) reduces to eqn. (9), derived without regard to ϕ_2, when C (or C_c) is less than about 1% as large as C_d (as may be the case in a $1F$ excess of supporting electrolyte). Equation (22) can be solved explicitly for any of its variables so that the value of any one variable can be calculated directly from the experimental results if the values of the others are known.

Equations (19) and (21) are entirely analogous to eqn. (8) except for the presence of the function, $Z(\phi_2)$. The effect of $Z(\phi_2)$ is to alter both the peak current and the peak potential: $Z(\phi_2)$ appears in eqn. (21) in combination with $\exp[(-\alpha n_0 F/RT)(E-E^0)]$; combining eqns. (18) and (20) gives

$$Z(\phi_2)\exp\left[\frac{-\alpha n_0 F}{RT}(E-E^0)\right] = \exp\left\{\frac{F}{RT}\left[\frac{C}{C_d}(Z_{ox}-\alpha n_0)E_z + \alpha n_0 E^0\right]\right\} \times$$
$$\times \exp\left[\alpha^* \frac{F}{RT}E\right] \tag{23}$$

where

$$\alpha^* \equiv (Z_{ox}-\alpha n_0)C/C_d + \alpha n_0 \tag{24}$$

Thus, under influence of the outer Helmholtz potential, the charge transfer coefficient, α, exhibits an apparent value α^*, and the peak current achieves a value different from that predicted by eqn. (10):

$${}_ci_p = \alpha^* nF^2 V(-r)C_{ox}^0/2.718\,RT \tag{25}$$

α^* is defined in eqn. (24). As eqns. (24) and (25) suggest, α^* and ${}_ci_p$ are expected to be smaller for anionic than for cationic reactants. Thin layer current–potential curves obtained with moderate and low concentrations of supporting electrolyte *may* provide a simple means for *estimation* of the ratio, C/C_d, of the total and diffuse differential double-layer capacitances. An implication of eqn. (23) is that ϕ_2 should alter the ap-

parent value of k^0 by a constant factor, the first exponential term on the r.h.s. of eqn. (23). Thus, the peak potential should differ, according to eqn. (22), from the value expected when $\phi_2 = 0$; the variance should be most pronounced when the quantity, $(Z_{ox} - \alpha n_0)C/C_d$, is large—that is, at low ionic strengths with highly charged reactant species.

3. *Thin layer current–potential curve for a totally irreversible stepwise reaction*

If reduction of the reactant takes place in two totally irreversible steps, for instance[12],

$$(PtCl_6)^{2-} + 2e^- \xrightarrow{k_1^0} (PtCl_4)^{2-} + 2Cl^-$$

and

$$(PtCl_4)^{2-} + 2e^- \xrightarrow{k_2^0} Pt + 4Cl^-$$

the current–potential curve (Fig. 3) is expected to exhibit two separate peaks if the first step is the faster one (Curve A), or a single peak if the second reaction is faster than, or comparable to, the first (curves B and C).

In the event that $k_1^0 \geqq 10^3 \cdot k_2^0$, the two-step reaction behaves formally as two separate reactions, so that the equations presented in the previous section apply. A general current–potential equation for totally irreversible stepwise (cathodic) reactions:

$$ox + n_1 e^- \rightarrow red_1 \quad \text{(step 1)}$$
$$red_1 + n_2 e^- \rightarrow red_2 \quad \text{(step 2)}$$

is obtained as follows: First, the contribution to the current due to the first reaction step is found by rewriting eqn. (8):

$$i_1 = n_1 F A k_1^0 \exp\left\{\frac{-(\alpha n_0)_1 F}{RT}(E - E_1^0)\frac{-ARTk_1^0}{(\alpha n_0)_1 FV(-r)}\exp\left[\frac{-(\alpha n_0)_1 F}{RT}(E - E^0)\right]\right\} \tag{26}$$

The current due to the second step is given by eqn. (27).

$$i_2 = -n_2 FV\frac{dC_2}{dt} + i_1 = n_2 FAC_2 k_2^0 \exp\left[\frac{-(\alpha n_0)_2 F}{RT}(E - E^0)\right] \tag{27}$$

Equation (27) is solved for C_2 and i_2 by the usual procedures for first-order, linear differential equations to give:

$$C_2 = C_1^0 H^{-1}\int_{E_i}^{E} GH\,dE \tag{28}$$

$$i_2 = n_2 FAk_2^0 C_1^0 H^{-1}\exp\left[\frac{-(\alpha n_0)_2 F}{RT}(E - E_2^0)\right]\int_{E_i}^{E} GH\,dE \tag{29}$$

where

$$G \equiv \frac{n_1 Ak_1^0 C_1^0}{n_2 Vr}\exp\left\{\frac{-(\alpha n_0)_1 F}{RT}(E - E_1^0) + \frac{Ak_1^0 RT}{(\alpha n_0)_1 FVr}\exp\left[\frac{-(\alpha n_0)_1 F}{RT}(E - E_1^0)\right]\right\}$$

$$H \equiv \exp\{[Ak_2^0 RT/V(-r)(\alpha n_0)_2 F]\exp[(-(\alpha n_0)_2 F/RT)(E - E_2^0)]\}$$

$C_1^0 \equiv$ (initial concentration of ox) and $C_2^0 \equiv$ (initial concentration of red_1) $= 0$.

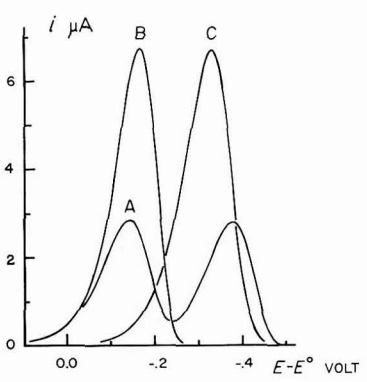

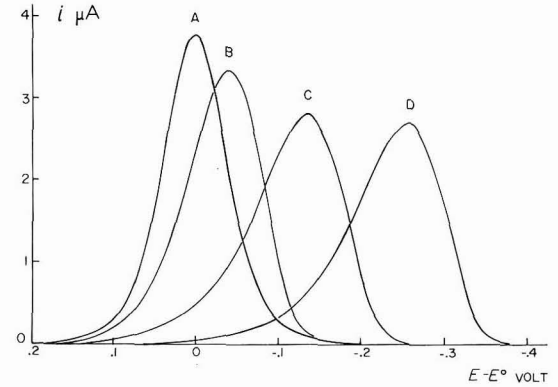

Fig. 3. Theoretical thin layer current–potential curves for a stepwise totally irreversible reaction. Graph of eqn. (30). (A), $k_1^0 = 10^{-5}$; $k_2^0 = 10^{-7}$; (B), $k_1^0 = k_2^0 = 10^{-5}$; (C), $k_1^0 = 3 \cdot 10^{-7}$; $k_2^0 = 10^{-5}$ cm sec^{-1}. Values for αn_0, V, r, n, A, C^0 and T are the same as in Fig. 1.

Fig. 4. Theoretical thin layer current–potential curves for reactions of intermediate reversibility. Graph of eqn. (32) for various values of k^0: (A), $\geqslant 4 \cdot 10^{-3}$; (B), 10^{-4}; (C), 10^{-5}; (D), 10^{-6} cm sec^{-1}. Values for αn_0, V, r, n, A, C^0 and T are the same as in Fig. 1.

Since $i = i_1 + i_2$, the current–potential expression is:

$$i = n_2 FVr\, C_1^0 G + n_2 FAk_2^0 C_1^0 H^{-1} \exp\left[\frac{-(\alpha n_0)_2 F}{RT}(E - E_2^0)\right] \int_{E_i}^{E} GH\, dE \quad (30)$$

The integral term on the r.h.s. of eqn. (30) does not appear to have an analytic solution, but graphs obtained by computerized numerical integration for $(\alpha n_0)_1 = (\alpha n_0)_2 = \frac{1}{2}$ and several pairs of values of k_1^0 and k_2^0 appear in Fig. 3.

4. *Thin layer current–potential curve for a semi-reversible reaction*

The current–potential expression obtained for a reaction of intermediate reversibility suffers from the limitation that it is not explicit in i or E. The result, obtained by combining eqns. (2), (7) and (31):

$$C_{ox}^0 = C_{ox} + C_{red} \quad (31)$$

is given by eqn. (32).

$$i = -nFA\left\{k_b C_{ox}^0 - \frac{AC_{ox}^0}{Vr}(k_f + k_b) X^{-1} \int_{E_i}^{E} X k_b\, dE\right\} \quad (32)$$

where

$$X \equiv \exp\left[\{ART/V(-r)n_0F\}(k_f/\alpha - k_b/(1-\alpha))\right]$$

$$k_f \equiv k^0 \exp\left[(-\alpha n_0 F/RT)(E - E^0)\right]$$

$$k_b \equiv k^0 \exp\left[\{(1-\alpha)n_0F/RT\}(E - E^0)\right]$$

The analogous equation for anodic reactions is obtained from eqn. (32) if C_{ox}^0 is replaced by C_R^0. A graph of eqn. (32) appears in Fig. 4. The value of the peak current varies steadily between the extremes represented by eqns. (3) and (10) for reversible ($k^0 > 4 \cdot 10^{-3}$ cm sec^{-1}) and totally irreversible ($k^0 < 1 \cdot 10^6$ cm sec^{-1}) reactions, respectively.

5. Thin layer current–potential curve for a totally irreversible reaction involving parallel reaction paths

In the event that two parallel reaction paths are available to a single reactant species,

$$\mathrm{ox} + n_1 e^- \rightarrow \mathrm{red}_1$$
$$\mathrm{ox} + n_2 e^- \rightarrow \mathrm{red}_2$$

the current–potential curve displays morphology (Fig. 5) not unlike that for a single reaction path (Fig. 1). In particular, only a single peak is expected regardless of the number of reaction paths available to the *single* reactant species.

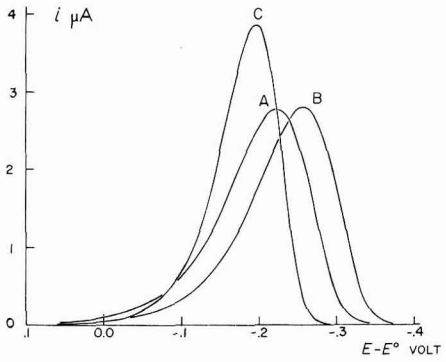

Fig. 5. Theoretical current–potential curves for irreversible reactions involving two parallel paths. Graph of eqn. (35). (A), $E_1^0 = E_2^0 = 0.0$, $(\alpha n_0)_1 = (\alpha n_0)_2 = 0.5$; (B), $E_1^0 = 0.0$, $E_2^0 = -0.20$, $(\alpha n_0)_1 = (\alpha n_0)_2 = 0.5$; (C), $E_1^0 = 0.0$, $E_2^0 = -0.2$, $(\alpha n_0)_1 = 0.7$, $(\alpha n_0)_2 = 0.5$. The following values were assumed in making the plots: $n_1 = n_2 = 1$; $k^0 = 10^{-6}$ cm sec^{-1}; $C_{ox}^0 = 10^{-6}$ mole cm^{-3}; V, r and A the same as in Fig. 1.

The experimental equations appropriate to this reaction type are obtained as follows. The current due to parallel, totally irreversible (cathodic) reactions is given by:

$$i = FAC_{ox}\,(n_1\ {}_1k_f + n_2\ {}_2k_f) \tag{33}$$

where ${}_1k_f \equiv {}_1k^0 \exp\left[\{-(\alpha n_0)_1 F/RT\}(E - E_1^0)\right]$

and ${}_2k_f \equiv {}_2k^0 \exp\left[\{-(\alpha n_0)_2 F/RT\}(E - E_2^0)\right]$

The current must also obey the relation:

$$i = -FV\left(\frac{n_1\ {}_1k_f + n_2\ {}_2k_f}{{}_1k_f + {}_2k_f}\right)\frac{dC_{ox}}{dt} \tag{34}$$

The term in brackets on the r.h.s. of eqn. (34) gives the instantaneous effective n-value of the mixed reaction. Equations (33) and (34) are readily solved to give

$$i = FAC_{ox}^0\,(n_1\ {}_1k_f + n_2\ {}_2k_f)\exp\left\{\frac{ART}{VFr}\left[\frac{{}_1k_f}{(\alpha n_0)_1} + \frac{{}_2k_f}{(\alpha n_0)_2}\right]\right\} \tag{35}$$

Graphs of eqn. (35) appear in Fig. 5.

APPENDIX

Conditions for reversible and totally irreversible behavior in thin layer voltammetry

In order to assure that eqn. (10) describes the current–potential curve of an *irreversible* reaction within a relative error of 2%, it is sufficient to ascertain that the exchange current is about 2% as large as the peak current. Employing eqn. (36)

$$i_0 = nFAk^0C^0 \tag{36}$$

as a convenient upper estimate of the exchange current, i_0, and eqn. (10) as a lower estimate of the peak current, i_p, gives:

$$i_0/i_p \leqq 2.718ARTk^0/\alpha n_0 FVr \geqq 0.02 \tag{37}$$

or

$$k^0 \leqq (\alpha n_0 FV|r|/2.718\ ART)\cdot 0.02 \tag{38}$$

For typical values of the experimental parameters ($\alpha n_0 = 0.5$; $V = 2\cdot 10^{-3}$ cm^3; $|r| = 2$ mV sec^{-1}; $T = 298°$K; and $A = 0.5$ cm^2) the simple theory applies whenever $k^0 \leqq 1.2\cdot 10^{-6}$ cm sec^{-1}. The difference, $E_p - E^0$, between the peak and standard potentials corresponding to this maximum value of k^0 is calculated from eqns. (9) and (37) to be:

$$|E_p - E^0| \geqq 4.9\ RT/\alpha n_0 F \approx 0.25\ \text{V} \tag{39}$$

In order to ensure that eqn. (5) describes the current–potential behavior of a *reversible* reaction within a relative error of 2% it is sufficient to ascertain that

$$i_0/i_p \geqslant 4ARTk^0/nFV|r| \geqq 50 \tag{40}$$

That is, if eqn. (41) is followed,

$$k^0 \geqslant (nFVr/4\ ART)\cdot 50 \tag{41}$$

Nernstian behavior will be observed in thin layer voltammetry. Evaluation of eqn. (41) using the same values of the parameters as for eqn. (38) gives:

$$k^0 \geqslant 4\cdot 10^{-3}\ \text{cm sec}^{-1}$$

The value of $|E_p - E^0|$ corresponding to the minimum value of k^0 is estimated from eqns. (5) and (10); the result is:

$$\exp\left[(-\alpha n_0 F/RT)(E - E^0)\right] - \exp\left[\{(1-\alpha)n_0 F/RT\}(E - E^0)\right] = 0.04 \tag{42}$$

Evaluation of eqn. (42) for $\alpha n_0 = 0.5$ gives

$$|E_p - E^0| \leqq 1\ \text{mV}.$$

ACKNOWLEDGEMENTS

This research was supported in part by the Petroleum Research Fund of the American Chemical Society (grant number PRF 1265-G-2,3) and the National Science Foundation (contract number GP 8880).

SUMMARY

Linear potential sweep voltammetry in thin layers of solution offers numerous

advantages for the study of irreversible reactions. The experimental equations, derived here for representative reaction types, are simpler than their counterparts in ordinary voltammetry, and may in some cases be solved directly for the electrochemical rate parameters, k^0 and αn_0. Rate measurements in thin layers do not require that both members of the reactant couple be present initially in solution. The physical and mathematical simplicity of thin layer voltammetry may allow the otherwise impossible study of irreversible systems involving multiple reactants, multiple charge-transfer steps or complicated stoichiometry. Experiments in which the theory is verified and exploited for studies of fundamental interest will be described in subsequent communications.

REFERENCES

1 A. T. HUBBARD AND F. C. ANSON, *J. Electroanal. Chem.*, 9 (1965) 163.
2 A. T. HUBBARD, R. A. OSTERYOUNG AND F. C. ANSON, *Anal. Chem.*, 38 (1966) 692.
3 A. T. HUBBARD AND F. C. ANSON, *Anal. Chem.*, 38 (1966) 1601.
4 A. T. HUBBARD AND F. C. ANSON, *Anal. Chem.*, 38 (1966) 58.
5 A. T. HUBBARD AND F. C. ANSON, *Anal. Chem.*, 38 (1966) 1887.
6 C. R. CHRISTENSEN AND F. C. ANSON, *Anal. Chem.*, 35 (1963) 205.
7 C. R. CHRISTENSEN AND F. C. ANSON, *Anal. Chem.*, 35 (1964) 495.
8 L. B. ANDERSON AND C. N. REILLEY, *J. Electroanal. Chem.*, 10 (1965) 295.
9 B. MCDUFFIE, L. B. ANDERSON AND C. N. REILLEY, *Anal. Chem.*, 38 (1966) 883.
10 D. M. OGLESBY, J. D. JOHNSON AND C. N. REILLEY, *Anal. Chem.*, 38 (1966) 385.
11 A. T. HUBBARD, Ph.D. Thesis, California Institute of Technology, 1967, (available from University Microfilms, Ann Arbor, Mich. Pub. No. 67-6066).
12 A. T. HUBBARD AND A. L. Y. LAU, article III in this series.
13 A. T. HUBBARD AND J. CUSHING, article II in this series.
14 A. T. HUBBARD AND F. C. ANSON, *The Theory and Practice of Electrochemistry with Thin-layer Cells*, in *Electroanalytical Chemistry*, Vol. 5, edited by A. J. BARD, Marcel Dekker, New York, in press.
15 K. S. VETTER, *Electrochemical Kinetics*, Academic Press, New York, 1967.

ELECTROANALYTICAL CHEMISTRY AND INTERFACIAL ELECTROCHEMISTRY
Elsevier Sequoia S.A., Lausanne – Printed in The Netherlands

VOLTAMMETRIC DETERMINATION OF BROMITE WITH A PLATINIZED PLATINUM MICROELECTRODE WITH PERIODICAL RENEWAL OF THE DIFFUSION LAYER

F. PERGOLA, G. RASPI AND A. MASSAGLI
Istituto di Chimica Analitica ed Electrochimica dell'Università di Pisa (Italy)
(Received February 18th, 1969)

INTRODUCTION

During our study of the polarographic determination of the halides and oxygenated compounds of the halogens[1,2] with the platinum electrode with periodical renewal of the diffusion layer, it appeared to be of interest to investigate bromite behaviour on this electrode and the possibility of its polarographic determination. Recently, this compound has become of some importance from an industrial point of view. Leclerc and Kircher[3] have found that by treating textile fibres with an alkaline solution of bromite the starch is completely eliminated and the fibres then exhibit excellent hydrophilic characteristics.

Several authors have dealt with the determination of bromite in the presence of hypobromite and bromate. Some methods are based on an iodometric chemical titration after elimination of hypobromite with phenol[4,5] or ammonium salts[6,8]. Both methods have been criticized because they give incorrect results: phenol acts slowly on iodine and interferes with the detection of the end-point; ammonium ion has a slight action on bromite. Other authors[9] base their methods on the different reaction rates of hypobromite and bromite with ferrocyanide and arsenious oxide. They suggest a direct determination of hypobromite with As_2O_3 with potentiometric detection of the final end-point and subsequent titration of bromite, also with As_2O_3, using osmium tetroxide as catalyst.

Velghe and Claeys[10] have determined bromite polarographically using a rotating platinum electrode; however, they studied the behaviour of bromite at only one value of pH and determined it in solution containing only bromite, via the amplitude of the reduction wave.

We propose a polarographic method of determination, with the platinum electrode with periodical renewal of the diffusion layer. This sensitive method is quite specific allowing the direct determination of bromite in the presence of hypobromite, bromate and other oxidants. Either the amplitude of the reduction wave of bromite into bromide or that of the oxidation wave of bromite into bromate may be used in the pH range 8–14. At lower pH-values bromite decomposes[5,11] to an extent that increases with decrease in pH.

EXPERIMENTAL

Reagents

All reagents were of analytical grade. The bromite solution was prepared daily by dissolving $Ba(BrO_2)_2 \cdot 2H_2O$ in alkaline solution. This solution was kept at 0°C and standardized against arsenious oxide before use. The solid $Ba(BrO_2)_2 \cdot 2H_2O$ was prepared by the method suggested by Kircher and Periat[12]. The results obtained with the salt supplied by the Société d'Etudes Chimiques pour l'Industrie et l'Agriculture, Paris, were indistinguishable from those obtained with our preparation.

The 0.05 *M* hypobromite solution was obtained by dissolving 24 g of pure NaOH in a litre of distilled water and adding slowly, at −4°C, 8 g of bromine. The solution was kept cold for 2 h. It was standardized by the method of Farkas and Lewin[13] and checked for the presence of bromate and bromite.

The chlorite solution was prepared according to Foerster and Dolch[14] by allowing chlorine dioxide to bubble through a solution containing sodium hydroxide and hydrogen peroxide. Runs performed on a technical product, recrystallized many times from water, gave the same results. The chlorite solution was standardized iodometrically in acetic acid solution.

Apparatus

A cell with a platinum electrode with periodical renewal of the diffusion layer as already described[15] was used. The measurements were made with the three-electrode technique at 25±0.1°C with a Metrohm Polarecord E261, modified to allow a slow variation of the applied voltage, and a Metrohm IR compensator type E446. The pHs of the supporting electrolytes were measured with a Metrohm E388 potentiometer using a glass electrode, except for the 1 *N* and 0.1 *N* NaOH solutions. In these cases the pH was taken as 14.0 and 13.0, respectively.

Procedure

A platinized electrode was used because the processes studied are characterized by a high degree of irreversibility on smooth platinum. An optimum had to be reached to reduce irreversibility and to avoid too great a capacity of the electrode–solution condenser. This capacity produces a non-faradaic current, which increases with the rate of variation of the applied voltage. The conditions for the platinization were: cleaning of the electrode with nitric acid, subsequent electrolytic hydrogen development on its surface for 1–2 min in a dilute sulphuric acid solution and platinizing for 5 sec with a current density of about 1.2 A/cm^2 in a 3% chloroplatinic acid and 0.025% lead acetate solution. Between any two treatments, the electrode was carefully washed with distilled water. Before every set of measurements a fresh platinization was made after dissolving the preceding one in diluted and boiling aqua regia. The counter and reference electrodes were of saturated mercurous sulphate, and were joined to the polarographic cell by a bridge of a solid mixture of silica gel and K_2SO_4 in the ratio of 3:2. The voltage was generally varied at a rate of 28 mV/min. Buffer solutions brought to an ionic strength, $\mu = 1$, by the addition of $NaNO_3$ were used as supporting electrolytes. Oxygen was removed by nitrogen bubbling. The tensions reported in the present work refer to SCE.

RESULTS

The current/voltage curve reported in Fig. 1 (curve a) was recorded by changing the voltage applied to the electrode towards less positive values, in the interval +1.00 and −0.10 V, in a deaerated solution containing $1 \cdot 10^{-4}$ *M* barium bromite

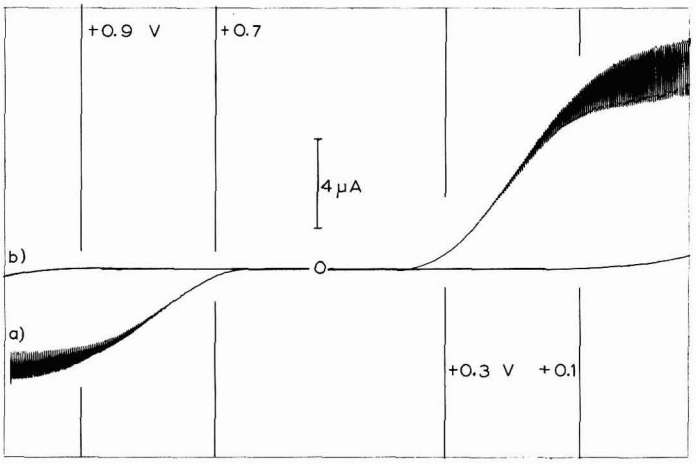

Fig. 1. Voltammetric curve of: (a), $1 \cdot 10^{-4}$ *M* bromite ion in soln. buffered at pH 10; (b), supporting electrolyte alone.

buffered at pH 10. This curve is characterized by two polarographic waves: the first in the anodic zone ($E_{\frac{1}{2}} = +0.79$ V), the second (having double amplitude) in the cathodic zone ($E_{\frac{1}{2}} = +0.20$ V).

Oxidation wave

The wave is well formed, independently of the direction of recording, and the limiting current is proportional to the bromite concentration (Table 1). $E_{\frac{1}{2}}$ depends on the pH of the solution: increase of alkalinity causes a half-wave potential displace-

TABLE 1

EFFECT OF BROMITE ION CONCENTRATION ON WAVE AMPLITUDE

$C_{BrO_2^-} \cdot 10^4$ (*M*)	*Anodic wave*		*Cathodic wave*	
	$i_d/(\mu A)$	$(i_d/c) \cdot 10^{-4}$	$i_d/(\mu A)$	$(i_d/c) \cdot 10^{-4}$
0.50	—	—	4.1	8.2
0.75	—	—	6.3	8.4
1.00	4.2	4.2	8.5	8.5
1.50	6.2	4.1	12.5	8.35
2.00	8.4	4.2	17.0	8.5
4.00	17.6	4.4	34.0	8.5
8.00	33.6	4.2	67.0	8.4
11.00	47.0	4.3	92.0	8.4
14.00	60.0	4.3	120.0	8.6

ment towards less positive values of about 25 mV/pH unit (Fig. 2, a). This displacement is far less than that corresponding to the oxygen discharge; as a consequence, this wave is obscured by the oxygen discharge when the pH of the solution is above

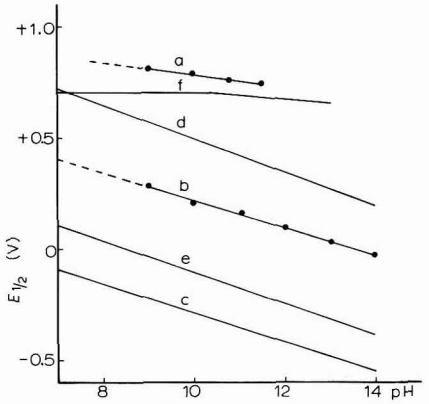

Fig. 2. Changes of $E_{\frac{1}{2}}$ as a function of pH for: (a), BrO_2^- oxidation wave; (b), BrO_2^- reduction wave; (c), BrO_3^- reduction wave; (d), BrO^- reduction wave; (e), ClO_2^- reduction wave; (f), ClO_2^- oxidation wave.

11.5. The results of the coulometric measurements (Table 2) show that bromite oxidation involves the global participation of 2 electrons/molecule, in accordance with the electrode reaction:

$$BrO_2^- + 2OH^- \rightarrow BrO_3^- + H_2O + 2e^-$$

The logarithmic analysis of the wave shows that the ratio, $\Delta E/\Delta \log[i/(i_d - i)]$ is equal to 51 mV, compared with the theoretical value of 29.5 mV expected for a reversible process.

TABLE 2

COULOMETRY OF 0.1625 *m*MOLES OF BROMITE IN BUFFER SOLUTION pH 9.0, AT A PLATINIZED PLATINUM ANODE (7.5 cm^2) POLARIZED AT +0.88 V

$C_{BrO_2^-}$ (*mmol/l*)	*Coulombs*		
	Calcd. (2 *e*)	*Exptl.*	*Difference*
2.58	—	—	—
2.25	4.0	3.9	−0.1
2.03	6.7	6.6	−0.1
1.88	8.5	8.6	+0.1
1.76	10.0	10.0	−
1.69	11.8	11.9	+0.1
1.43	14.0	13.9	−0.1
1.20	16.8	16.8	−
0.96	19.7	19.8	+0.1

Reduction wave

This wave takes place near the wave of the oxygen reduction and deaeration

is therefore essential. The wave amplitude is proportional to the bromite concentration (Table 1). The half-wave potential depends on the alkalinity of the solution: there is an $E_{\frac{1}{2}}$ displacement of about 70 mV/pH unit (Fig. 2, b). The coulometric results (Table 3) show that the bromite reduction process involves the global participation of 4 electrons/molecule, according to the scheme:

TABLE 3

COULOMETRY OF 0.158 *m*MOLES OF BROMITE, IN BUFFER SOLUTION pH 9.0 AT A PLATINIZED PLATINUM CATHODE (7.5 cm^2) POLARIZED AT —0.10 V

$C_{BrO_2^-}$/(*mmol/l*)	*Coulombs*		
	Calcd. (4 *e*)	*Exptl.*	*Difference*
3.16	—	—	—
2.90	5.0	5.1	+0.1
2.72	8.5	8.5	–
2.54	12.0	12.1	+0.1
2.33	16.0	15.9	−0.1
2.07	21.0	20.9	−0.1
1.86	25.1	25.2	+0.1
1.61	29.9	29.7	−0.2
1.40	34.0	34.1	+0.1

$$BrO_2^- + 2\,H_2O + 4e^- \rightarrow Br^- + 4OH^-$$

The process is characterized by an appreciable overvoltage: the logarithmic analysis of the wave shows that the ratio, $\Delta E/\Delta \log[(i_d - i)/i]$, is equal to 110 mV, well above the theoretical value of 15 mV for a reversible process. The mean limiting current, $\bar{i}_d$, is related to the diffusion coefficient, D, by the equation[15]:

$$\bar{i}_d = a + (b/t_{tot})(2t_{tot}^{\frac{1}{2}} - 1.5t_p^{\frac{1}{2}})$$

where: $a = nFADC/r$, $\quad b = nFAD^{\frac{1}{2}}C/\pi^{\frac{1}{2}}$

t_p = the washing period of the electrode,
t_{tot} = period between two subsequent washings,
n = number of Faradays (F)/mole required by the reaction at the electrode,
r = radius of the platinum sphere,
C = molar concentration of electroactive substance,
A = effective electrode surface area, obtained by measurements of the limiting current of solutions of electroactive species with known D.

When the measured values of $\bar{i}_d$, A and r were inserted in this expression the diffusion coefficient value for bromite was found to be $1.20 \cdot 10^{-5}$ cm^2 sec^{-1}.

DISCUSSION

The simultaneous presence of two independent polarographic waves enables either the anodic or cathodic wave to be chosen for the quantitative determination of bromite when compounds that interfere in the cathodic or anodic zone are present in the test solution.

The amplitude of the cathodic bromite wave can be measured down to a concentration of $4 \cdot 10^{-5}$ *M*. At lower concentrations the results are uncertain. The evaluation of the anodic wave is possible at a bromite concentration as low as $1 \cdot 10^{-4}$ *M*.

The effect of bromate, hypobromite and chlorite was investigated. In the pH range useful for bromite determination, bromate[16], hypobromite[16] and chlorite[2] give a reduction wave the amplitude of which is proportional to concentration.

In the presence of bromate the reduction wave of bromite is followed by the reduction wave of bromate into bromide. Figure 2 (b and c) shows a large separation between the two waves, making it possible to determine bromite down to a concentration of $5 \cdot 10^{-5}$ *M*, provided that the molar ratio, BrO_3^-/BrO_2^-, is not above 120 (Table 4). Bromite at concentrations above $1 \cdot 10^{-4}$ *M* (Table 4) can also be determined for higher values of this ratio by using the anodic wave in buffered solution at pH 8–9.

TABLE 4

DETERMINATION OF BROMITE IN THE PRESENCE OF BROMATE IN BUFFER SOLUTION pH 9.0

(*a*)			(*b*)		
$C_{BrO_2^-} \cdot 10^4$ *present* (*M*)	$C_{BrO_2^-} \cdot 10^4$ *found* (*M*)	*Error* (%)	$C_{BrO_2^-} \cdot 10^4$ *present* (*M*)	$C_{BrO_2^-} \cdot 10^4$ *found* (*M*)	*Error* (%)
1.1	1.07	−3.0	0.5	0.48	−4.0
2.2	2.24	+1.8	1.0	0.94	−6.0
4.5	4.52	+0.5	2.0	1.98	−1.0
7.5	7.65	+2.0	3.5	3.52	+0.6
10.0	9.90	−1.0	8.0	7.91	−1.1
16.0	15.89	−0.7	11.0	11.05	+0.5
32.0	32.25	+0.8	25.0	25.10	+0.4
40.0	40.05	−0.1	40.0	40.40	+1.0
50.0	50.15	−0.3	50.0	49.60	−0.8

(a) All data obtained with 0.2 *M* $KBrO_3$ by using the anodic bromite wave.
(b) All data obtained with $6.18 \cdot 10^{-3}$ *M* $KBrO_3$ by using the cathodic bromite wave.

In the presence of hypobromite, the reduction wave of bromite is preceded by the reduction wave of hypobromite to bromide. As shown in Fig. 2 (b–d), the two waves are sufficiently separated for bromite to be determined in the pH range investigated. However, this determination must be carried out at pH 13 in order to avoid the decomposition of hypobromite into bromite and bromide which is appreciable in the pH range 9–12[5]. The determination of bromite is possible for values of the molar ratio, BrO^-/BrO_2^-, below 16 (Table 5) but above this value the determination is unsatisfactory because the reduction current of BrO_2^- appears on the reduction plateau of BrO^-. Most of the BrO^- can be eliminated by the careful addition of ammonia (avoiding any excess) to the solution at 0°C. When the hypobromite concentration has been reduced to the same order of magnitude as that of bromite, the latter can be determined by using its cathodic wave.

The analysis of a hypobromite–bromite–bromate mixture should be carried out at pH 13, at which hypobromite is stable and where there is still a good separation between the single waves (see Fig. 3). Good results are obtained for hypobromite at bromite/hypobromite molar ratios below 15; bromate did not interfere for bromate/hypobromite molar ratios below 100. For bromite, what has already been said about

TABLE 5

DETERMINATION OF BROMITE IN THE PRESENCE OF HYPOBROMITE OR CHLORITE ION IN 1 *N* NaOH SOLUTION

(*a*)			(*b*)		
$C_{BrO_2^-} \cdot 10^4$ *present* (*M*)	$C_{BrO_2^-} \cdot 10^4$ *found* (*M*)	*Error* (%)	$C_{BrO_2^-} \cdot 10^4$ *present* (*M*)	$C_{BrO_2^-} \cdot 10^4$ *found* (*M*)	*Error* (%)
0.8	0.78	−2.5	0.8	0.83	+3.8
1.0	1.06	+6.0	1.0	1.02	+2.0
2.0	1.98	−1.0	2.0	1.91	−4.5
3.2	3.22	+0.6	3.5	3.48	−0.6
8.0	8.71	−1.1	5.5	5.41	−1.6
12.0	12.18	+1.5	11.0	11.04	+0.4
25.0	25.37	+1.5	22.0	22.21	+1.0
40.0	40.20	+0.5	33.0	33.30	+0.9
			50.0	49.80	−0.4

(a) All data obtained with 10^{-3} *M* NaBrO solution.
(b) All data obtained with $9 \cdot 10^{-4}$ *M* $NaClO_2$ solution.

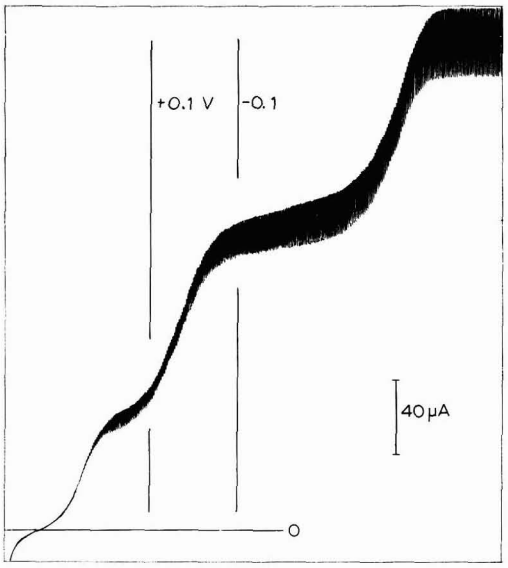

Fig. 3. Voltammetric curve of $1.4 \cdot 10^{-3}$ *M* hypobromite, $1.2 \cdot 10^{-3}$ *M* bromite, $8 \cdot 10^{-4}$ *M* bromate in 0.1 *N* NaOH soln.

the single separations still holds. For bromate, good results are obtained provided that the molar ratio, (hypobromite + bromite)/bromate, does not exceed 20; above this value the error in the quantitative determination of bromate is considerable. The results are shown in Table 6.

The determination of bromite in the presence of chlorite is also feasible. In fact, chlorite ion also gives a reduction wave and an oxidation wave[2]. However, Fig. 2 shows (b–e) that the reduction wave of chlorite develops at more negative tensions than that of bromite reduction, whereas the oxidation waves of the two species (a–f) develop at about the same voltage. Bromite was therefore determined in 1 *N* NaOH solution, via its reduction wave. The results (Table 5) show that the determination of

TABLE 6

SIMULTANEOUS DETERMINATION OF HYPOBROMITE, BROMITE AND BROMATE IN 1 N NaOH SOLUTION

$BrO^- \cdot 10^4$ present (M)	$BrO_2^- \cdot 10^4$ present (M)	$BrO_3^- \cdot 10^4$ present (M)	$BrO^- \cdot 10^4$ found (M)	$BrO_2^- \cdot 10^4$ found (M)	$BrO_3^- \cdot 10^4$ found (M)	Error (BrO^-) (%)	Error (BrO_2^-) (%)	Error (BrO_3^-) (%)
20.0	40.0	1.5	20.10	40.20	1.39	+0.5	+0.5	−7.4
15.0	20.0	15.0	14.90	19.90	14.84	−0.7	−0.5	−1.1
30.0	15.0	20.5	30.52	14.91	20.32	+1.7	−0.6	−0.9
11.0	25.0	12.5	10.80	24.87	12.87	−1.8	−0.5	+3.0
8.0	4.5	6.0	7.91	4.58	5.90	−1.1	+1.8	−1.7
5.0	30.0	50.0	5.12	29.80	50.10	+2.4	−0.7	+0.2
8.0	6.5	50.0	8.11	6.60	49.80	+1.4	+1.5	−0.4
3.0	3.5	65.0	3.18	3.40	65.06	+6.0	−3.0	+0.1
12.5	1.0	25.0	12.31	1.08	25.25	−1.5	+8.0	+1.0

TABLE 7

DETERMINATION OF CHLORITE IN THE PRESENCE OF BROMITE IN 1 N NaOH, $3.82 \cdot 10^{-3}$ M BrO_2^- SOLUTION

$C_{ClO_2^-} \cdot 10^4$ present (M)	$C_{ClO_2^-} \cdot 10^4$ found (M)	Error (%)
4.0	4.08	+2.0
8.0	8.14	+1.8
12.0	12.13	+1.1
16.0	15.84	−1.0
20.0	20.20	+1.0
29.0	29.15	+0.5
38.0	37.70	−0.8
55.0	54.89	−0.2
75.0	74.70	−0.4

bromite is possible when the chlorite/bromite molar ratio is not above 18, provided that the bromite concentration is not below $4 \cdot 10^{-5}$ M.

Finally, the determination of chlorite in the presence of bromite was considered. The determination is possible for chlorite/bromite molar ratios greater than 0.1. The results are reported in Table 7.

ACKNOWLEDGEMENTS

The present work was partially supported by C.N.R. (Consiglio Nazionale delle Ricerche) under contract No. 115/1332.0/0469.

SUMMARY

A new method is presented for the polarographic determination of bromite alone or in the presence of bromate, hypobromite and chlorite, with a cell with platinized platinum electrode with periodical renewal of the diffusion layer. The simultaneous determination of bromite, bromate and hypobromite is also possible. Dilute

bromite solutions with pH > 8 show two distinct waves, the amplitude of which is proportional to the concentration, one in the anodic range and the other in the cathodic range; the former is caused by the oxidation of bromite to bromate and the latter by the reduction of bromite to bromide. Above pH 11.5 the anodic step is masked by the oxygen discharge. The presence of two independent polarographic steps enables either the anodic or the cathodic step to be chosen for the quantitative determination of bromite when compounds that interfere in the cathodic or anodic zone, respectively, are present in the test solution. The method gives good reproducibility in a wide field of concentrations, is sensitive and simple to use.

REFERENCES

1 G. RASPI, F. PERGOLA AND D. COZZI, *J. Electroanal. Chem.*, 15 (1967) 35.
2 G. RASPI AND F. PERGOLA, *J. Electroanal. Chem.*, 20 (1969) 419.
3 J. LECLERC AND R. KIRCHER, Fr. Addn., 71,747 (Jan. 19, 1960).
4 J. CLARENS, *Compt. Rend.*, 157 (1913) 216.
5 R. M. CHAPIN, *J. Am. Chem. Soc.*, 56 (1934) 2211.
6 J. CLARENS, *Compt. Rend.*, 156 (1913) 1998.
7 M. H. HASHMI AND A. A. AYAZ, *Anal. Chem.*, 35 (1963) 908.
8 M. H. HASHMI AND A. A. AYAZ, *Analyst*, 89 (1964) 147.
9 T. ANDERSEN AND H. E. LUNDAGER MADSEN, *Anal. Chem.*, 37 (1965) 49.
10 N. VELGHE AND A. CLAEYS, *Bull. Soc. Chim. Belges*, 75 (1966) 498.
11 P. ENGEL, A. OPLATKA AND B. PERLMUTTER-HAYMAN, *J. Am. Chem. Soc.*, 76 (1954) 2010.
12 R. KIRCHER AND R. PERIAT, German Patent, 1.076.096 (Feb. 25, 1960).
13 L. FARKAS AND M. LEWIN, *Anal. Chem.*, 19 (1947) 662.
14 F. FOERSTER AND P. DOLCH, *Z. Elektrochem.*, 23 (1917) 138.
15 D. COZZI, G. RASPI AND L. NUCCI, *J. Electroanal. Chem.*, 12 (1966) 36.
16 G. RASPI AND F. PERGOLA, unpublished data.

ELECTROANALYTICAL CHEMISTRY AND INTERFACIAL ELECTROCHEMISTRY
Elsevier Sequoia S.A., Lausanne – Printed in The Netherlands

VOLTAMMETRIC INVESTIGATION OF THE NEPTUNYL GLYCINATE COMPLEX AT THE ROTATED GLASSY CARBON ELECTRODE

C. E. PLOCK

Chemistry Research and Development, The Dow Chemical Company, Rocky Flats Division, Golden, Colo. (U.S.A.)

(Received February 20th, 1969)

The investigation of metal–glycinate complexes prior to 1961 has been well documented by Sillén and Martell[1]. Since 1961 the glycinate complexes of neodymium[2,4], praseodymium[3,4] and lanthanium[4] have been investigated. Kriss[5] determined the first-order stability constants of the glycinate complexes of the lanthanum rare earths using a potentiometric titration. Pankratova *et al.*[6] found that zirconium does not form a glycinate complex at low glycine concentrations.

The only glycinate complex of the actinide rare earths investigated is the uranium(VI) glycinate studied polarographically by Lai *et al.*[7].

The investigation of the organic complexes of neptunium(VI) has been limited to the spectrophotometric investigation of the acetate[8] complex, and the voltammetric investigation of the malonate[9] and the glutamate[10] complexes. Keller and Eberle[11] attempted to prepare neptunium(VI) complexes with 8-hydroxyquinoline and some of its derivatives, but neptunium(VI) was rapidly reduced by the complexing ligand.

The complexes of neptunium(V) have been more thoroughly investigated by spectrophotometry[11–14] and ion-exchange[11,15–18] methods.

This paper describes the investigation of the neptunium(VI) glycinate complex at the rotated glassy carbon electrode.

EXPERIMENTAL

Apparatus

All voltammograms were obtained at 25°C with a Sargent Model XV recording polarograph. The applied potential was monitored by a Hewlett Packard Model DY-2401C integrating digital voltmeter. None of the measurements was damped. The electrolysis cell and the glassy carbon electrode (GCE) have been described[9,19]. The electrode was mounted in a Sargent synchronous rotator, rotation speed 600 rev./min. The electrode was cleaned at the end of each measurement by allowing the electrode to rotate for 15–30 sec in concentrated nitric acid.

The pH-values of the solutions were measured using a Beckman Model 76 Expanded Scale pH-meter and a glass electrode. The pH was adjusted with perchloric acid or sodium hydroxide.

The conductometric titrations were performed using a YSI Model 31 (Yellow Springs Instrument Co., U.S.A.) line operated conductivity bridge. The amperometric titrations were performed using the Sargent Model XV recording polarograph and a 10-ml Sargent Model C automatic constant rate burette.

A Cannon–Fenske–Ostwald viscometer (Cannon Instrument Co., U.S.A.) was used to obtain the viscosity values.

Reagents

The preparation and standardization of the neptunium(VI) and the neptunium(V) stock solutions have been described[9,19]. The glycinate solution was prepared by dissolving sodium glycinate (K and K Laboratories, U.S.A.) in water and was standardized by an amperometric titration against a ferric iron solution whose concentration had been determined by controlled potential coulometry.

All other chemicals were reagent-grade and were prepared in the usual manner. Purified nitrogen was used to deaerate the test solutions when necessary.

DISCUSSION AND RESULTS

Effect of pH

The effect of changes in acidity on the half-wave potential and on the limiting current of the neptunium(VI)–glycinate complex was determined in solutions $7.50 \cdot 10^{-4}$ *M* in neptunium(VI), 1.0 *M* in sodium glycinate, and 0.5 *M* in sodium perchlorate.

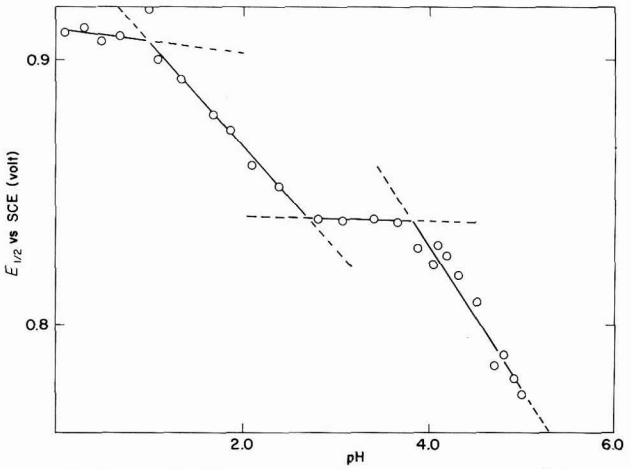

Fig. 1. Variation of half-wave potential with pH. $7.50 \cdot 10^{-4}$ *M* neptunium(VI), 0.5 *M* $NaClO_4$, 1.0 *M* $NaC_2H_4O_2N$.

The plot in Fig. 1 can be divided into four straight line portions, corresponding to the pH-regions, 0.1–1.0, 1.0–2.7, 2.7–3.8, and 3.8–5.0. Above pH 5.0 the reduction waves become ill-defined.

In the pH range 0.1–1.0, the half-wave potential is constant with change of acid concentration indicating that no hydrogen ions are involved in the reduction of neptunium(VI). The half-wave potential in this pH-range averages 0.909 V *vs.* the saturated calomel electrode (SCE). This value is in good agreement with the potential reported for the reduction of the simple neptunium(VI) ion[19–21]. This indicates that no complexation has taken place, or that the dissociation constant of neptunium(VI)–glycinate is equal to the dissociation constant of neptunium(V)–glycinate. It is more

common to find the dissociation constant of the oxidized complex to be less than that of the reduced complex than to find them equal. It seems likely, therefore, that no complexation of neptunium(VI) has taken place at this low pH.

In the pH-ranges 1.0–2.7 and 3.8–5.0, the half-wave potential is a function of the pH. The respective slopes can be represented by the equations:

$$E_{\frac{1}{2}} = 0.942 - 0.034 \text{ pH} \quad (1)$$

$$E_{\frac{1}{2}} = 1.048 - 0.054 \text{ pH} \quad (2)$$

Equation (1) indicates that one hydrogen ion is involved in the reduction of two neptunium(VI) ions in the pH-range 1.0–2.7. In the pH-range 3.8–5.0, eqn. (2) indicates that one hydrogen ion is involved in the reduction of each neptunium(VI) ion.

In the pH range 2.7–3.8, the slope of the curve is zero, which indicates that in this pH-range the half-wave potential is independent of the pH, and that neither hydrogen nor hydroxyl ions are involved in the reduction of neptunium(VI).

Reversibility of the reduction of neptunium(VI) in the pH-range 0.1–5.0 was demonstrated by the value of the slopes for the plots of $\log[i/i_1 - i)]$ *vs.* E_{RGC}. The average value of these slopes was 0.0637 V which compares well with the theoretical value of 0.0591 V for a one-electron, reversible reduction.

To confirm the reversibility of the electrode reaction, solutions were prepared which were $7.83 \cdot 10^{-4}$ *M* in neptunium(V), 0.5 *M* in sodium perchlorate, and 1.0 *M* in glycinate in the pH range 0.1–5.0. Neptunium(V) in these solutions was oxidized, and the half-wave potential of the anodic waves $(E_{\frac{1}{2}})_a$ was compared with the half-wave potential of the cathodic waves $(E_{\frac{1}{2}})_c$ (Table 1). $(E_{\frac{1}{2}})_a$ compares well with $(E_{\frac{1}{2}})_c$ indicating that the electrode reduction of neptunium(VI) in the pH-range 0.1–5.0 at 1.00 *M* glycinate is reversible.

TABLE 1

COMPARISON OF ANODIC HALF-WAVE POTENTIAL WITH CATHODIC HALF-WAVE POTENTIAL AT VARIOUS pH-VALUES

$7.50 \cdot 10^{-4}$ *M* neptunium(VI), $7.83 \cdot 10^{-4}$ *M* neptunium(V), 0.5 *M* $NaClO_4$, 1.0 *M* $NaC_2H_4O_2N$.

pH	$(E_{\frac{1}{2}})_c$/*V vs. SCE*	$(E_{\frac{1}{2}})_a$/*V vs. SCE*	*pH*	$(E_{\frac{1}{2}})_c$/*V vs. SCE*	$(E_{\frac{1}{2}})_a$/*V vs. SCE*
0.5	0.907	0.912	3.3	0.840	0.846
1.1	0.914	0.911	3.7	0.840	0.843
1.6	0.887	0.884	4.3	0.815	0.823
1.9	0.872	0.864	4.8	0.788	0.795

The pH has no effect on the limiting current over the pH-range 0.1–5.0. The average of the limiting current in this pH-range is 30.4 ± 0.8 μA indicating that the diffusion coefficient for uncomplexed neptunium(VI) and that for the neptunium(VI)–glycinate complex are approximately equal.

Effects of glycinate concentration

The effect of changes in the sodium glycinate concentration on the half-wave potential and on the limiting current of the neptunium(VI)–glycinate complex was determined in solutions which were $7.50 \cdot 10^{-4}$ *M* in neptunium(VI), and 0.5 *M* in sodium perchlorate in the pH-ranges, 1.0–2.7, 2.7–3.8 and 3.8–5.0. In these pH-ranges,

the half-wave potential is independent of the glycinate concentration below 0.30 M, $8.3 \cdot 10^{-2}$ M, and $5.9 \cdot 10^{-2}$ M, respectively (Fig. 2) and has average values of 0.911 V, 0.909 V, and 0.897 V *vs.* SCE, which compare favorably with the potential reported for the reduction of the simple neptunium(VI) ion[19-21]. This indicates as described above that no complexation of neptunium(VI) has taken place under these experimental conditions (pH < 2.7, $C_x < 0.30$ M; pH 2.7–3.8, $C_x < 8.3 \cdot 10^{-2}$ M; and pH 3.8–5.0, $C_x < 5.9 \cdot 10^{-2}$ M, where C_x is the glycinate concentration). This is taken as an indication of the instability of the neptunium(VI)–glycinate complex under these conditions.

Reversibility of the reduction of neptunium(VI) was demonstrated by the value of the slopes for the plots of $\log[i/(i_1 - i)]$ *vs.* E_{RGC}. The average values of the slopes were 0.064 V (pH < 2.7, $C_x < 0.30$ M), 0.060 V (pH 2.7–3.8, $C_x < 8.3 \cdot 10^{-2}$ M), and 0.061 V (pH 3.8–5.0, $C_x < 5.9 \cdot 10^{-2}$ M). These values compare well with theoretical value of 0.0591 V for a one-electron, reversible reduction.

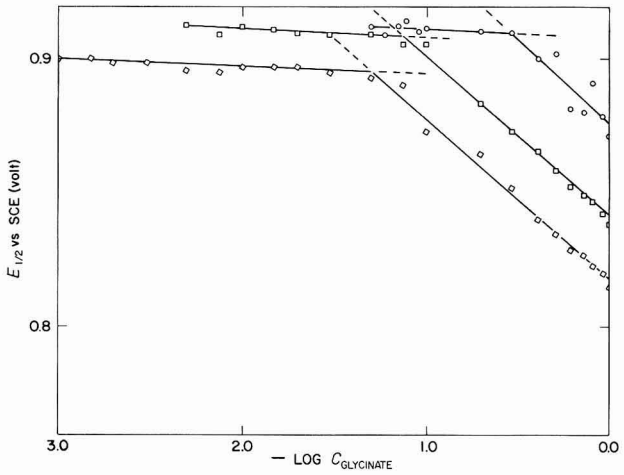

Fig. 2. Variation of half-wave potential with sodium glycinate concentration. $7.50 \cdot 10^{-4}$ M neptunium(VI), 0.5 M $NaClO_4$. pH: (○), 2.00; (□), 3.30; (◇), 4.30.

To confirm the reversibility of the electrode reaction, solutions were prepared which were $7.83 \cdot 10^{-4}$ M in neptunium(V), and 0.5 M in sodium perchlorate, with various concentrations of glycinate in the pH-ranges, 1.0–2.7, 2.7–3.8, and 3.8–5.0. Neptunium(V) in these solutions was oxidized, and $(E_{\frac{1}{2}})_a$ was found to compare well with $(E_{\frac{1}{2}})_c$ (Table 2). This indicates that the electrode reduction of neptunium(VI) is reversible below the glycinate concentrations given above.

In glycinate concentrations greater than these the plot of $\log C_x$ *vs.* the half-wave potential (Fig. 2) showed that the half-wave potential is a function of the glycinate concentration. The slopes of the plots were -0.064 V, -0.061 V and -0.061 V, respectively, which indicates that neptunium(VI) has one more glycinate ligand bound to it than neptunium(V) under these experimental conditions.

The reversibility of the electrode reaction was determined by $\log[i/(i_1 - i)]$ *vs.* E_{RGC} plots. The average values of the slopes were 0.063 V (pH < 2.7, $C_x > 0.30$); 0.063 V (pH 2.7–3.8, $C_x > 8.3 \cdot 10^{-2}$ M) and 0.061 V (pH 3.8–5.0, $C_x > 5.9 \cdot 10^{-2}$ M).

The values of these slopes compare well with the theoretical value of 0.0591 V for a one-electron, reversible reduction.

To confirm the reversibility of the electrode reaction, solutions were prepared which were $7.83 \cdot 10^{-4}$ *M* in neptunium(V) and 0.5 *M* in sodium perchlorate with various concentrations of glycinate at pH-values of 2.00, 3.30, and 4.30. Neptunium(V) in these solutions was oxidized, and $(E_{\frac{1}{2}})_a$ was found to compare well with $(E_{\frac{1}{2}})_c$ (Table 2). This indicates that the electrode reduction of neptunium(VI) at the above glycinate concentrations is reversible.

TABLE 2

COMPARISON OF ANODIC HALF-WAVE POTENTIAL WITH CATHODIC HALF-WAVE POTENTIAL AT VARIOUS GLYCINATE CONCENTRATIONS AND AT pH 2.00, 3.30 AND 4.30

$7.50 \cdot 10^{-4}$ *M* neptunium(VI), $7.83 \cdot 10^{-4}$ *M* neptunium(V), 0.5 *M* $NaClO_4$

$[NaC_2H_4O_2N]$/	*pH* 2.00		*pH* 3.30		*pH* 4.30	
moles l^{-1}	$(E_{\frac{1}{2}})_c/V$ *vs. SCE*	$(E_{\frac{1}{2}})_a/V$ *vs. SCE*	$(E_{\frac{1}{2}})_c/V$ *vs. SCE*	$(E_{\frac{1}{2}})_a/V$ *vs. SCE*	$(E_{\frac{1}{2}})_c/V$ *vs. SCE*	$(E_{\frac{1}{2}})_a/V$ *vs. SCE*
$1.0 \cdot 10^{-3}$					0.901	0.905
$5.0 \cdot 10^{-3}$			0.912	0.915	0.896	0.910
$1.0 \cdot 10^{-2}$			0.912	0.919	0.897	0.900
$5.0 \cdot 10^{-2}$	0.911	0.915	0.909	0.914	0.893	0.895
0.1	0.911	0.912	0.905	0.910	0.873	0.882
0.5	0.901	0.907	0.858	0.868	0.835	0.834
1.0	0.872	0.869	0.839	0.842	0.815	0.820

In the glycinate concentration ranges of $5.0 \cdot 10^{-2}$–1.00 *M* (pH < 2.7), $5.0 \cdot 10^{-3}$–1.00 *M* (pH 2.7–3.8), and $1.0 \cdot 10^{-3}$–1.00 *M* (pH 3.8–5.0), the limiting current is constant with average values of 30.0 ± 0.8, 31.0 ± 0.8, and 30.9 ± 1.2 μA, respectively, again indicating that the diffusion coefficients of the uncomplexed neptunium(VI) and of the neptunium(VI)–glycinate complex are approximately equal.

Composition of neptunium(VI)–glycinate complex

To determine the composition of the metal:ligand ratio, a conductometric titration was used. The titrations were performed at pH < 2.7, pH 2.7–3.8, and pH > 3.8 by using 5 ml of $14.36 \cdot 10^{-3}$ *M* neptunium(VI) solution diluted to 350 ml with water. The titrant was 0.144 *M* sodium glycinate. Three sodium glycinate solutions were prepared as titrants, and the pH of these was adjusted to correspond with the pH-range in which they were to be used. Figures 3 and 4 show the result of these titrations. At pH < 2.7 the titration curve indicates the presence of two complexes with metal: ligand ratios, 1 : 2 and 1 : 3, whereas in the pH-ranges 2.7–3.8 and > 3.8 the titration curves show that four complexes exist with the metal : ligand ratios of, 1 : 1, 1 : 2, 1 : 3, and 1 : 4.

Keefer[22] and Lai *et al.*[7] have reported that at the lower concentration of glycinate, the metal : ligand ratio is 1 : 2, while at high concentrations glycinate forms a 1:3 metal:ligand ratio. It has recently been reported that uranium(VI) forms a tetraacetate complex[23] and by analogy, the conductometric results seem to be valid. To verify this, however, attempts were made to confirm the conductometric results

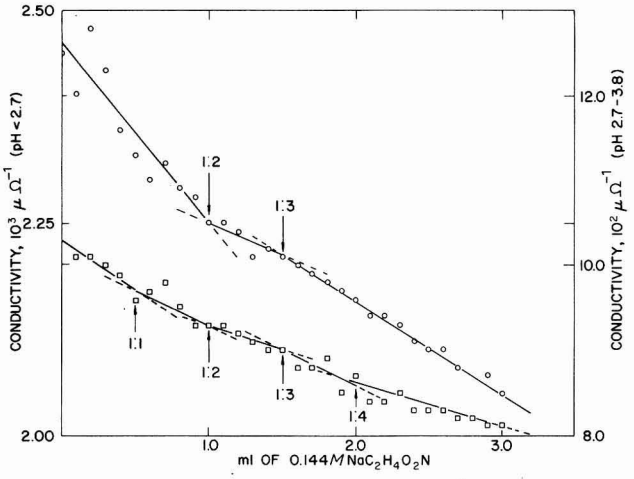

Fig. 3. Conductometric titrations. 5 ml $14.36 \cdot 10^{-3}$ *M* neptunium(VI), 345 ml water, pH: ○, < 2.7; □, 2.7–3.8.

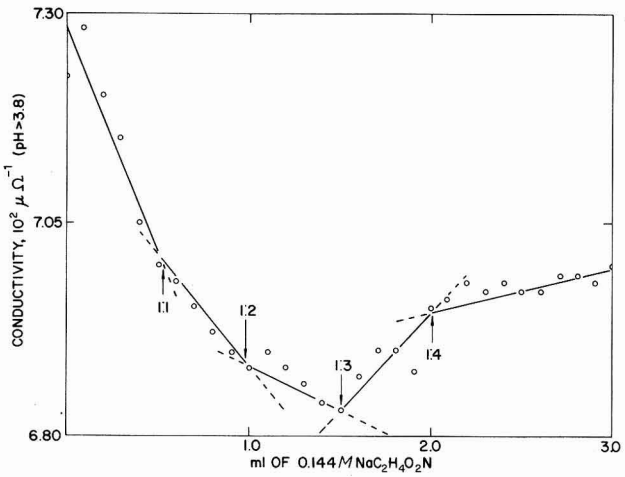

Fig. 4. Conductometric titration with pH > 3.8. 5 ml $14.36 \cdot 10^{-3}$ *M* neptunium(VI), 345 ml water.

by amperometric titrations. The results of these titrations are shown in Fig. 5, and indicate only the maximum metal : ligand ratio in the various pH-ranges. These maximum metal : ligand ratios confirm the conductometric results. The shift in the location of the break at pH 2.7–3.8 and pH > 3.8 is probably due to hydrolysis of neptunium.

Electrode reaction

Goldberg[24] has shown that the complexation of a metal ion with glycinate is due to the displacement of the weakly acidic proton of the dipolar glycinate ion *via*:

$$M^{2+} + H_3N^+-CH_2-COO^- \rightarrow M(NH_2-CH_2-COO)^+ + H^+$$

Since neptunium(VI) forms both a 1 : 3 and a 1 : 4 complex at higher glycinate concentrations, these reactions must be:

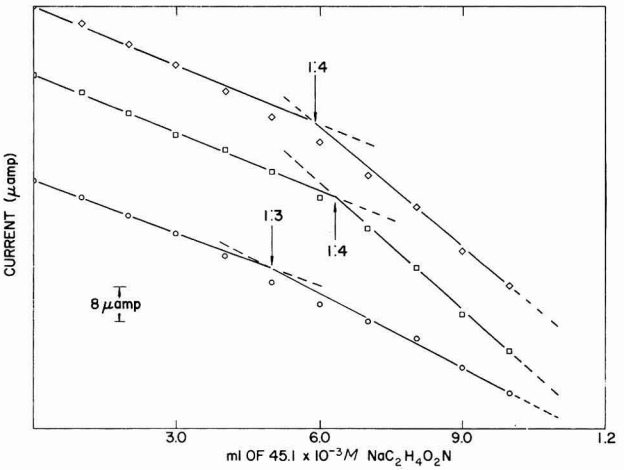

Fig. 5. Amperometric titrations. 5 ml $14.36 \cdot 10^{-3}$ *M* neptunium(VI), 10 ml 2.5 *M* $NaClO_4$, 10 ml water. pH: ○, < 2.7; □, 2.7–3.8; ◇, > 3.8.

pH > 1.0, but < 2.7

$$NpO_2^{2+} + 3\ NH_3^+–CH_2–COO^- \rightarrow NpO_2(NH_2–CH_2–COO)_3^- + 3\ H^+$$

pH > 2.7

$$NpO_2^{2+} + 4\ NH_3^+–CH_2–COO^- \rightarrow NpO_2(NH_2–CH_2–COO)_4^{2-} + 4\ H^+$$

The electrode reactions based on the foregoing data and discussion are postulated as follows (sodium glycinate concentration, 1.0 *M*; glycinate ion designated by A^-):

pH < 1.0

$$NpO_2^{2+} + e^- \rightarrow NpO_2^+$$

pH > 1.0, but < 2.7, and $q = p - 1$

$$2\ NpO_2A_3^- + H^+ + 2e^- \rightarrow 2\ NpO_2A_2^- + HA + A^-$$

pH > 2.7, but < 3.8, and $q = p - 1$

$$NpO_2A_4^{2-} + e^- \rightarrow NpO_2A_3^{2-} + A^-$$

pH > 3.8, but < 5.0, and $q = p - 1$

$$NpO_2A_4^{2-} + 2\ H_2O + e^- \rightarrow NpO_2(OH)A_3^{3-} + A^- + H_3O^+$$

When the glycinate concentration is below 0.30 *M* (pH < 2.7), $8.3 \cdot 10^{-2}$ *M* (pH 2.7–3.8), and $5.9 \cdot 10^{-2}$ *M* (pH > 3.8), the electrode reaction is:

$$NpO_2^{2+} + e^- \rightarrow NpO_2^+$$

Diffusion coefficients

The diffusion coefficient of neptunium(VI)–glycinate complex was determined at 25°C in solutions which were $7.50 \cdot 10^{-4}$ *M* in neptunium (VI), 0.5 *M* in sodium perchlorate, 1.0 *M* in sodium glycinate, at pH-values < 2.7, 2.7–3.8, and > 3.8

using the equation[25]:

$$D^{\frac{2}{3}} = i_1 v^{\frac{1}{6}}/1.500 \cdot 10^5 \, n \, ACN^{\frac{1}{2}}$$

where i_1 = limiting current (μA)
v = kinematic viscosity
n = number of Faradays
A = electrode area (cm^2)
C = concentration, mmoles/l
N = No. revs./sec.

The value for the diffusion coefficient was $0.45 \cdot 10^{-5}$ cm^2/sec at pH < 2.7, and $0.48 \cdot 10^{-5}$ cm^2/sec at pH > 2.7. It was expected that the diffusion coefficient for these pH-ranges would be approximately the same since the limiting current is the same.

Calibration curve

A calibration curve for neptunium was prepared by pipetting the proper aliquot of the standard neptunium stock solution into a 25-ml volumetric flask. To the volumetric flask were added 5 ml of 2.5 *N* sodium perchlorate, 10 ml of 2.50 *M* sodium glycinate, and sufficient perchloric acid to adjust the pH of the final solution to pH 2.7–3.8. The solution was then diluted to volume with water. A portion was transferred to the electrolysis cell, and the solution was purged of oxygen by bubbling purified nitrogen through the solution for 5 min. Neptunium solutions of eight different concentrations were prepared, and three voltammograms were recorded for each concentration.

The results given in Table 3 show that the limiting current is proportional to the concentration of neptunium in the pH range 2.7–3.8 under the conditions noted. The relative standard deviation of the limiting current quotient, i_1/C, is 4.83%.

TABLE 3

VARIATION OF LIMITING CURRENT WITH NEPTUNIUM(VI) CONCENTRATION IN THE pH RANGE 2.7–3.8
1.00 *M* $NaC_2H_4O_2N$, 0.5 *M* $NaClO_4$

$[NpO_2^{2+}]/M \cdot 10^4$	$i_1/\mu A$	$i_1/C/\mu A\ mm^{-1}$	$[NpO_2^{2+}]/M \cdot 10^4$	$i_1/\mu A$	$i_1/C/\mu A\ mm^{-1}$
0.75	3.43	45.7	7.5	31.2	41.6
1.88	7.67	40.8	11.2	46.3	41.3
3.75	15.6	41.6	15.0	62.1	41.4
5.62	22.6	40.2	18.8	77.5	41.2

ACKNOWLEDGEMENT

This work was carried out under U.S. Atomic Energy Commission contract AT(29-1)-1106.

SUMMARY

The voltammetric behavior of neptunium(VI)–glycinate complex has been investigated over widely varying conditions of ligand concentration and pH. Under

all the conditions investigated, a reversible, one-electron wave corresponding to the reduction of neptunium(VI) to neptunium(V) was obtained. The half-wave potential was found to be independent of the pH in the pH-ranges, 0.1–1.0 and 2.7–3.8. In the pH-ranges 1.0–2.7 and 3.8–5.0, the half-wave potential is a function of pH. In each of these pH-ranges except 0.1–1.0, neptunium(VI) has one more glycinate ligand bound to it than neptunium(V). The metal : ligand ratio was found to be 1 : 3 and 1 : 4 by conductometric and amperometric titrations. The limiting current is proportional to the concentration of neptunium(VI) from $7.50 \cdot 10^{-5}$–$1.88 \cdot 10^{-3}$ M. The diffusion coefficient is $0.48 \cdot 10^{-5}$ cm^2 sec^{-1}.

REFERENCES

1 L. G. Sillén and A. E. Martell, *Stability Constants of Metal-Ion Complexes, Chem. Soc., London, Spec. Publ.*, 17 (1964) 377.
2 O. E. Zvyagintsev and E. V. Goncharov, *Zh. Neorgan. Khim.*, 7 (1962) 1880.
3 O. E. Zvyagintsev and E. V. Goncharov, *Zh. Neorgan. Khim.*, 8 (1963) 349.
4 I. M. Batyaev and S. V. Larionov, *Izv. Sibirsk. Otd. Akad. Nauk SSSR*, 12 (1962) 69; *Nucl. Sci. Abstr.*, 17 (1963) 23326.
5 E. E. Kriss, *Ukr. Fiz. Zh.*, 31 (1965) 153; *Nucl. Sci. Abstr.*, 19 (1965) 22227.
6 L. N. Pankratova, L. G. Vlasov and A. V. Lapitskii, *Zh. Neorgan. Khim.*, 9 (1964) 1763.
7 T.-T. Lai, H.-T. Lin and C.-C. Hsieh, *J. Chinese Chem. Soc. (Taiwan)*, 10 (1963) 33.
8 M. P. Mefod'eva, P. I. Artyukhin and A. D. Gel'man, *Radiokhimiya*, 1 (1959) 309.
9 C. E. Plock, *J. Inorg. Nucl. Chem.*, 30 (1968) 3023.
10 C. E. Plock, *Anal. Chim. Acta*, 43 (1968) 281.
11 V. C. Keller and S. H. Eberle, *Radiochim. Acta*, 8 (1967) 65.
12 Yu. A. Zolotov and Yu. P. Novikov, *Zh. Neorgan. Khim.*, 4 (1959) 1693.
13 G. Gibson, D. M. Gruen and J. J. Katz, *J. Am. Chem. Soc.*, 74 (1952) 2103.
14 D. M. Gruen and J. J. Katz, *J. Am. Chem. Soc.*, 75 (1953) 3772.
15 Yu. A. Zolotov, I. N. Marov and A. I. Moskvin, *Zh. Neorgan. Khim.*, 6 (1961) 1055.
16 A. I. Moskvin, I. N. Marov and Yu. A. Zolotov, *Zh. Neorgan. Khim.*, 6 (1961) 1813.
17 Yu. A. Zolotov and I. P. Alimarin, *J. Inorg. Nucl. Chem.*, 25 (1963) 691.
18 A. I. Moskvin and M. P. Medof'eva, *Radiokhimiya*, 7 (1965) 410.
19 C. E. Plock, *J. Electroanal. Chem.*, 18 (1968) 289.
20 R. W. Stromann, R. M. Peekema and F. A. Scott, *U.S. At. Energy Comm. Rept.* HW-58212 (1958)
21 L. Meites, *Handbook of Analytical Chemistry*, edited by L. Meites, McGraw-Hill, New York, 1963, p. 5–10.
22 R. M. Keefer, *J. Am. Chem. Soc.*, 68 (1946) 2329.
23 J. L. Ryan and W. E. Keder, *Lanthanide Actinide Chemistry*, edited by R. F. Gould, American Chemical Society, Washington, D.C., 1967, p. 335.
24 R. D. Goldberg, *Instrument News*, (Perkin-Elmer Corp.) 18, No. 3 (1968) 8.
25 L. Meites, *Polarographic Techniques*, Interscience, New York, 2nd ed., 1965, p. 424.

ELECTROANALYTICAL CHEMISTRY AND INTERFACIAL ELECTROCHEMISTRY
Elsevier Sequoia S.A., Lausanne – Printed in The Netherlands

CATHODIC STRIPPING VOLTAMMETRY OF MANGANESE

E. HRABÁNKOVÁ, J. DOLEŽAL AND V. MAŠIN
Department of Analytical Chemistry, Charles University, Prague 2 (Czechoslovakia)
(Received February 25th, 1969)

INTRODUCTION

A systematic study of the determination of trace elements by the stripping voltammetry technique[1] carried out in our Institute included the determination of trace impurities in pure acids[2-5]. To determine impurities in alkali hydroxides, which can be used similarly to decompose materials, a procedure had to be evolved for determining small concentrations of manganese[6]. Manganese forms only a very dilute amalgam, and therefore the determination by means of amalgam polarography is not sufficiently sensitive[7]. Brainina[8] suggested the determination of small amounts of manganese after preliminary oxidation to MnO_2. This method was later studied in detail with regard to practical applications, as well as from the point of view of the electrode process involved[9-11]. The authors used an indicator electrode of graphite or graphite paste, the minimum concentration determined being about 10^{-8} *M*. The reaction was studied in ammonia, borate and acetate buffer solutions[9,11], and in solutions of different concentrations of ammonium chloride and ammonium sulphate[10].

In the present work, the possibility of using stationary and rotating platinum electrodes for the preliminary accumulation of manganese in the form of MnO_2 was studied, and the effect of some factors on the sensitivity of the determination was investigated in detail.

THEORETICAL

It is known that manganese can be determined electrogravimetrically from acid medium on a platinum anode, Mn^{2+} being oxidized anodically to Mn^{4+} which immediately hydrolyses to form manganese dioxide (or the hydrate). When small concentrations of manganese are to be determined, the electrolytic oxidation process can be used for preliminary accumulation on the indicator electrode, the current–potential relationship being studied on repeated reduction (*i.e.*, dissolution) of the oxide layer. The height of the characteristic peak on the cathodic polarisation curve is proportional to the manganese concentration. The reaction taking place is:

$$Mn^{2+}(H_2O)_x \rightleftarrows MnO_2(H_2O)_{x-y}(s) + 4\,H^+ + (y-2)H_2O + 2\,e^- \qquad (1)$$

The reverse process takes place on dissolution and recording. This overall process consists of several steps[10]:

$$2\,Mn(H_2O)_x^{2+} \rightarrow 2\,Mn(H_2O)_x^{3+} + 2\,e^- \qquad (2)$$

$$2\,Mn(H_2O)_x^{3+} \rightarrow Mn(H_2O)_x^{2+} + Mn(H_2O)_x^{4+} \quad (3)$$

$$Mn(H_2O)_x^{4+} \rightarrow MnO_2(H_2O)_{x-y} + 4\,H^+ + (y-2)H_2O \quad (4)$$

The rate-determining step is reaction (3), the rate of which is proportional to the pH of the solution (the reaction product, Mn^{4+}, undergoes hydrolysis accompanied by simultaneous liberation of protons). For this reason the process does not have a purely diffusion character, as confirmed by a study of the relationship between the peak height or peak potential, and the pH of the solution, and temperature[10].

EXPERIMENTAL

Apparatus and reagents

Platinum indicator electrode. Two types of electrodes, stationary and rotating, were used. The stationary electrode consisted of a platinum wire, 0.3 mm in diameter and 1.5–2 mm long, sealed into a glass tube; the rotating electrode was a product of the Radiometer Co. (surface roughly 6 mm^2). The method of cleaning the platinum electrode surface is very important. During the reduction cycle, the MnO_2 layer is not entirely dissolved, and peaks will decrease in height and the reproducibility of the results will be worsened unless the electrode is properly regenerated. The possibility of using concentrated HCl, HNO_3, H_2SO_4, $H_2SO_4+H_2O_2$ was tested. Of this series, the effect of concentrated nitric acid during 1–3 min was found to be optimum. The efficiency of the cleaning procedure is improved when a "blank" curve is recorded before the analysis (scanning in the potential range to be employed, *i.e.*, +0.8–0 V) without preceding electrolysis.

The electrode was also cleaned by applying a constant potential, more negative than the peak potential (*i.e.*, +0.1 to −0.1 V). This procedure was not suitable for the stationary electrode, the original peak height not being achieved even after a prolonged period of time (up to 2 h). With the rotating electrode, however, this method is sufficiently efficient after 2 min, and in this case is more advantageous than cleaning with nitric acid.

Reference electrode. Saturated calomel electrode, connected to the solution by means of a bridge containing saturated KCl solution. All potential values are given *versus* SCE. The polarograph was Type PO4 (Radiometer Co.). The solution was stirred by means of a glass stirrer with an electromotor, or with the rotating electrode.

Reagent-grade materials and bi-distilled water were used throughout for all measurements. Oxygen was removed from the solutions with nitrogen freed from oxygen traces in a reductor containing an alkaline solution of anthraquinone sulphonate. The volumetric $MnSO_4$ solution was prepared as a 10^{-2} *M* stock solution, which was diluted before use. A set of borate buffers, 0.1 *N* (pH 7–12) or ammonia buffers was used as supporting electrolyte.

RESULTS

In a medium of borate or ammonia buffers, Mn^{2+} can be oxidized on the platinum electrode; the solid oxidation product adheres to the electrode and forms an inverse peak (Fig. 1) in the reduction half-cycle. With higher manganese concen-

trations, a second, less developed peak (curve b) appears. The position and height of the two peaks depend on the pH of the solution, while the shape of the curve (see Fig. 1) is independent of the nature of the supporting electrolyte. Similar curves may also be obtained in 0.1 N HNO_3, but the determination is not sufficiently sensitive for trace analysis in this case[6].

The peak height depends on many factors. The following relationships were investigated:

The dependence of the peak height on the manganese concentration and duration of preliminary electrolysis is linear in the manganese concentration range, 10^{-6}–10^{-5} M, with a limit at concentrations above $2 \cdot 10^{-5}$ M (the exact value of this concentration depends, among other factors, on the electrode surface and the procedure employed for its regeneration).

The dependence of the peak height on the potential of preliminary electrolysis, E_{el}, has a maximum at E_{el}-values between +0.6 and +0.8 V (see Fig. 2); a further slight

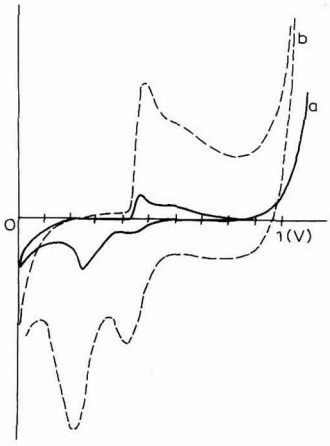

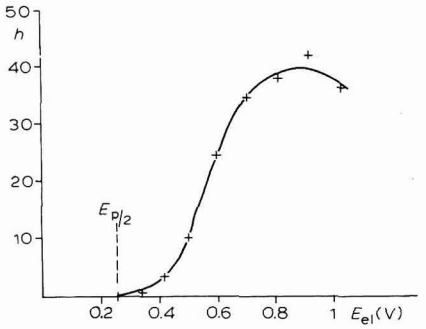

Fig. 1. Polarisation curves of manganese in borate buffer, pH 7; $v = 400$ mV/sec; sensitivity 3 μA. Manganese concn.: (a), $2 \cdot 10^{-5}$; (b), 10^{-4} M.

Fig. 2. Dependence of peak height on electrolysis potential. $3 \cdot 10^{-6}$ M Mn^{2+} + buffer soln., pH 8.4; time of pre-electrolysis, 30 sec.

decrease is caused by a decrease of the current efficiency with respect to oxygen evolution which takes place at the same time. The difference, $E_{el} - E_{p/2}$, needed to attain the maximum peak is about 0.6 V.

The peak is intensified on more vigorous stirring of the solution during electrolysis, and stirring of the solution during the recording of the curve also causes the peak to deepen. This is probably due to the fact that stirring facilitates the transport of the reaction product from the electrode, thus increasing the rate of dissolution. The peak is higher when the rate of potential change on recording is increased. In Fig. 3 this relationship is illustrated for different rates of stirring during the recording of the curve. The curves show clearly that the peak height increases when the rotating electrode is used. Increase in the electrode surface also causes a rise in peak height, only, however, up to a certain value, as the capacitance current increases with increasing surface.

Oxygen dissolved in the solution does not affect the peak height, but the shape of the curves is improved when oxygen is removed, as the residual current value is decreased: this is especially important with low manganese concentrations.

The pH of the solution is significant. The pH-dependence of the peak height is presented in Fig. 4. The decrease of the peak height in acid solutions is due to incomplete precipitation of MnO_2, while aerial oxidation of Mn^{2+} and precipitation of $Mn(OH)_2$ take place in alkaline solutions. (It follows from the solubility product

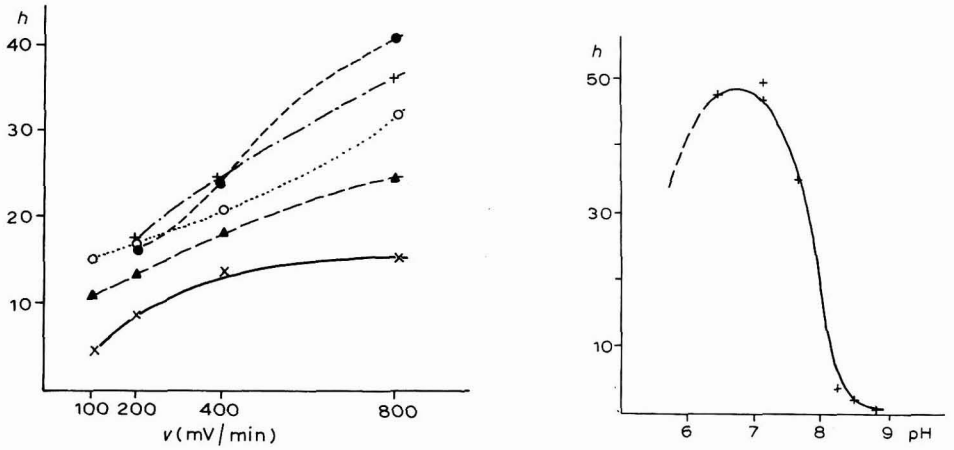

Fig. 3. Dependence of peak height on rate of polarization, v. $6 \cdot 10^{-6}$ M Mn^{2+} + borate buffer, pH 7.8; pre-electrolysis 1 min at potential +0.8 V; soln. stirred during electrolysis at 600 rev./min; surface of electrode, 6 mm^2.

(————), Soln. not stirred;
(—▲—▲—), soln. stirred, 600 rev./min;
(○...○...○), rotating electrode, 600 rev./min;
(–·–·–·–·–), rotating electrode, 1200 rev./min;
(----------), rotating electrode, 1800 rev./min.
} during the recording

Fig. 4. Dependence of peak height on pH of soln. $3 \cdot 10^{-6}$ M Mn^{2+} + 0.1 N borate buffer, pH 6.8–9.

of $Mn(OH)_2$ that the manganese concentration in solutions of pH 9 must be lower than 10^{-5} M, and lower than 10^{-7} M in solutions of pH 10 in order that precipitation should not take place.) The relationships established agree with the results reported[10].

The peak potential shifts linearly towards more negative values with increase of pH of the solution (see Fig. 5), indicating that H^+ ions are liberated in the reaction (see eqn. (1)[10]).

The general equation may be written as:

$$Me^{(p-n)} + p\,H_2O \rightarrow Me(OH)_p + pH^+ + ne^-$$

The relationship between the redox potential and pH may be stated as:

$$E = A + p(RT/nF) \ln a_{H^+} \quad (5)$$

$$A = E^\circ + (RT/nF) \ln (S/K_v) - (RT/nF) \ln a_{Me} \quad (6)$$

p = number of H^+ ions
n = number of electrons
} exchanged in the reaction
S = solubility product of the compound formed
K_v = ionic product of water
Similarly, for the half-peak potential, $E_{p/2}$[10],

$$E_{p/2} = A' + p(RT/nF) \ln a_{H^+} \quad (7)$$

The number of H^+ ions liberated may, therefore, be determined from the shift, $\Delta E_{p/2}/\Delta pH$. The value determined experimentally is 110 mV, which agrees well with the theoretical value of 118 mV obtained from eqn. (1). It may be concluded, therefore, that the overall process is described by eqn. (1).

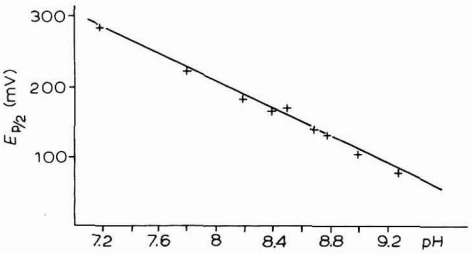

Fig. 5. Dependence of half-peak potential, $E_{p/2}$, on pH of soln. $3 \cdot 10^{-6}$ M Mn^{2+} + buffer soln.; pre-electrolysis 1 min at potential, +0.8 V.

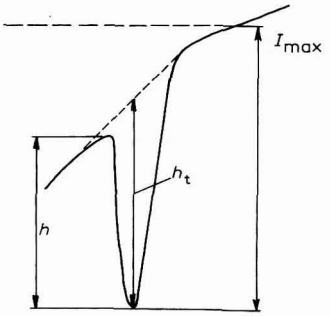

Fig. 6. Different methods of evaluating peak height.

TABLE 1

REPRODUCIBILITY OF THE MANGANESE PEAK

Relative deviation in 10 repeated measurements.

	Stationary electrode (%)	*Rotating electrode* (%)
I_{max}	3	3
h	6.2	4.9
h_t	7.5	3.1
Deriv.	8.8	6.5

The most suitable conditions for the determination of manganese can be determined on the basis of the above relationships. The sensitivity of the analysis may be further improved by using an electronic derivative unit built into the instrument because the derivative of the charging and residual current is very small as the potential is changed linearly while the sensitivity to a rapidly changing signal (i.e., of the peak) is increased[10].

The reproducibility of the method was tested with the stationary and the rotating electrodes, in the normal and in the derivative circuit (see Table 1). For illustration, the Table includes three ways of evaluating the peak height: for the significance of the individual symbols, see Fig. 6. It should be stressed that inaccurate

results will be obtained if the value, I_{max}, is considered in the study of some of the relationships and the values, h or h_t, should therefore be used instead (all the relationships discussed were evaluated with the use of the value, h). It can be seen from the Table, that the rotating platinum electrode, in general, enables more reproducible results to be achieved. On the other hand, although the sensitivity is considerably improved with the derivative wiring, the reproducibility is inferior, because the curves are obtained in a stirred solution which lowers the quality of the derivative curves (sudden oscillations etc. are observed).

Manganese determinations may be carried out on the basis of the above results down to concentrations of about 10^{-9} M. A rotating platinum electrode is used with an electrolysis for 3 min at a potential of +0.8 V: in a solution of pH 7 with a manganese concentration of 2.10^{-9} M, the peak height, h, is 0.06 μA.

Alkali and alkali-earth metals, and Zn, Cd, Co, Cu do not interfere in the determination even when present in a 10000-fold excess. Iron and aluminium interfere if present at concentrations of more than 10^{-5} M as they are precipitated in solution and Mn^{2+} is adsorbed on the fresh precipitate. Lead interferes markedly: at ratios as low as Mn : Pb = 1 : 0.5–1 : 1 (the value depends on the pH of the solution) the manganese peak is lowered by some 50%. No improvement was obtained by using NH_4Cl solution (pH 5), in which manganese can be determined in the presence of a 500-fold excess of lead with the use of a graphite electrode, as described in a previous study[11]. The material used for the electrode is probably the dominating influence here. The effect of lead could not be eliminated even by binding it in a complex. This problem continues to be a subject of study. Among conventional anions, tartrate and EDTA interfere if present in concentrations above 0.01 M.

Procedure for the determination of manganese in alkali hydroxides

Weigh 4 g of the hydroxide to be analysed, dissolve in 100 ml of 1.5 M NH_4Cl. Place a platinum electrode (with a freshly cleaned surface) in the solution and electrolyse in the stirred solution at a potential of +0.6 V. At the end of the electrolysis, record a polarisation curve from +0.6 to 0 V without interrupting the stirring. Measure the peak height by means of one of the techniques described and evaluate either with the use of a calibration curve or by means of the standard addition method. In this modification, manganese may be determined in concentrations down to 10^{-7}%. The relative deviation of individual determinations is not greater than 20%.

SUMMARY

A procedure is described for determining manganese in concentrations down to 10^{-9} M using a cathodic stripping voltammetry technique. The conditions for the determination and the effect of the composition of the solution and of variations of the technique employed were studied. The use of a rotating platinum electrode was found to be especially advantageous as this increased the sensitivity and the reproducibility of the method.

The method was applied to the determination of small quantities of manganese in alkali hydroxides.

REFERENCES

1 E. HRABÁNKOVÁ AND J. DOLEŽAL, *Chem. Listy*, 62 (1968) 1164.
2 P. BERAN, J. DOLEŽAL AND E. HRABÁNKOVÁ, *Collection Czech. Chem. Commun.*, 33 (1968) 308.
3 P. BERAN, J. DOLEŽAL AND D. MRÁZEK, *J. Electroanal. Chem.*, 6 (1964) 381.
4 P. BERAN, J. DOLEŽAL AND P. PACÁK, *Chem. Zvesti*, 18 (1964) 333.
5 P. BERAN, J. DOLEŽAL AND E. TVRZICKÁ, *Collection Czech. Chem. Commun.*, 32 (1967) 4139.
6 V. MAŠÍN, Thesis, Charles University, 1967.
7 W. KEMULA AND Z. GALUS, *Roczniki Chem.*, 36 (1962) 1223.
8 CH. BRAININA, *Zh. Analit. Khim.*, 19 (1964) 810.
9 C. O. HUBER AND L. LEMMERT, *Anal. Chem.*, 38 (1966) 128.
10 G. FARSANG AND L. TOMCSANYI, *Acta Chim. Acad. Sci. Hung.*, 52 (1967) 123.
11 H. MONIER AND K. ZINKE, *Z. Anal. Chem.*, 240 (1968) 32.
12 C. V. ELVINS AND S. P. PERONE, *Anal. Chem.*, 39 (1967) 309.

ELECTROANALYTICAL CHEMISTRY AND INTERFACIAL ELECTROCHEMISTRY
Elsevier Sequoia S.A., Lausanne – Printed in The Netherlands

CATHODIC STRIPPING VOLTAMMETRY OF LEAD

E. HRABÁNKOVÁ, J. DOLEŽAL AND P. BERAN
Department of Analytical Chemistry, Charles University, Prague 2 (Czechoslovakia)
(Received February 25th, 1969)

INTRODUCTION

In our previous paper[1] we studied the application of the cathodic stripping technique to the determination of manganese, utilising the oxidation to MnO_2 on the platinum electrode. Since it is known from electrogravimetry that the determination of lead on the platinum electrode by anodic oxidation to PbO_2 is similar to the determination of manganese, we investigated the possibility of determining lead by the stripping technique.

The method has already been described[2] but in the case cited the determination is carried out on a graphite electrode in ammonium chloride solution and the minimum concentration is 10^{-7} M.

The use of stationary and rotating platinum electrodes and the mechanism of the reaction are discussed in the present work.

THEORETICAL

Bivalent lead is oxidized on a platinum electrode in solutions of acetate or borate buffers to Pb^{4+}, which hydrolyses immediately to form PbO_2:

$$Pb(H_2O)_y^{2+} \rightleftharpoons PbO_2(H_2O)_{y-x} + 4\,H^+ + (x-2)H_2O + 2\,e^- \qquad (1)$$

The equilibrium potential value reported for this reaction is $E_0 = 1.4$ V, $pK = 49.1$[3].

The solubility product of $Pb(OH)_4$ or of the hydrated oxide ($pK_s = -65.9$) is considerably less than that of $Pb(OH)_2$ ($pK_s = -14$) and this can be used for preliminary electrolytic accumulation of lead on the surface of the indicator electrode, the reduction of the oxide layer being studied after a certain period of time.

EXPERIMENTAL

Apparatus and reagents

The apparatus employed has already been described[1]. In this case also, the surface of the platinum electrode must be purified and regenerated in order to achieve reproducible results, although the process of decrease of peak height of lead is slower compared to that of manganese under the same conditions. Purification by means of concentrated nitric acid for 1–2 min is again recommended. For the rotating electrode, regeneration is best achieved by applying a constant potential of +0.42 to +0.48 V to the electrode for 1–2 min.

A volumetric 10^{-2} *M* stock solution was prepared from $Pb(NO_3)_2$; this was diluted appropriately before use. A set of 0.2 *N* acetate buffers was used as supporting electrolytes.

RESULTS

Figure 1 shows the anodic and cathodic polarisation curve of lead in acetate buffer solution. The anodic peak is hardly visible, as its potential is nearly identical with that of oxygen evolution. A well-developed peak ($E_{p/2} = +0.65$ V), the exact value depends on pH and the lead concentration) is seen on the cathodic curve. At lead concentrations above 10^{-4} *M*, a second, more positive but substantially smaller and less well-developed, peak is obtained, probably because there are two crystal modifications of PbO_2, the orthorhombic, α, and the tetragonal, β, modifications[4].

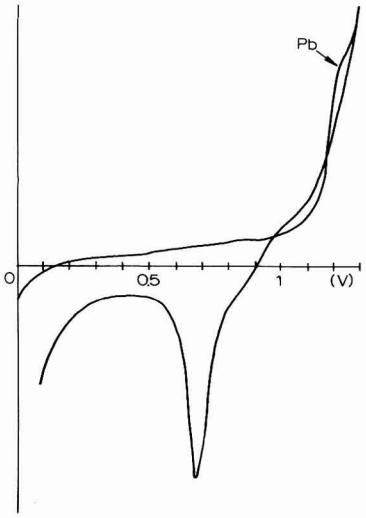

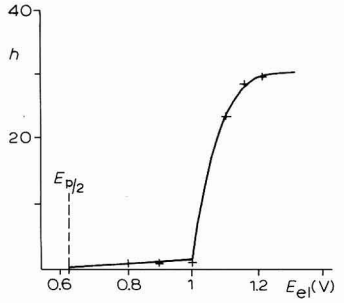

Fig. 1. Polarisation curves of lead (10^{-4} *M*) in acetate buffer soln., pH 4.9; sensitivity 3 μA; $v = 800$ mV/sec.

Fig. 2. Dependence of peak height on electrolysis potential. $5 \cdot 10^{-6}$ *M* Pb^{2+} + buffer soln. pH 4.9; pre-electrolysis, 1 min.

The dependence of the peak height on lead concentration and the duration of electrolysis is linear: under the conditions specified (*i.e.*, electrode surface and procedure used for its regeneration, etc.) the limiting character of this dependence is apparent for lead concentrations above 10^{-5} *M* and electrolysis times longer than 2 min.

The dependence of the peak height on the electrolysis potential, E_{el}, rises sharply with E_{el}-values of +0.9 to +1.2 V (see Fig. 2). At higher potential values, the electrode becomes excessively passivated. The difference $(E_{el} - E_{p/2})$ needed to achieve a maximum peak is about 0.55 V.

The peak is increased in height with more rapid transport of Pb^{2+} ions to the electrode surface during the preliminary electrolysis process, *i.e.*, with more vigorous stirring of the solution or use of the rotating electrode. Stirring of the solution during the recording of the curve, or increasing the rate of stirring in this period, will not

influence the peak height to any great extent, thus differing from the analysis of manganese. The dependence of the peak height on the rate of polarisation, v, is presented in Fig. 3.

It follows from eqn. (1), that the height as well as potential of the peak depend on the pH of the solution. The dependence of the peak height, h, on pH is shown in Fig. 4, from which it can be seen that the highest and best developed peaks are ob-

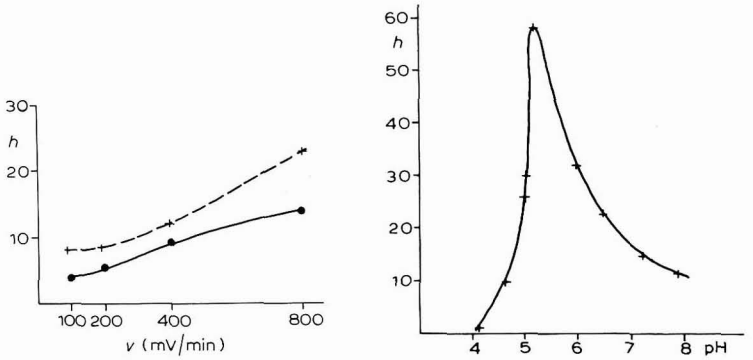

Fig. 3. Dependence of peak height on rate of polarization. $6 \cdot 10^{-6}$ M Pb^{2+} + buffer soln. pH 5.2; pre-electrolysis, 1 min at +1.2 V.
(——), Unstirred soln.
(– – –), stirred soln. (600 rev./min) } during the recording.

Fig. 4. Dependence of peak height on pH of soln. $5 \cdot 10^{-6}$ M Pb^{2+} + buffer soln. pH 5.2; pre-electrolysis, 1 min at +1.2 V.

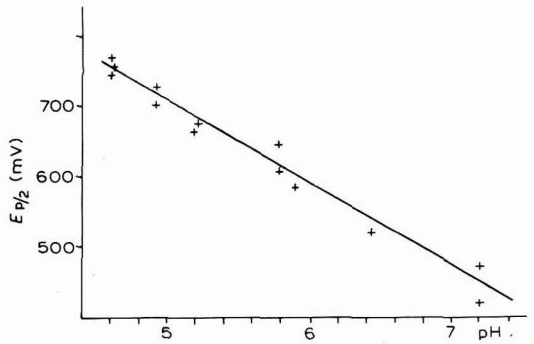

Fig. 5. Dependence of half-peak potential on pH of soln. $5 \cdot 10^{-6}$ M Pb^{2+} + buffer pH 5.2; pre-electrolysis, 1 min at +1.2 V.

tained in a pH 5 buffer (acetate). In NH_4Cl of pH 5 the peak height is roughly the same. The precipitation of PbO_2 is incomplete, and peaks are lower and wider in strong acid and alkaline solutions.

The peak half-potential, $E_{p/2}$, shifts towards negative values with increase of pH (see Fig. 5); the $\Delta E_{p/2}/\Delta$ pH value is 120 mV, agreeing well with the theoretical value of 118 mV derived from the equations[5]:

$$E_{p/2} = A' + p(RT/nF) \ln a_{H^+} = A' + 4(RT/2F) \ln a_{H^+} = A' + 0.118 \text{ pH}$$

The most advantageous conditions for maximum sensitivity are obtained on the basis of the above relationships and the sensitivity may be further increased with the use of a derivative unit built into the instrument. The reproducibility of the method is illustrated in Table 1 for the case of the stationary and rotating electrodes. The technique of evaluating the peak height is similar to that reported in the previous study[1]. It will be seen from the Table that reproducibility is improved to some extent by using the derivative unit.

TABLE 1

REPRODUCIBILITY OF THE LEAD PEAK
Relative deviations of 10 repeated determinations

	Stationary electrode (%)	*Rotating electrode* (%)
I_{max}	5	3.2
h	12.5	5.2
Deriv.	6.9	4.6

Under the above conditions, lead may be determined at concentrations of at least $5 \cdot 10^{-9}$ M with an error not greater than 10%. Oxygen dissolved in the solution does not directly influence the peak height, but the residual current value may be diminished somewhat by removing oxygen from the solution.

Manganese interferes in the analysis of lead to the same extent as does lead in the determination of manganese.

SUMMARY

A method of lead analysis by the cathodic stripping voltammetry technique is suggested in the present study. The experimental conditions and the influence of these factors on the behaviour of lead and sensitivity of the analysis are discussed. The use of the rotating platinum electrode and of a derivative circuit is found to be useful.

Compared with amalgam polarography, the cathodic stripping technique has the advantage of easy separation from copper, cadmium, zinc, etc., although the amalgam polarography procedure is more sensitive. The errors of the two methods are approximately the same.

REFERENCES

1 E. HRABÁNKOVÁ, V. MAŠÍN AND J. DOLEŽAL, *J. Electroanal. Chem.*, 22 (1969).
2 H. MONIER AND K. ZINKE, *Z. Anal. Chem.*, 240 (1968) 32.
3 L. G. SILLÉN, *Stability Constants of Metal-Ion Complexes*, The Chemical Society, London, 1964.
4 N. A. HAMPSON, P. C. JONES AND R. F. PHILIPS, *Can. J. Chem.*, 45 (1967) 2041.
5 G. FARSANG AND L. TOMSCANYI, *Acta Chim. Acad. Sci. Hung.*, 52 (1967) 123.

ELECTROANALYTICAL CHEMISTRY AND INTERFACIAL ELECTROCHEMISTRY
Elsevier Sequoia S.A., Lausanne – Printed in The Netherlands

THE ANODIC BEHAVIOUR OF MERCURY IN SOLUTIONS OF OXYACIDS

R. D. ARMSTRONG, W. P. RACE AND H. R. THIRSK

Electrochemistry Research Laboratory, Department of Physical Chemistry, University of Newcastle upon Tyne, Newcastle upon Tyne, NE1 7RU (England)

(Received February 3rd, 1969; in revised form, February 27th, 1969)

INTRODUCTION

The anodic dissolution of mercury in perchloric acid has been studied extensively[1-7]. It has been found that the magnitude of the double-layer capacity at anodic potentials is unusually high, and this has been attributed to the specific adsorption of Hg(I). The purpose of the present investigation was to determine the behaviour of the reaction

$$2\,Hg \rightleftharpoons Hg_2^{2+} + 2\,e$$

in solutions of perchloric, sulphuric and nitric acids, using interfacial impedance measurements, and to evaluate this behaviour relative to that of Hg in solutions of other anions (OH^-, $H_2PO_4^-$, S^{2-}) studied in these laboratories[8-10]

EXPERIMENTAL

Solutions of $HClO_4$ (9.4 *M* and 1 *M*), HNO_3 (1 *M* and 0.5 *M*), and H_2SO_4 (1 *M* and 0.1 *M*) were prepared in triply-distilled water, from BDH AristaR grade reagents. Mercury was purified under nitric acid, then distilled twice *in vacuo*. Measurements were made at $25.0 \pm 0.1°C$.

Electrode impedance measurements were made using a cell containing a hanging mercury drop electrode (of areas down to 0.004 cm^2) and a large platinum cylinder as counter electrode. A conventional Wien bridge was used to measure the cell impedance in the frequency range, 60 Hz–24 kHz. Some measurements (1 *M* $HClO_4$) were also made at 100 kHz using a Wayne–Kerr precision radio frequency bridge (B221) applying the method proposed previously to overcome the difficulties associated with the uncertainty in the areas of very small Hg drops[11].

Potentials were generally measured with respect to SCE. In the case of 1 *M* H_2SO_4, in order to examine the anodic behaviour with respect to the reversible Hg_2SO_4 potential (avoiding any uncertainty arising from liquid junction potentials) measurements were made using a mercurous sulphate electrode in the same solution as reference electrode, and a second Hg_2SO_4 electrode to stabilise the potential of the counter electrode.

In the case of 1 *M* $HClO_4$, measurements were also made using hydrogen electrodes in the same solution as reference electrodes, to avoid the inclusion of errors arising from the irreproducibility of liquid junction potentials when correlating sepa-

rate audio- and radio-frequency investigations. For the latter, no d.c. polarising circuit was employed, but the potential was set by adding small quantities of a solution of $Hg_2(ClO_4)_2$ in $HClO_4$ to the cell solution. This method gives much better control of the d.c. potential than when the large capacitor (1,000 μF in this case) isolating the cell from the bridge is to be charged through the necessarily resistive polarising circuit[11].

RESULTS

For an interfacial impedance corresponding to a Randles' circuit with a negligible charge transfer resistance[8]

$$R_p = 2\sigma/\omega^{\frac{1}{2}} c_0$$
$$C_p = C_{dl} + c_0/2\sigma\omega^{+\frac{1}{2}}$$

For all the solutions studied, the experimental data in the frequency range, 300 Hz–25 kHz, were found to correspond to these equations within the accuracy of the observations.

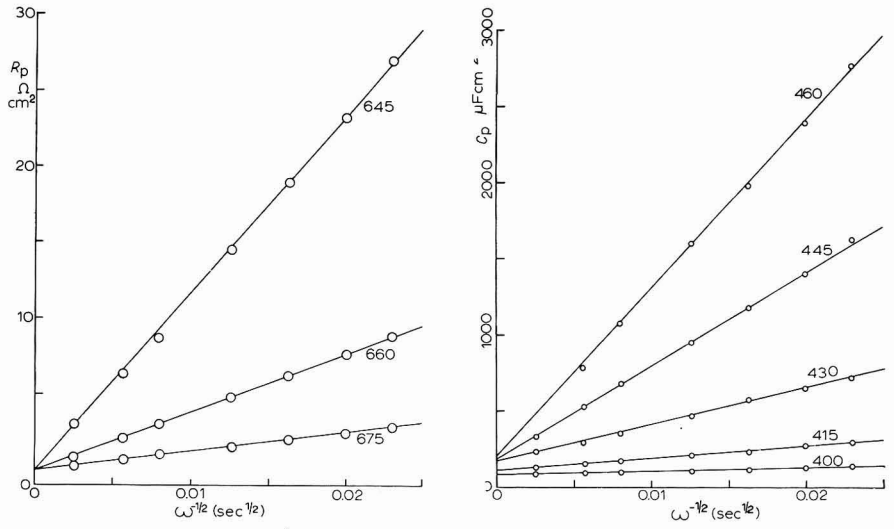

Fig. 1. Dependence of R_p on $\omega^{-\frac{1}{2}}$ in 1 M $HClO_4$; numbers below lines denote potentials relative to hydrogen electrodes.

Fig. 2. 1 M HNO_3, dependence of C_p on $\omega^{-\frac{1}{2}}$; numbers above lines denote potentials with respect to SCE.

Figure 1 shows typical R_p–$\omega^{-\frac{1}{2}}$ dependences, the graphs extrapolating at infinite frequency to the origin as is required for a substantially reversible process. Figure 2 is an example of the C_p–$\omega^{-\frac{1}{2}}$ behaviour, with the infinite frequency extrapolations giving estimates of the double-layer capacity, C_{dl}.

From the slopes of such graphs, values of $c_0 D_0^{\frac{1}{2}}$ were estimated, and their potential-dependence is shown in Fig. 3. The lines drawn through the points have slope, 1 decade/29.5 mV, confirming the occurrence of a two-electron transfer reaction. In the case of the $HClO_4$ solutions, the relative displacement of the $c_0 D_0^{\frac{1}{2}}$ lines is due

primarily to differences in D_0 between 1 M and 9.4 M solutions. On the assumptions that in $HClO_4$ there is negligible complexation of Hg_2^{2+}, and that the D_0-values in the remaining solutions are close to that in 1 M $HClO_4$, Table 1 shows estimates of the ratio of complex to Hg_2^{2+} for the HNO_3 and H_2SO_4 solutions.

Figure 4 shows the potential-dependence of C_{dl} (plotted on logarithmic scale) for the various solutions, estimated from the intercepts of the C_p–$\omega^{-\frac{1}{2}}$ plots. Addi-

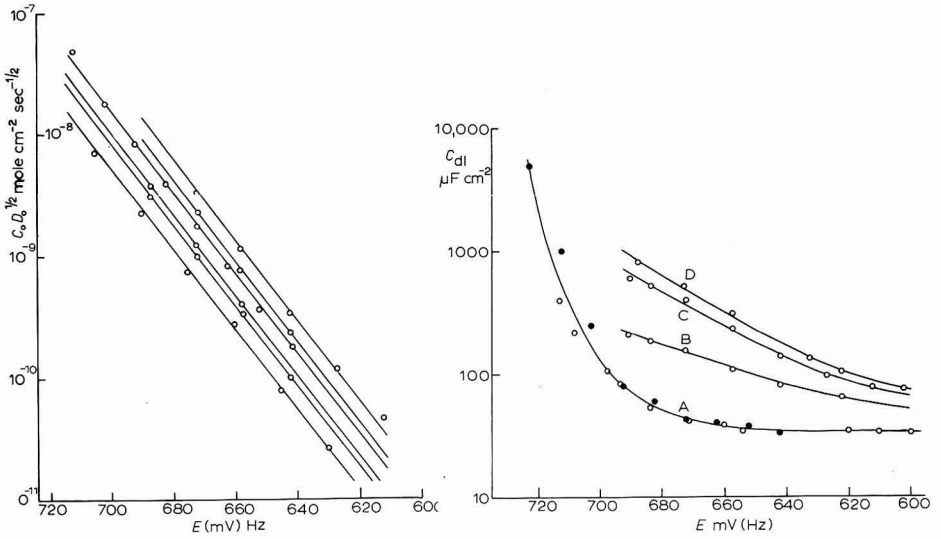

Fig. 3. Dependence of $c_0 D_0^{\frac{1}{2}}$ on potential, for solns, of 1 M $HClO_4$, 0.5 M HNO_3, 0.1 M H_2SO_4, 9.4 M $HClO_4$, 1 M HNO_3, and 1 M H_2SO_4, respectively, moving cathodic.

Fig. 4. Potential-dependence of the double-layer capacity (log scale). (A), (○), 1 M $HClO_4$, (●), 9. 4 M $HClO_4$; (B), 1.0 M HNO_3; (C), 1.0 M H_2SO_4; (D), 0.1 M H_2SO_4.

TABLE 1

RATIO OF COMPLEXED TO UNCOMPLEXED Hg_2^{2+} SPECIES

H_2SO_4		*HNO_3*	
Solution	*Ratio*	*Solution*	*Ratio*
1.0 M	4.5	1.0 M	2.6
0.1 M	0.85	0.5 M	0.55

tional values at more cathodic polarisations were obtained by direct measurement of C_s at high frequencies. In the case of 1 M $HClO_4$, C_{dl} was estimated at anodic potentials by subtracting the calculated faradaic parallel circuit capacitance from the 100-kHz data, treated as outlined in Appendix II.

In 1 M H_2SO_4, the behaviour of the interface at potentials positive to the reversible Hg_2SO_4 potential was examined. At a potential of about +100 mV, a discontinuous change in the electrode impedance showed that an anodic phase was

formed on the mercury surface. Also, the anodic current due to the dissolution reaction decreased greatly at this potential. The anodic phase could be removed at potentials near +10 mV. It is of interest to note that the 100-mV potential difference between the reversible potential for the bulk phase, and the potential at which film formation can be detected, is considerably greater than that found for most other anions[12]. Also, since the film can in fact be reduced anodic to the reversible potential, it is shown that the properties of the anodic surface phase are not identical with those of bulk Hg_2SO_4.

In the presence of the anodic phase, the impedance of the interface was markedly frequency-dependent. The dispersion did not correspond to a faradaic process, but rather to the limiting high frequency behaviour associated with a slow relaxation process. Figure 5 shows an analysis of the parallel circuit interfacial impedance at potentials of +100 and +150 mV. Although the relaxation time cannot be spanned by the data, it is evident that the order of the times is about 1 sec, and that the time is substantially increased on moving anodic by 50 mV. In both cases, the capacity at

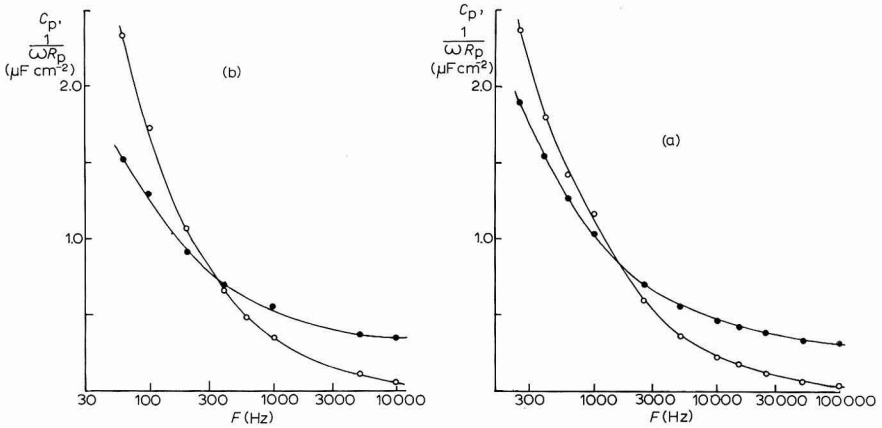

Fig. 5. Analysis of sulphate film relaxation process: (○), $1/\omega R_p$; (●), C_p. (a), +100; (b), +150 mV.

high frequencies tends to a limiting value of about 0.3 μF cm^{-2}, which is consistent with other examples of thick anodic films, and would in this case indicate a film thickness of about 10 nm.

Similar limiting anodic behaviour in HNO_3 and $HClO_4$ was not observable, mainly owing to the much higher solubilities of the respective mercurous salts prohibiting the separation of the double-layer capacitance from the (dominant) faradaic terms, although a visible thick film could be formed in 9.4 *M* $HClO_4$ at about 742 mV (H_2) under potentiostatic conditions.

DISCUSSION

(i) *The interpretation of* C_{dl}

For the present impedance measurements, C_{dl} has the significance

$$C_{dl\ \omega \to 0} = -\left(\frac{\partial^2 \gamma}{\partial E^2}\right) = \frac{\partial}{\partial E}(q_M + 2F\Gamma_{Hg_2^{2+}})$$

Figure 4 shows that C_{dl} is a function of the nature of the anion of the supporting electrolyte, but not markedly dependent on its concentration. Thus a ten-fold change in the anion concentration would be expected to produce a shift of the steeply rising part of the *C–E* curve by $\geqslant 60/n$ mV, were anion adsorption responsible for the rise (see Appendix I). In fact, in the case of H_2SO_4 the change is in the opposite sense. This finding is very different from the behaviour of the interphase, $Hg/NaOH_{aq}$, where the shift of the *C–E* curve followed the anion concentration, and the steep rise was attributable to the adsorption of OH^- anions. Therefore, it is considered that the present abnormal behaviour of Hg is due to the presence of mercury species on the electrode surface, in a configuration such that a small change in surface concentration causes a large change in the interfacial potential. The different behaviour in solutions of different oxy-anions is attributed to the (slight) specific adsorption of these anions, which in turn causes a change in the concentration of Hg species.

(ii) Comparison with other investigations

The present results are similar to those obtained by Sluyters[5] in the comparison of 0.1 *M* and 1 *M* $HClO_4$. The degree of irreversibility of the dissolution reaction may be observed from the significance of deviations from the linear dependences of C_p and R_p on $\omega^{-\frac{1}{2}}$. Figure 6 shows the data for 1 *M* $HClO_4$ at 690 mV (H_2), the broken lines

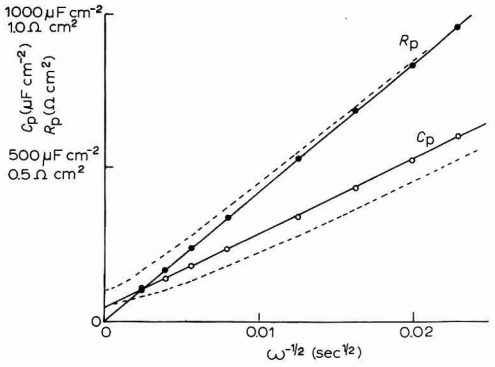

Fig. 6. 1 *M* $HClO_4$, 690 mV (H_2) dependence on $\omega^{-\frac{1}{2}}$ of the parallel circuit impedance components (full lines drawn through experimental points) and comparison with form taken if $i_0 = 130$ mA cm^{-2} (broken curves).

show the form these plots would have taken had the reaction been irreversible to the degree corresponding to $i_0 = 0.13$ A cm^{-2}, assuming a Randles circuit. The deviation of this behaviour from the experimental points at frequencies between 5 kHz and 25 kHz is well outside experimental error. Thus, such an estimate of i_0, which is not far removed from values reported recently by Kooijman*, is considerably lower than the experimental value. At more anodic potentials in 1 *M* $HClO_4$, and also in 9.4 *M* $HClO_4$, such an analysis of the C_p-data is necessarily less successful, due primarily

* Kooijman[7] assumed that the surface Hg species were always in equilibrium with $c_{Hg_2^{2+}}$ $(x=0)$. Another possibility is equilibrium with the metal, although this would not be expected to lead to a frequency-dependent capacity.

to the greater importance of instrumental errors at high frequencies, when measuring capacities of 5,000 μF cm^{-2}. The corresponding resistance data, however, are less affected and give much higher minimum values of i_0, so that in 9.4 M $HClO_4$, at 712 mV, $i_0 > 20$ A cm^{-2}. It seems probable that this minimum i_0-value may well apply to the reaction in all the solutions studied, though it can only be demonstrated in the case of 9.4 M $HClO_4$ where the high Hg_2^{2+} concentration achievable leads to favourable conditions for the study of the reaction kinetics. This is consistent with the observation of no systematic deviation from reversible behaviour in any of the solutions studied. Thus, the irreversibility found by Kooijman is not consistent with the present data. It is unlikely that fortuitous accumulation of errors could lead to similar observations of reversible behaviour in widely differing conditions of conductivity, and C_{dl}.

APPENDIX I

The shift in C–E curves with change in the bulk concentration of specifically adsorbed anions

This shift is expressed by the coefficient $(\partial\varphi_M/\partial \ln a_\pm)_{C_{dl}}$

We can write

$$\left(\frac{\partial\varphi_M}{\partial \ln a_\pm}\right)_{C_{dl}} = -RT\left(\frac{\partial\varphi_M}{\partial C_{dl}}\right)_\mu \left(\frac{\partial C_{dl}}{\partial\mu}\right)_{\varphi_M}$$

For the inner layer capacity, C^i

$$C^i = \left(\frac{\partial q_M}{\partial\varphi_{M-2}}\right)_{q_1,\mu} + \left(\frac{\partial q_M}{\partial q_1}\right)_{\varphi_{M-2},\mu}\left(\frac{\partial q_1}{\partial\varphi_{M-2}}\right)_\mu$$

The general expression for the coefficient is rather complex. If, however, we recognise that $(\partial q_M/\partial\varphi_{M-2})_{q_1,\mu}$ and $(\partial q_M/\partial q_1)_{\varphi_{M-2}}$ are found experimentally to be only weakly dependent on μ, φ_{M-2}, we may write

$$\left(\frac{\partial\varphi_M}{\partial \ln a_\pm}\right)_{C_{dl}} \approx -RT\frac{\partial}{\partial\mu}\left[\left(\frac{\partial q_1}{\partial\varphi_{M-2}}\right)_\mu\right]_{\varphi_{M-2}} \Big/ \frac{\partial}{\partial\varphi_{M-2}}\left[\left(\frac{\partial q_1}{\partial\varphi_{M-2}}\right)_\mu\right]_\mu$$

To proceed further requires the use of an adsorption isotherm. For a situation where Henry's Law is applicable and where the constant field approximation is also valid

$$q_1 = K\exp(\mu/RT)\exp(-\overline{x_2 - x_1}\,nF\varphi_{M-2}/x_2RT)$$

So that in this case

$$\left(\frac{\partial\varphi_M}{\partial \ln a_\pm}\right)_{C_{dl}} \approx \frac{-\overline{x_2 - x_1}\,nF}{x_2RT}$$

i.e., an Esin–Markov effect is predicted and experimentally this is found. Thus for sodium benzene *m*-disulphonate[13] at low coverages

$$\left(\frac{\partial\varphi_M}{\partial \ln a}\right)_{C_{dl}} = -0.130 \text{ V}$$

whilst

$$-\overline{x_2 - x_1}\,nF/x_2RT \approx -0.120 \text{ V}$$

APPENDIX II

Parallel circuit impedance measurements in the presence of an electrode reaction

It was shown previously that the uncertainty in the areas of minute Hg electrodes can be overcome using the "plateau" method, *i.e.*, by determining the value of C_p that is independent of the electrode area. This method may still be applied in the presence of an electrode reaction provided drop areas are used such that the faradaic contribution to the resistive term is insignificant. In such a case, the conversion to the equivalent series circuit capacity yields the sum $(C_{dl}+C_{pf})$ where C_{pf} is the parallel circuit faradaic capacity at the particular frequency of the determination* (the case of no reaction gives simply C_{dl}).

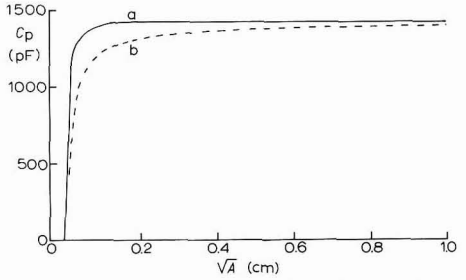

Fig. 7. Dependence of measured parallel capacitance on $A^{\frac{1}{2}}$, for the hypothetical conditions outlined in the text.

Figure 7 shows a simulated comparison of the plateaux which would be found under the following conditions at 100 kHz:

(a) No reaction, $C_{dl}=59.2\ \mu F\ cm^{-2}$.

(b) Process occurring such that $C_{pf}(100\,kHz)=29.2\ \mu F\ cm^{-2}$; $C_{dl}=30\ \mu F\ cm^{-2}$.

Thus, it is seen that the plateau may still be observed in the presence of a reaction, but the small area deviation (deviation I, ref. 11) is more pronounced. In the present work, therefore, values of $(C_{dl}+C_{pf})$ for Hg in 1 M $HClO_4$ at 100 kHz were obtained from the measured plateau values. C_{pf} was calculated from audio-frequency data at less anodic potentials, and extrapolated anodically (assuming reversibility, and continued 1 decade/29.5 mV dependence of $c_0 D_0^{\frac{1}{2}}$ on E). Subtraction of C_{pf} gives C_{dl}.

NOTATION

a Activity
A Electrode area (cm^2)
C_s Series circuit interfacial capacity ($\mu F\ cm^{-2}$)
C_p Parallel circuit interfacial capacity ($\mu F\ cm^{-2}$)
C_{pf} Faradaic component of C_p
C'_p Measured parallel circuit capacitance (pF)

* Similarly, in the case of the relaxation of the adsorption of neutral species, it should be noted that the high frequency capacity values expressed as C_s are in fact the sum of C_∞ with the parallel interfacial capacity arising from the adsorption at each frequency.

C_{dl} Double-layer capacitance (μF cm^{-2})
c_0 Pseudo bulk concentration of dissolving species (M)
D_0 Diffusion coefficient (cm^2 sec^{-1})
E Potential (mV)
i_0 Apparent exchange current (A cm^{-2})
K Henry's law constant (cm)
n Charge
q_M Charge on the metal electrode (C cm^{-2})
q_1 Specifically adsorbed charge
R_p Parallel circuit interfacial resistance (Ω cm^2)
T Temperature (°K)
x_1 Distance to I.H.P.
x_2 Distance to O.H.P.
γ Interfacial tension (dyn cm^{-1})
Γ Surface concentration (mole cm^{-2})
μ Chemical potential
$\bar{\mu}$ Electrochemical potential
φ Potential (V)
ω Angular frequency (sec^{-1})

SUMMARY

The anodic behaviour of mercury in solutions of sulphuric, nitric and perchloric acids has been investigated by a.c. impedance measurements. There is no significant deviation from reversible behaviour at frequencies up to 100 kHz. The values of the double-layer capacity vary markedly with the nature of the anion, but only slightly with anion concentration.

REFERENCES

1 H. GERISCHER AND K. STAUBACH, *Z. Physik. Chem. (Frankfurt)*, 6 (1956) 118; H. GERISCHER AND M. KRAUSE, *Z. Physik. Chem. (Frankfurt)*, 14 (1952) 184.
2 H. MATSUDA, S. OKA AND P. DELAHAY, *J. Am. Chem. Soc.*, 81 (1959) 5077.
3 R. L. BIRKE AND D. K. ROE, *Anal. Chem.*, 37 (1965) 450, 455.
4 W. D. WEIR AND C. G. ENKE, *J. Phys. Chem.*, 71 (1967) 280.
5 M. SLUYTERS-REHBACH AND J. H. SLUYTERS, *Rec. Trav. Chim.*, 83 (1964) 967, 983.
6 D. J. KOOIJMAN AND J. H. SLUYTERS, *J. Electroanal. Chem.*, 13 (1967) 152.
7 D. J. KOOIJMAN, *J. Electroanal. Chem.*, 19 (1968) 365.
8 R. D. ARMSTRONG, W. P. RACE AND H. R. THIRSK, *J. Electroanal. Chem.*, 19 (1968) 233.
9 R. D. ARMSTRONG, M. FLEISCHMANN AND J. W. OLDFIELD, *J. Electroanal. Chem.*, 14 (1967) 235.
10 R. D. ARMSTRONG, D. F. PORTER AND H. R. THIRSK, *J. Electroanal. Chem.*, 16 (1968) 219.
11 R. D. ARMSTRONG, W. P. RACE AND H. R. THIRSK, *Electrochim. Acta*, 13 (1968) 215.
12 R. D. ARMSTRONG AND J. D. MILEWSKI, *J. Electroanal. Chem.*, 21 (1969) 547.
13 R. PARSONS AND J. M. PARRY, *Trans. Faraday Soc.*, 59 (1963) 241.

ELECTROANALYTICAL CHEMISTRY AND INTERFACIAL ELECTROCHEMISTRY
Elsevier Sequoia S.A., Lausanne – Printed in The Netherlands

STANDARD ELECTRODE POTENTIALS OF Cd/Cd(II), In/In(III), Pb/Pb(II), Tl/Tl(I), Zn/Zn(II) IN MOLTEN ALKALI ACETATES

ROBERTO MARASSI, VITO BARTOCCI, PAOLO CESCON AND MARIO FIORANI
Istituto Chimico dell'Università di Camerino, Camerino (Italy)
(Received February 27th, 1969)

INTRODUCTION

In connection with previous work carried out in alkali nitrates [1–4], we have undertaken a study of the potentials of redox couples in molten alkali acetates.

The acetate solvent is interesting especially from the view point of its acid–base properties and its strong complexing power but there is a paucity of data in the literature for this solvent. Diogenov[5] and Pochtakova[6] have determined state diagrams of the ternary system (Li, Na, K) acetates and there has been a preliminary polarographic study of some redox couples in this solvent[7].

This paper deals with the determination of the potentials of the redox couples, Cd/Cd(II), In/In(III), Pb/Pb(II), Tl/Tl(I) and Zn/Zn(II) in a mixture of (Li, Na, K) acetates in the temperature range, 470–520°K.

The data have been obtained from e.m.f. measurements of the cell with an amalgam electrode

$$\mathrm{Pt}\left|\mathrm{M(Hg)}\right|\begin{matrix}\mathrm{M}^{n+}\\ \text{(Li,Na,K)acetates}\end{matrix}\Big|\mathrm{glass}\Big|\begin{matrix}\mathrm{Ag}^{+}\\ \text{(Li,Na,K)nitrates}\end{matrix}\Big|\mathrm{Ag}\left|\mathrm{Pt}\right. \qquad (1)$$

The glass reference electrode[8,9] has been standardized by means of the cell

$$\mathrm{Pt}\left|\mathrm{Zn(Hg)}\right|\begin{matrix}\mathrm{Zn}^{2+}\\ \text{(Li,Na,K)acetates}\end{matrix}\Big|\mathrm{glass}\Big|\begin{matrix}\mathrm{Ag}^{+}\\ \text{(Li,Na,K)nitrates}\end{matrix}\Big|\mathrm{Ag}\left|\mathrm{Pt}\right. \qquad (2)$$

All the potentials measured are referred to the standard Zn/Zn(II) (1 *m*) (mol kg^{-1}) electrode. Amalgam electrodes have been used in order to prevent metal oxidation[1,10].

EXPERIMENTAL

Chemicals

CH_3COONa and CH_3COOK were reagent-grade (C. Erba, Milan); CH_3COOLi was kindly prepared by C. Erba for our work. $Cd(CH_3COO)_2 \cdot 2H_2O$ and $Zn(CH_3COO)_2 \cdot 2H_2O$ (Merck), CH_3COOTl and $Pb(CH_3COO)_2 \cdot 3H_2O$ (C. Erba) and $In_2(SO_4)_3$ (B.D.H.), were used without further purification. Metals, Cd, Tl, Pb, Zn (C. Erba) and In (B.D.H.) were reagent grade. Mercury was distilled twice *in vacuo*.

Apparatus

Measurements were carried out in a Pyrex glass cell (a) (Fig. 1) made up of two vessels (A, B) connected to a third smaller compartment in which was dipped the glass reference electrode. A glass bridge, connecting compartments A and B to the central one, allowed vacuum or gas flow through the entire cell without mixing of the melts. The electrical contacts between the central and side compartments were realized by means of two thin asbestos fibres. The vessels A and B were equipped with five necks with standard glass joints; three of these were on one side compartment, two on the other. By means of these necks, two dropping amalgam electrodes (DAE) (one in A and the other in B), a gas inlet and a glass sheath, (b), with a side branch for connection to *vacuo* and containing the Chromel-Alumel thermocouple, were introduced into the

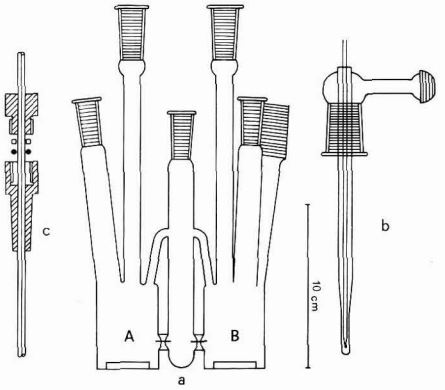

Fig. 1. Cell and accessories.

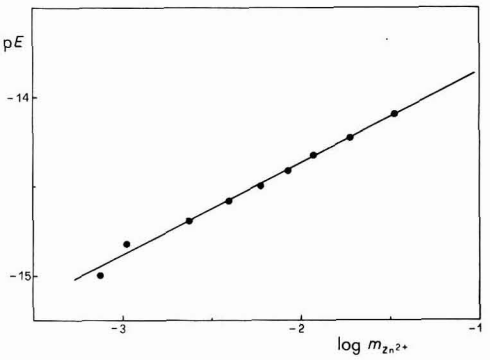

Fig. 2. pE *vs.* log(m) for the Zn/Zn(II) couple at 497.5°K (amalgam concn., $3.71 \cdot 10^{-3}$ mole kg^{-1}).

cell. Vacuum tightness on the gas inlet and on the two DAE's was ensured by O-ring-gaskets, (c). The fifth neck and the gas inlet served also for introducing solutes into the two vessels as weighed pellets containing a known amount of metal (Cd, Tl, Pb, Zn) acetates in (Li, Na, K) acetates mixture. Indium(III) was introduced with a small platinum spoon into the melt as pure $In_2(SO_4)_3$. The cell necks and the accessories were constructed in such a way that thermal convection was practically absent. The temperature was controlled with a fused nitrate bath to within ± 0.2°C. Vessels A and B had an annular groove at the bottom in which amalgams collected; the solutions were stirred by means of a small magnetic bar. Amalgams were prepared in a C-shaped ampoule as already described[1].

Procedure

The solvent was prepared by mixing CH_3COOLi, CH_3COONa and CH_3COOK (20, 30, 50 mole%). The mechanical mixture was dried under vacuum 24 h and a weighed quantity (about 40 g) was introduced into compartments A and B and melted under vacuum. A small quantity of solvent was also introduced into the central compartment in order to establish electrical contact between each solution and the glass reference electrode. This electrode (resistance in the range, 0.1–1 MΩ) was

dipped into a separate vessel containing pure solvent in order to avoid any possible effect on its potential of the cations added[9]. The cell was maintained under vacuum for about 2 h and then filled with dry nitrogen. The measurements were carried out with varying concentrations of the cations in the two vessels in the range 10^{-4}–10^{-2} *m*. The amalgam concentration in each experiment was about 10^{-3} mole kg^{-1}.

The e.m.f. of cells 1 and 2 was measured by means of a Solartron type LM 1420 digital integration voltmeter. The direct measurement of e.m.f. of the cell:

$$Pt\left|Zn(Hg)\right|Zn^{2+}\left|\;\right|M^{n+}\left|M(Hg)\right|Pt$$

is not accurate because the DAE potentials varied during the life of the drop[1]. The e.m.f. measured reached a stable value as soon as dissolution of the pellets was completed (about 10 min).

RESULTS AND DISCUSSION

The reversible behaviour of amalgam electrodes was tested for all couples by plotting pE ($= EF/RT \ln 10$) *vs.* $\log(m_{M^{n+}})$ at constant amalgam activity. In all cases, slopes are very near to the theoretical values for the reactions: $Cd \rightleftarrows Cd^{2+} + 2e$; $In \rightleftarrows In^{3+} + 3e$; $Tl \rightleftarrows Tl^{+} + e$; $Pb \rightleftarrows Pb^{2+} + 2e$; $Zn \rightleftarrows Zn^{2+} + 2e$. The limit values for each redox couple are given in Table 1 (column 5). A typical plot of pE *vs.* $\log(m_{M^{n+}})$ for the Zn/Zn(II) couple is given in Fig. 2. Slopes for the Pb/Pb(II) couple were always greater than the theoretical value. This discrepancy must be ascribed to slowness in reaching equilibrium conditions.

TABLE 1

STANDARD ELECTRODE POTENTIAL DATA

(Standard state, 1 mole kg^{-1})

Reaction	E°_{495}/mV	$(dE^{\circ}/dT)/mV\ deg^{-1}$	*No. of exptl. points*	*Limit values of* $1/n$
$Cd \rightleftarrows Cd^{2+} + 2e$	375.26 ± 0.04	-0.155 ± 0.004	80	0.480–0.525
$In \rightleftarrows In^{3+} + 3e$	376.87 ± 0.03	0.230 ± 0.005	75	0.321–0.345
$Tl \rightleftarrows Tl^{+} + e$	531.15 ± 0.12	-0.427 ± 0.009	85	0.997–1.040
$Pb \rightleftarrows Pb^{2+} + 2e$	602.38 ± 0.25	-0.124 ± 0.009	68	0.526–0.538
$Zn \rightleftarrows Zn^{2+} + 2e$	—	—	154	0.485–0.520

The activity of the metals in the amalgams was calculated by extrapolating the thermodynamic selected data[11] at every temperature assuming the pure metal as standard state. The e.m.f. values of cells 1 and 2 were used to obtain the standard electrode potential (E°_{M}) for each couple from the difference between the quantities, $E^{\circ\prime}_{M}$ and $E^{\circ\prime}_{Zn}$, where

$$E^{\circ\prime}_{M} = E_{v} - E^{\circ}_{M}$$
$$E^{\circ\prime}_{Zn} = E_{v} - E^{\circ}_{Zn}$$

E_{v} is the potential of the glass reference electrode and E°_{Zn} has been assumed, conventionally, as equal to zero. The number of values of $E^{\circ\prime}_{M}$ and $E^{\circ\prime}_{Zn}$ at each temperature is

equal to the number of variations of molality in the two cells. These potentials are distributed at random around the "true value". Equal weight has been given to each experimental $E^{\circ\prime}$-value, and E°_{M} has been calculated as the average of all the possible differences, $E^{\circ\prime}_{M} - E^{\circ\prime}_{Zn}$. This procedure has also been used to obtain the values of the constants in the equation:

$$E^{\circ}_{M(T)} = E^{\circ}_{M(495)} + dE^{\circ}_{M}/dT\,(T-495)$$

by means of the least-squares method. These constants are given in Table 1. In Table 2 are given the standard thermodynamic data for the electrode reactions, with the corresponding probable errors.

TABLE 2

STANDARD THERMODYNAMIC QUANTITIES

(Standard state, 1 mole kg^{-1})

Reaction	ΔH°/*kcal mole*$^{-1}$	ΔS°/*cal mole*$^{-1}$ *deg*$^{-1}$	ΔG°_{495}/*kcal mole*$^{-1}$
$Cd \rightleftarrows Cd^{2+} + 2e$	-20.85 ± 0.06	-7.15 ± 0.18	-17.309 ± 0.002
$In \rightleftarrows In^{3+} + 3e$	-18.19 ± 0.12	15.91 ± 0.34	-26.075 ± 0.002
$Tl \rightleftarrows Tl^{+} + e$	-17.12 ± 0.07	-9.85 ± 0.21	-12.249 ± 0.003
$Pb \rightleftarrows Pb^{2+} + 2e$	-30.62 ± 0.14	-5.72 ± 0.41	-27.785 ± 0.012

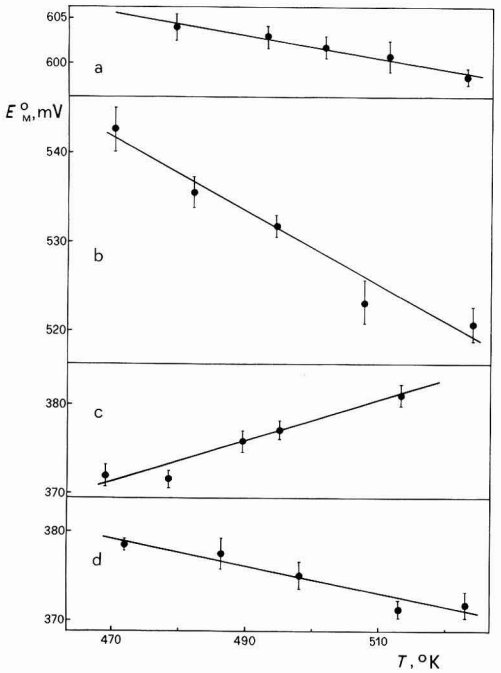

Fig. 3. Temperature-dependence of standard electrode potentials for: (a), Pb/Pb(II); (b), Tl/Tl(I); (c), In/In(III); (d), Cd/Cd(II) couples.

The plots of E°_{M} *vs.* T for each redox couple, obtained from the calculated equations, are presented in Fig. 3. The vertical segments are probable errors calculated from the experimental points.

ACKNOWLEDGEMENT

This work was supported by the Italian National Research Council (C.N.R.).

The calculations have been carried out by means of the Olivetti model 101 computer of the Istituto di Zoologia, Camerino.

SUMMARY

The standard potentials of the redox couples, Cd/Cd(II), In/In(III), Pb/Pb(II), Tl/Tl(I) and Zn/Zn(II) in molten alkali acetates in the range 470–520°K, have been determined.

REFERENCES

1 G. A. MAZZOCCHIN, G. G. BOMBI AND M. FIORANI, *Ric. Sci.*, 36 (1966) 338.
2 M. FIORANI, G. G. BOMBI AND G. A. MAZZOCCHIN, *Ric. Sci.*, 36 (1966) 580.
3 G. A. MAZZOCCHIN, G. G. BOMBI AND M. FIORANI, *J. Electroanal. Chem.*, 17 (1968) 95.
4 G. A. SACCHETTO, G. G. BOMBI AND M. FIORANI, *J. Electroanal. Chem.*, 20 (1969) 89.
5 G. G. DIOGENOV, *Zh. Neorgan. Khim.*, 1 (1956) 2551.
6 E. I. POCHTAKOVA, *Russ. J. Inorg. Chem. English Transl.*, 10 (1965) 1268.
7 G. G. BOMBI, M. FIORANI AND C. MACCA', *Chem. Commun. (London)*, (1966) 455.
8 D. INMAN, *J. Sci. Instr.*, 39 (1962) 391.
9 G. G. BOMBI, G. A. MAZZOCCHIN AND M. FIORANI, *J. Electroanal. Chem.*, 20 (1969) 195.
10 M. STEINBERG AND N. N. NACHTRIEB, *J. Am. Chem. Soc.*, 72 (1950) 3558.
11 R. HULTGREN, R. ORR, P. D. ANDERSON AND K. K. KELLEY, *Selected Values of Thermodynamic Properties of Metals and Alloys*, J. Wiley and Sons, New York, 1963.

ELECTROANALYTICAL CHEMISTRY AND INTERFACIAL ELECTROCHEMISTRY
Elsevier Sequoia S.A., Lausanne – Printed in The Netherlands

ZUM MECHANISMUS DER REDUKTION VON MOLYBDÄNIONEN AN QUECKSILBERKATHODEN IN SALZSAUREN LÖSUNGEN

M. WOLTER, D. O. WOLF UND M. VON STACKELBERG
Institut für Physikalische Chemie der Universität Bonn (Deutschland)
(Eingegangen den 27. Februar 1969)

Mo(VI) wird in neutralen und alkalischen Lösungen an der Quecksilbertropfelektrode nicht reduziert. In Lösungen von Schwefelsäure geringer und hoher Konzentration sind 2 polarographische Stufen sichergestellt, die den Vorgängen Mo(VI) $\rightarrow$ Mo(V) $\rightarrow$ Mo(III) zugesprochen werden[1].

Komplizierter ist das Verhalten in Salzsäure. Ueber den Mechanismus der Reduktion gibt es mehrere Deutungsversuche (Höltje und Geyer[2], Carritt[3], Haight[4], Wittick und Rechnitz[5]), denen wir hier einen weiteren hinzufügen wollen. Und zwar auf Grund von Versuchen, die wir sowohl mit einer grossflächigen als auch mit einer tropfenden Quecksilberelektrode durchgeführt haben.

DIE EXPERIMENTELLE ANORDNUNG

Die *grossflächige Quecksilberelektrode* bestand aus einer runden Fläche von $A = 35$ cm^2. Darüber war ein Propellerrührer angebracht, der mit variabler aber jeweils konstanter Drehgeschwindigkeit betrieben werden konnte. Das Volumen der Lösung betrug stets $V = 50$ ml. Durch Diaphragmen abgetrennt waren eine grossflächige Kalomel-Anode und eine Ag/AgCl-Bezugselektrode. Jedoch sind die nachfolgenden Potentialangaben stets auf die Kalomelnormalelektrode (NKE) umgerechnet. Die Temperatur betrug 25 ± 0.3°C.

Die Elektrolyse erfolgte stets bei konstantem Potential mit Hilfe eines Potentiostaten, wobei die mit der Konzentration C abnehmende Stromstärke i verfolgt wurde (Controlled Potential Electrolysis = "CPE"-Methode).

Nach den Gesetzen von Faraday und von Nernst ist

$$i = nFV \frac{-\mathrm{d}C}{\mathrm{d}t} = nFDAC/\delta \qquad (1)$$

wenn D der Diffusionskoeffizient (cm^2/sec) des reduzierbaren Stoffes und δ die von der Rührgeschwindigkeit abhängige (mittlere) Dicke der Nernst'schen Diffusionsschicht ist.

Aus Gl. (1) folgt

$$-\mathrm{d}\ln C/\mathrm{d}t (= -\mathrm{d}\ln i/\mathrm{d}t) = DA/V\delta \equiv \alpha = \text{konst.} \qquad (2)$$

für einen Versuch bei dem D und δ konstant sind. Dann ist

$$\alpha = -\mathrm{d}i/i\,\mathrm{d}t = (i_0 - i_t)/i_0 t = 2.3 \log(i_0/i_t)/t$$

und somit

$$\delta = DAt/V \cdot 2.3 \log(i_0/i_t) \qquad (3)$$

Bei einer einfachen Rührvorrichtung hat δ nur die Bedeutung eines Mittelwertes (z.B. in Tab. 3).

$$n = \frac{i_0}{C_0 F V \alpha} = \frac{i_0 t}{C_0 F V \cdot 2.3 \log(i_0/i_t)} = \frac{i_0(\text{mA}) \cdot t(\text{Min}) \cdot 2.7 \cdot 10^{-4}}{C_0(M) \cdot \log(i_0/i_t) \cdot V(\text{ml})} \quad (4)$$

Bei unserem Problem ist zu beachten, dass bei HCl-Konzentrationen >1 M die Reduktion $Mo^{6+} + Hg + Cl^- = Mo^{5+} + \frac{1}{2} Hg_2Cl_2$ stattfindet[2]. Ab 3 M HCl liegt das Gleichgewicht ganz rechts.

An die *Tropfelektrode* wurde ein Metrohm-Polarecord E 261 angeschlossen. Die verwendeten Tropfkapillaren hatten bei der normalerweise auf 80 cm eingestellten Höhe des Hg-Niveaugefässes Tropfzeiten von $\vartheta = 5$–6 sec und Hg-Ausflussgeschwindigkeiten von $m = 1.0$–1.4 mg/sec. Die Temperatur der entlüfteten Lösung betrug 25.0°C. Als Maximadämpfer wurden stets $1 \cdot 10^{-3}\%$ Triton X-305 zugesetzt. Potentialangaben beziehen sich stets auf die NKE.

Chemikalien

Als Mo(VI)-Präparat wurde p.a.-Natriummolybdat $Na_2MoO_4 \cdot 2\,H_2O$ der Firma Merck benutzt. Das MoO_4^{2-} liegt in der 0.6 M HCl wahrscheinlich als $MoO_2(OH)_2$ oder $Mo(OH)_6$ vor[6]. Eine Polymerisation zu Isopolysäuren, z.B. $H_2Mo_7O_{24}^{4-} + 4\,H^+$, ist bei den von uns benutzten geringen Mo(VI)-Konzentrationen in saurer Lösung nur in ganz unbedeutendem Ausmass möglich[7].

Als Mo(V)-Präparat wurde $MoCl_5$ reinst der Firma Schuchardt verwendet. Dass Mo(V) in verdünnter Salzsäure dimer vorliegt[8], wird im Abschnitt "Die zweite Stufe" besprochen werden.

Die 1. Stufe

Nach Abb. 1 scheint die Höhe der 1. Stufe mit zunehmender HCl-Konzentration (0.3–1.86 M) grösser zu werden. Dies beruht jedoch darauf, dass durch anodische Hg-Oxydation gebildete lösliche Hg–Cl-Komplexe (z.B. $HgCl_4^{2-}$) mitreduziert werden[9]. Ausserdem wird der linke Teil des Grenzstromes mit steigender HCl-Konzentration in zunehmendem Masse durch die erwähnten anodischen Reaktionen abgeschnitten. Da die Stufenhöhen somit nur in HCl-Lösungen nicht zu grosser Konzentration einwandfrei festgestellt werden können, benutzten wir für die quantitativen Versuche eine 0.6 M HCl-Lösung.

Dabei ergab sich, dass die Stufenhöhe

1. proportional der Mo(VI)-Konzentration ($1 \cdot 10^{-4}$–$1 \cdot 10^{-3}$) ist.
2. proportional $\sqrt{h}$, wobei h die Niveauhöhe des Quecksilbergefässes der Tropfkapillare ist ($h = 40$–80 cm), s. Abb. 2,
3. im Temperaturbereich 25°–50°C nimmt die Stufenhöhe um 1.6% pro Grad zu.

Diese Ergebnisse weisen darauf hin, dass es sich um einen diffusionsbegrenzten Strom handelt. Nimmt man eine Reduktion von Mo^{6+} zu Mo^{5+} an (also $n = 1$), so ergibt sich der Diffusionskoeffizient zu etwa $D = 4$–$5 \cdot 10^{-6}$ cm²/sec, also ein durchaus plausibler Wert.

Auch eine Reduktion von $1 \cdot 10^{-3}$ M Mo(VI) in 0.6 M HCl an der grossflächigen Elektrode bei -0.08 V gegen NKE, entsprechend dem Potential des Grenzstromes der ersten polarographischen Stufe, ergibt bei Darstellung von log i als Funktion der Elektrolysenzeit t eine Gerade, aus deren Neigung nach Gl. (4) $n = 1 \pm 3\%$ folgt, und

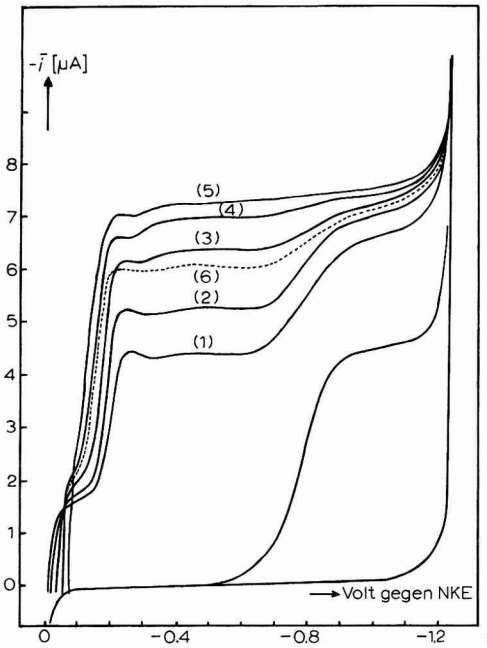

Abb. 1. Polarogramme einer $1 \cdot 10^{-3}$ *M* Mo(VI)-Lösung in HCl-Lösungen verschiedener Konzentration (s. Tabelle 1) und von einer $1 \cdot 10^{-3}$ *M* Mo(V)-Lösung in 0.6 *M* HCl. Dazu das Polarogramm der Grundlösung mit 0.6 *M* HCl. Allen Lösungen ist $1 \cdot 10^{-3}$% Triton X-305 beigefügt, trotzdem zeigt die 2. Stufe noch eine kleines Maximum. Bei Mo(VI)-Konzentrationen über 10^{-3} *M* treten an dieser Stelle erhebliche Störungen des Polarogrammes auf.

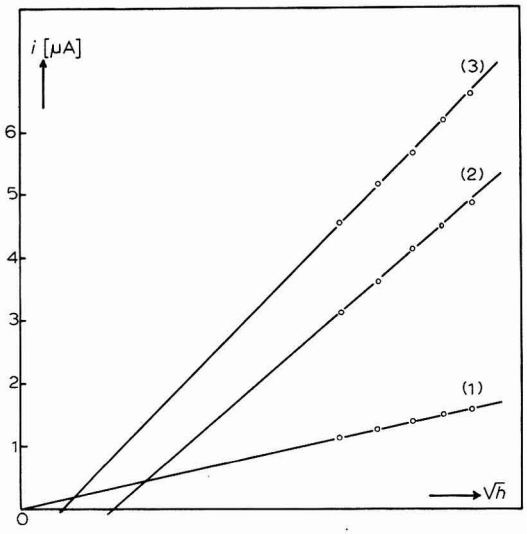

Abb. 2. Der polarographische Gesamtgrenzstrom der drei Mo(VI)-Stufen in Abhängigkeit von der Wurzel der Hg-Niveauhöhe *h*. 10^{-3} *M* Mo(VI) in 0.6 *M* HCl.

zwar auch bei verschiedener Rührgeschwindigkeit und daher verschiedener Neigung der Geraden, die aber i_0 proportional ist. Die reduzierte Mo(VI)-Lösung hat die schwach gelbbraune Farbe einer Mo(V)-Lösung angenommen. Eine titrimetrische Oxydation zu Mo(VI) mit einer Ce^{4+}-Lösung entspricht $n=1$.

Es scheint uns also wahrscheinlich, dass die erste Stufe einer normalen diffusionsbegrenzten Mo(VI)–Mo(V)-Reduktion entspricht.

TABELLE 1

ANGABEN ZU DEN 3 POLAROGRAPHISCHEN STUFEN* $1\cdot10^{-3}$ *M* Mo(VI)

HCl-Konz. (*Mole/l*)	$E_{\frac{1}{2}}$ *gegen NKE* (*V*)			*Gesamtstufenhöhen* (*μA*)			*Verhältnis der Stufenhöhen*
	1.	2.	3.				
0.3	−0.01	−0.20	−0.78	(1.8)	4.6	6.8	1 : 2.5 : 3.6
0.6	(−0.02)	−0.18	−0.78	1.9	5.5	7.2	1 : 2.9 : 3.8
1.0	—	−0.16	−0.78	(2.2)	6.7	7.5	1 : 3.5 : 3.9
1.6	—	−0.14	(−0.78)	(2.4)	7.3	7.6	1 : 3.8 : 4
1.86	—	(−0.12)		—	7.6		1 : 4
0.6 *M* HCl + 1.26 *M* KCl	—	−0.15	−0.8	—	6.4	7.3	1 : 3.4 : 3.8
		$1\cdot10^{-3}$ *M* Mo(V)					
0.6		−0.77			4.4		2.3

* Vgl. Abb. 1. Die wahren Halbstufenpotentiale sind etwas positiver, da keine Widerstandskorrektur angebracht worden ist. Bei der Berechnung des Verhältnisses der Stufenhöhen wurde die Höhe der 1. Stufe stets gleich 1.9 μA gesetzt.

Die 2. Stufe

Nach Abb. 1 verschiebt sich das Halbstufenpotential der 2. Stufe mit steigender HCl-Konzentration in positiver Richtung und die Stufenhöhe nimmt stark zu (s. Tabelle 1). In 0.6 *N* HCl mit $1\cdot10^{-3}$ *M* Mo(VI) ist die vom Grundstrom aus gemessene Gesamthöhe der 2. Stufe 2.9 mal höher als die erste Stufe. Aber beim Herabsetzen der Mo(VI)-Konzentration nähert sich dieses Verhältnis dem Werte 4:1 (nach Tabelle 2 bei 10^{-4} *M* Mo(VI) 3.5:1). Dabei muss also Mo(VI) bei der 2. Stufe um 4 Einheiten zu Mo(II) reduziert werden. Dass das Verhältnis bei höherer Mo(VI)-Konzentration kleiner wird, kann darauf beruhen, dass Mo(II) bereits in der Diffusionsschicht der Tropfelektrode mit herandiffundierendem Mo(VI) reagiert, wodurch die Menge des an die Elektrode gelangenden Mo(VI) herabgesetzt wird.

Die Reaktion von Mo(II) mit Mo(VI) muss zu einem beim Potential der 2. Stufe nicht reduzierbaren Produkt führen. Wir nehmen an, dass dies die dimerisierte Form von Mo(V) ist, die sich also nach der Bruttoreaktion

$$3\,Mo^{6+} + Mo^{2+} = 2(Mo^{5+})_2 \qquad (5)$$

bilden würde. Sacconi und Cini[8] haben durch magnetochemische Untersuchungen die nicht paramagnetische dimere Form in HCl-Lösungen nicht zu hoher Konzentration nachgewiesen. Bei 2.5 *M* HCl beginnt die Dissoziation und ist in 7 *M* HCl beendet. Nach Jakob, Ogorzalek und Sikorski[10] sowie Haight[11] handelt es sich um das Gleichgewicht

$$[(MoOCl_4)_2O]^{4-}\,(\text{braun}) + 2\,H^+ + 2\,Cl^- \rightleftharpoons 2[MoOCl_5]^{2-}\,(\text{grün}) + H_2O$$

Auch eine Lösung von $MoCl_5$ in 0.6 *M* HCl bildet das braune Dimere. Dieses wird erst beim Potential der 3. Stufe einer Mo(VI)-Lösung reduziert. Setzt man der Mo(VI)-Lösung $MoCl_5$ zu, so wird die Höhe und Lage der ersten und zweiten polarographischen Reduktionsstufen nicht verändert. Nur die dritte Stufe wird erhöht.

Die Zunahme der Höhe der 2. Stufe mit der HCl-Konzentration (Abb. 1) ist vielleicht auf die Verminderung der Stabilität der dimeren Form des Mo(V) zurückzuführen. In 1.86 *M* HCl ist die zweite Stufe fast 4 mal so hoch wie die erste. Die Reduktion führt also fast vollständig zu Mo(II), die 3. Stufe ist verschwunden.

Das Verhältnis der Höhe der zweiten Stufe zu der der ersten nimmt auch mit abnehmender Mo(VI)-Konzentration zu (Tabelle 2). Da hierbei auch die Mo(II)-Konzentration abnimmt, wird der Bruchteil x (von Mo(II)), der noch in der Diffusionsschicht (mit Mo(VI)) nach Gl. (5) reagiert, abnehmen. In Tabelle 2 ist x nach $i(2)/i(1) = 4/(3x+1)$ berechnet.

TABELLE 2

Mo(VI)-Konz./ 10^4 *M (in 0.6 M HCl)*	*Verhältnis der Gesamtstufenhöhen*	*Bruchteil x*
	1.St. : 2.St. : 3.St.	
1	1 : 3.5 : 3.9	0.05
3	1 : 3.2 : 3.7	0.08
10	1 : 2.9 : 3.6	0.15

Auch die Ergebnisse von CPE-Reduktionen von $1 \cdot 10^{-3}$ *M* Mo(VI) in 0.6 *M* HCl entsprechen der Annahme einer Reduktion zu Mo(II) bei der 2. polarographischen Stufe mit der nachgelagerten Reaktion (5). Bei kleiner Rührgeschwindigkeit ist es gleichgültig, ob man bei −0.08 V (Potential des Grenzstromes der 1. Stufe) oder bei −0.40 V (2. Stufe) elektrolysiert. Man erhält eine gelblichbraune Mo(V)-Lösung. Während der Elektrolyse aufgenommene Polarogramme zeigen in beiden Fällen ein allmähliches Verschwinden der ersten und der zweiten Stufe, wobei aber das Verhältnis ihrer Höhen von 1:2.9 auf 1:4 steigt.

Die Abnahme von $\log i$ mit der Zeit t bei der CPE-Reduktion entspricht nach Gl. (4) dem Werte $n = 1$ ($\pm 2\%$). Eine Reduktion bei −0.40 V mit grösserer Rührgeschwindigkeit ergibt jedoch $n > 1$, wie die 2. und 3. Zeile der Tabelle 3 zeigen. In diesem Fall ist Mo(VI) verbraucht, bevor die Oxydation von Mo(II) in der Gesamtlösung restlos bis Mo(V) erfolgt ist. Nach Geske und Bard[12] ist $\log i$ (und $\log C$) auch bei einer nachgelagerten Reaktion eine lineare Funktion der Elektrolysezeit, wenn diese Reaktion relativ schnell ist. Aber wenn sie nicht sehr schnell ist (oder die Rührgeschwindigkeit langsam, die Stromstärke gering), so hat sie aus dem genannten Grunde im vorliegenden Fall nicht die $n = 1$ entsprechende Neigung.

Die 3. Stufe

Die CPE-Reduktion einer Mo(V)-Lösung bei −1.0 V liefert nach Gl. (4) auch bei Variation der Rührgeschwindigkeit $n = 3.0 \pm 0.1$. Die Reduktion bei −1.0 V liefert also Mo(II).

Das Polarogramm einer Mo(V)-Lösung (Abb. 1) zeigt nur eine Stufe, deren Potential und flacher Anstieg dem der 3. Stufe einer Mo(VI)-Lösung entsprechen.

TABELLE 3
(s. Abb. 3)

$i_t = i_0/100$ *nach Min.*	*Diffusionsschichtdicke (mm) (nach Gl. (3))*	*n*
38	0.017	1.00 ± 0.05
16.5	0.008	1.40 ± 0.1
9	0.004	1.75 ± 0.2

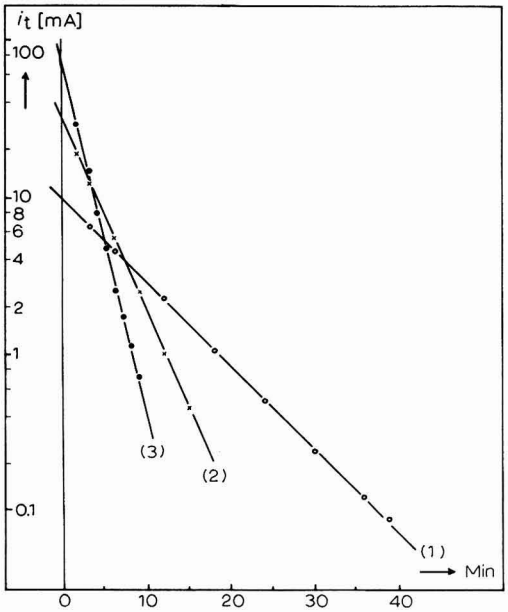

Abb. 3. Log i_t der 2. polarographischen Gesamtstufenhöhe in Abhängigkeit von der Zeit t bei CPE-Elektrolysen einer 10^{-3} *M* Mo(VI)-Lösung in 0.6 *M* HCl bei verschiedener Rührgeschwindigkeit (s. Tabelle 3).

Eine mit CPE-Anordnung bei -0.08 oder -0.40 V reduzierte Mo(VI)-Lösung ergibt das gleiche Polarogramm wie eine Mo(V)-Lösung. Die Höhe der polarographischen Stufe einer Mo(V)-Lösung ist proportional $\sqrt{h}$ und proportional der Mo(V)-Konzentration, entsprechend einer Diffusionsbegrenzung. Der bei -1.0 V liegende Grenzstrom lässt eine Reduktion zu Mo(II) annehmen. Mit $n=3$ ergibt sich $D=2.5\cdot 10^{-6}$ cm^2/sec (in 0.6 *M* HCl), also ein erheblich kleinerer Diffusionskoeffizient als für Mo(VI) ($D=4.5\cdot 10^{-6}$, die Genauigkeit dieser Angaben ist nicht gross). Das infolge Zusammenlagerung von zwei Mo^{5+} hochgeladene dimere $(Mo^{5+})_2$ hat sicher infolge Anlagerung zahlreicher Cl^--Ionen und H_2O-Molekulen ein grosses Volumen.

Die 3. Stufe eines Mo(VI)-Polarogramms ist also wahrscheinlich der Reduktion des stabilisierten $[Mo(V)]_2$ zuzuschreiben. Die Stabilisierung erfolgt um so schneller, je geringer die HCl-Konzentration ist. Damit nimmt die Höhe der 2. Stufe ab, die Höhe der 3. Teilstufe (Anstieg des Stromes bei -0.8 V) zu (Abb. 1).

Bei Verringerung der Mo(VI)-Konzentration nimmt das Verhältnis der Gesamthöhe der 3. Stufe zu der der 1. Stufe zu und nähert sich dem Werte 4, wie Tabelle 2

zeigt, entsprechend der Reduktion von Mo(VI) zu Mo(II). Von der Gesamthöhe der 3. Stufe ist also nur der Teil einer Mo(V)-Reduktion zuzusprechen, der dem Stromanstieg bei -0.8 V entspricht. Nur die Höhe dieses Teiles der 3. Stufe ist durch den kleineren Diffusionskoeffizienten herabgesetzt.

Das Abfangen von herandiffundierenden Mo(VI)-Ionen durch Mo(II)-Ionen setzt die Höhe der 3. Stufe nicht herab, denn durch das Abfangen wird der Konzentrationsgradient in die Diffusionsschicht verstärkt.

Die Gesamthöhe der 3. Stufe ist nicht proportional $\sqrt{h}$, wie Abb. 2 zeigt, weil mit zunehmendem h ein zunehmender Anteil des Stromes durch Mo(VI)-Reduktion bedingt ist.

ZUSAMMENFASSUNG

Auf Grund von Versuchsergebnissen, die bei Reduktionen von Mo(VI)- und Mo(V)-Lösungen in HCl-Lösungen einerseits an einer grossflächigen Elektrode bei konstantem Potential (und konstanter Rührung unter zeitlicher Verfolgung der Stromstärke), andererseits an einer Hg-Tropfelektrode gewonnen wurden, wird eine Deutung der Vorgänge bei den 3 polarographischen Stufen der Mo(VI)-Reduktion in HCl-Lösungen gegeben, die von den bisherigen Deutungen abweicht.

Die erste Stufe schreiben wir einer normalen diffusionsbegrenzten Reduktion von Mo(VI) zu Mo(V) zu; die 2. Stufe einer Reduktion von Mo(VI) zu Mo(II), wobei jedoch das Mo(II) mit dem herandiffundierenden Mo(VI) reagiert und in einer (im einzelnen noch nicht angebbaren) Reaktionskette dimeres Mo(V) bildet. Dieses ist erst bei dem Potential der 3. Stufe reduzierbar, so dass hier Mo(VI) restlos zu Mo(II) reduziert wird.

SUMMARY

A new interpretation of the reactions occurring in the three polarographic steps of Mo(VI) reduction in HCl solution is proposed on the basis of experimental results on the reduction of Mo(VI) and Mo(V) in HCl solution, both at a large surface electrode at constant potential (and constant stirring, with observation of the time-dependence of the current) as well as at the dropping mercury electrode.

The first step is ascribed to a normal diffusion-limited reduction of Mo(VI) to Mo(V); the second to a reduction of Mo(VI) to Mo(II); however, the Mo(II) reacts with the Mo(VI) diffusing to the electrode and produces dimeric Mo(V) by a reaction chain, the particulars of which cannot yet be defined. This is reducible only in the third step, so that Mo(VI) is finally completely reduced to Mo(II).

LITERATUR

1 I. M. KOLTHOFF UND I. HODARA, *J. Electroanal. Chem.*,4 (1962) 369; M. v. STACKELBERG, *Tech. Mitt. Krupp*, 2 (1939) 59; A. A. VLCEK, *Chem. Listy*, 47 (1953) 1162.
2 R. HÖLTJE UND R. GEYER, *Z. Anorg. Allgem. Chem.*, 246 (1941) 243, 265.
3 D. E. CARRITT, Ph.D. Thesis, Harvard Univ., 1947; I. M. KOLTHOFF, *Polarography*, Vol. II, 1952, p. 457.
4 G. P. HAIGHT JR., *J. Inorg. Nucl. Chem.*, 24 (1962) 673.
5 J. J. WITTICK UND G. A. RECHNITZ, *Anal. Chem.*, 37 (1965) 816.
6 G. SCHWARZENBACH UND J. MEIER, *J. Inorg. Nucl. Chem.*, 8 (1958) 302.

7 Y. SASAKI, I. LINDQUIST UND L. G. SILLEN, *J. Inorg. Nucl. Chem.*, 9 (1959) 93; J. AVESTON, E. W. ANACKER UND J. S. JOHNSON, *Inorg. Chem.*, 3 (1964) 735; H. M. NEUMANN UND N. C. COOK, *J. Am. Chem. Soc.*, 79 (1957) 3026.
8 L. SACCONI UND R. CINI, *J. Am. Chem. Soc.*, 76 (1954) 4239.
9 B. BEHR UND J. TARASZEWSKA, *J. Electroanal. Chem.*, 19 (1968) 373.
10 W. JAKOB, M. OGORZALEK UND H. SIKORSKI, *Roczniki Chem.*, 35 (1961) 3.
11 G. P. HAIGHT JR., *J. Inorg. Nucl. Chem.*, 24 (1962) 663.
12 D. H. GESKE UND A. J. BARD, *J. Phys. Chem.*, 63 (1959) 1057.

ELECTROANALYTICAL CHEMISTRY AND INTERFACIAL ELECTROCHEMISTRY
Elsevier Sequoia S.A., Lausanne – Printed in The Netherlands

PULSE POLAROGRAPHY

V. KINETICS OF PYRUVIC AND GLYOXYLIC ACID REACTIONS

A. W. FONDS*, J. L. MOLENAAR AND J. M. LOS**
Laboratory of Physical Chemistry, Vrije Universiteit, Amsterdam (The Netherlands)
(Received February 24th, 1969)

INTRODUCTION

In the investigation of the various equations derived for diffusion and kinetic waves in pulse polarography[1a–d] some new data and facts evolved from the study of the kinetic behaviour of pyruvic and glyoxylic acids.

Recent kinetic and thermodynamic studies pertaining to these acids have used methods such as polarography[2–6], cyclic voltammetry[5], temperature[7] and pressure jumps[8], and u.v.[3,4] and NMR[9–11] spectroscopy. These studies contain earlier literature references.

The interpretation of results has been based almost exclusively on the following reaction scheme:

$$\begin{array}{ccc} \overset{1}{\mathrm{RCOCOO^-}} + \mathrm{H^+} + \mathrm{H_2O} & \underset{k_{2,1}}{\overset{k_{1,2}}{\rightleftharpoons}} & \overset{2}{\mathrm{RCOCOOH}} + \mathrm{H_2O} \\ k_{1,4}\downarrow\uparrow k_{4,1} & & k_{2,3}\downarrow\uparrow k_{3,2} \\ \underset{4}{\mathrm{RC(OH)_2COO^-}} + \mathrm{H^+} & \underset{k_{3,4}}{\overset{k_{4,3}}{\rightleftharpoons}} & \underset{3}{\mathrm{RC(OH)_2COOH}} \end{array} \qquad (1)$$

where R = H (glyoxylic acid) or R = CH_3 (pyruvic acid). The enol form of pyruvic acid or its anion does not seem to occur to any significant extent[9].

Hydrates 3 and 4 are not reducible at a mercury electrode, while the non-hydrated acid, 2, is reduced more readily than its anion, 1. In a certain pH range (several units higher than pK_i, K_i being the dissociation constant of the corresponding acid) separate polarographic waves of species 2 and 1 occur side by side. These "first" and "second" or "total" waves seem to be controlled by a kinetic process dictated by reaction scheme (1), except for the second wave of pyruvic acid, which is diffusion controlled.

In the pulse-polarographic analysis of the problem, the experimental evidence obtained could be handled by using the most exact solutions available for the simple kinetic scheme preceding the electrode reaction of A

$$\mathrm{B} \underset{k_2}{\overset{k_1}{\rightleftharpoons}} \mathrm{A} \qquad (2)$$

* Present address: Rijks Instituut voor de Volksgezondheid, Bilthoven (The Netherlands)
** Requests for reprints should be addressed to this author.

Either one of the following two formulations can be used, depending on the magnitudes of the (pseudo-) first-order rate constants, k_1 and k_2. Both formulations refer to $\vartheta = t/t_1 < 1$, where t denotes the time of pulse application and t_1 the time of drop growth prior to pulse application. They are to be used for cylindrical capillaries since correction for shielding has been applied, *i.e.*, the spherical correction term has been multiplied by $\frac{1}{2}(1+\vartheta)$(see ref. 1b). Finally, both formulations refer to instantaneous currents, as these are expected to give more sensitive indications of devious behaviour than average currents.

(a) If the equilibrium of scheme (2) is established rapidly with a relaxation time much shorter than 1 sec, or better,

$$k_1 + k_2 \gg t^{-1} \tag{3a}$$

we have the following equation for the instantaneous limiting current (ref. 1c, eqn. (16) with shielding correction from ref. 1b)

$$\mathrm{i} = 4nF\alpha^2(\pi D)^{\frac{1}{2}} t_1^{\frac{1}{6}} \frac{(1+\vartheta)^{\frac{3}{3}}}{\vartheta^{\frac{1}{2}}} \omega^* \sum_{j=0} \frac{(-1)^j \chi_1^{j+1} \vartheta^{(j+1)/2}}{p_0 \cdot p_1 \cdots p_j}$$

$$\cdot \left[\left\{ 1 - \frac{j}{3(j+2)}\vartheta + \frac{j(4j+15)}{18(j+2)(j+4)}\vartheta^2 + \ldots \right\} \right.$$

$$\left. + \frac{D^{\frac{1}{2}} t_1^{\frac{1}{2}} \vartheta^{\frac{1}{2}}(1+\vartheta)}{\alpha p_{j+1}} \left\{ -j + \frac{j(3j+7)}{6(j+3)}\vartheta + \ldots \right\} \right] \tag{3b}$$

where i is expressed in amperes and n = number of electrons per unit of reaction; F = Faraday constant (96500 C equiv.$^{-1}$); $\alpha = (3m/4\pi d)^{\frac{1}{3}} = 0.26\ m^{\frac{1}{3}}$ (25°C); m = rate of flow of mercury (g sec^{-1}); d = density of mercury (g cm^{-3}); D = diffusion coefficient of both A and B (cm^2 sec^{-1}); ω^* = total concentration of A and B in bulk (moles cm^{-3}); $\chi_1 = 2(k_1+k_2)^{\frac{1}{2}} t_1^{\frac{1}{2}} K^{-1}$; $K = k_2/k_1$; $p_0 = 2\pi^{-\frac{1}{2}}$; $p_j \cdot p_{j+1} = 2(j+1)$.

If reaction (2) becomes infinitely fast or $\chi_1 \to \infty$, eqn. (4) leads to the diffusion equation in ω^*, *i.e.*, for species A and B together, as Dr. Brinkman of this laboratory has shown by calculating the current for a series of large χ_1-values with a computer programme. This diffusion current has been given in ref. 1b, eqn. (24)

$$i_d = 7.06_5 \cdot 10^4 n D^{\frac{1}{2}} m^{\frac{2}{3}} t_1^{\frac{1}{6}} \omega^* \frac{(1+\vartheta)^{\frac{4}{3}}}{\{(1+\vartheta)^{7/3} - 1\}^{\frac{1}{2}}}$$

$$\cdot [1 + 2.23\ D^{\frac{1}{2}} m^{-\frac{1}{3}} t_1^{\frac{1}{6}} \{(1+\vartheta)^{7/3} - 1\}^{\frac{1}{2}}] \tag{4}$$

(b) If the concentration of B retains its bulk value, b^*, up to the surface of the electrode, which is the case if

$$k_1 \ll t^{-1}, \tag{5a}$$

there exists a situation which has been treated as a formal analogue of the solution for catalytic currents, and the result is (*cf.* ref. 1d, eqn. (11), with shielding correction from ref. 1b):

$$i = 4nF\alpha^2(\pi D)^{\frac{1}{2}} t_1^{\frac{1}{6}} \frac{(1+\vartheta)^{\frac{2}{3}}}{\vartheta^{\frac{1}{2}}} a^* \left[\sum_{j=0} \frac{(-1)^{j+1} \chi_2^j \vartheta^j}{j!} \right.$$

$$\cdot \left\{ \frac{1}{2j-1} - \frac{1}{3(2j+1)} \vartheta + \frac{11-2j}{18(2j+1)(2j+3)} \vartheta^2 + \ldots \right\}$$

$$\left. + \frac{(\pi D)^{\frac{1}{2}}}{2\alpha} t_1^{\frac{1}{6}} \vartheta^{\frac{1}{2}} (1+\vartheta) \left(1 - \frac{\vartheta}{3} \ldots\right) \right] \qquad (5b)$$

where $\chi_2 = k_2 t_1$ and a^* is the bulk concentration of A. We note that $a^* = b^*/K = \omega^*/(K+1)$. Condition (5a) is certainly obeyed if $i \ll i_d$, the diffusion current of A and B together (in that case $K = k_2/k_1 \gg 1$ applies as well).

In the case that $k_2 \to 0$—for practical purposes $k_2 \ll 1/t$ will suffice— besides k_1 being small, the relaxation time of reaction (2), $(k_1 + k_2)^{-1}$, becomes so large that the system appears as if frozen and in the summation of eqn. (5b) only the term with $j = 0$ remains; this is the principal term of the diffusion equation for A (*cf.* ref. la, eqn. (38)). Also, the spherical term is approximately the same as that in the diffusion equation[1d]. Generally, eqn. (5b) can be written as an equation with $j = 0$ (which is the diffusion equation of A, *i.e.*, eqn. (4) with ω^* replaced by a^*) added to one containing all terms with $j \geq 1$ (the kinetic part: all χ_2-terms).

There may be occasions where both eqns. (3b) and (5b) could be applied. It must be borne in mind that because of the conditions of their validity, eqn. (3b) may fail when pulse times become too short and eqn. (5b) when they become too long.

The use of eqns. (3b) and (5b) is quite straightforward because of the availability of extensive tables which correlate the summation factor in eqn. (3b) (F and f in ref. 1c) to χ_1 and the summation $j = 1,2\ldots$ (which is proportional to $i - i_d$) in eqn. (5b) to χ_2, and which permit linear interpolation. Table 1 of ref. 1c is not detailed enough for this purpose.

In order to justify the reduction of scheme (1) to scheme (2) we shall occasionally make use of reaction-volume theory, if only as a guiding device.

EXPERIMENTAL

Aqueous solutions of freshly-distilled (under reduced pressure) pyruvic acid in phosphate buffers at two different pH-values, in an acetate buffer and in 0.3 *M* HCl, were investigated.

Experiments with glyoxylic acid were carried out in citrate buffer solutions at different pH-values and in 0.3 *M* HCl. Glyoxylic acid was added in the form of its calcium salt (reagent-grade).

Buffer components and KCl (used for adjusting to a certain ionic strength I) were at least of reagent-grade quality (phosphates and KCl[1b] were further recrystallized). Standard solutions used for calibration in the pH determinations were 0.025 *M* KH_2PO_4 + 0.025 *M* Na_2HPO_4 (pH = 6.86; 25°C) and 0.05 *M* potassium hydrogen phthalate (pH = 4.005; 25°C).

The pulse polarograph used for measurement of instantaneous currents, has already been described[1b]. The pH-meter was a Philips PR 9400 with a combination electrode. Both a mercury-pool cell with external reference and an H-type cell with

an extra intermediate compartment (to avoid contamination of the test solution) have been used. Capillaries were siliconed. The mercury used was extremely pure and very pure nitrogen was used for deaeration. The rate of flow of mercury, m, could be determined to better than 0.5% by weighing individual drops on a Cahn Electrobalance (precision 1 μg). Cell solutions were thermostatted at $25.0 \pm 0.1^{\circ}$C.

Since the second (total) polarographic wave is closely followed by the hydrogen wave, especially in the case of pyruvic acid, blank polarograms were recorded for subtraction. When the H-type cell was used, corrections for the voltage drop across it had to be applied in view of the subtraction procedure. The cell resistance was evaluated from the initial sharp current peak at the start of a calibrated pulse with a potential prior to the beginning of the wave, as shown by means of the fast sweep on an oscilloscope. Cell resistances, which were of the order of 1000 Ω, required significant corrections especially for the total wave of pyruvic acid.

Separation between first and second waves is not ideal in spite of a distance of at least 200 mV between the half-wave potentials. The inflection point between the two waves was taken as the limiting current of the first wave.

RESULTS AND DISCUSSION

For each of the two acids studied we shall investigate to what extent reaction scheme (2) can replace scheme (1). If this replacement is valid, we have to deal with 3 types of limiting currents for each acid:

(i) The total wave in the pH-range where two waves co-exist. This wave may be either diffusion-controlled or involve the dehydration kinetics of the anion (left-hand side of scheme (1)). The rate constants, $k_{4,1}$ and $k_{1,4}$, will be measured at constant c_{H_2O} (very dilute solution) and take the place of k_1 and k_2, respectively, of scheme (2).

(ii) In the two-wave region, the first wave may be controlled by the proton transfer to the non-hydrated anion A^- and the dissociation of the non-hydrated acid HA (top of scheme (1)). The rate constants, $k_{1,2}$ and $k_{2,1}$, are correlated with k_1 and k_2 of scheme (2) by

$$k_1 = k_{1,2}\, a_{H^+}\, \gamma_A \tag{6a}$$

$$k_2 = k_{2,1}\, \gamma_{HA} \tag{6b}$$

while

$$K = k_2/k_1 = k_{2,1}\, \gamma_{HA}/k_{1,2}\, a_{H^+}\, \gamma_A = (K_{2,1}/a_{H^+})(\gamma_{HA}/\gamma_A) = c_{A^-}/c_{HA} \tag{6c}$$

where a_{H^+} = activity of H_3O^+ as measured by a pH-meter, $K_{2,1} = k_{2,1}/k_{1,2}$ = thermodynamic equilibrium constant of HA, γ is the activity coefficient and $\gamma_H/\gamma_{\pm}$ is taken as unity ($\gamma_{\pm}$ being the mean activity coefficient of HCl).

(iii) The wave in 0.30 M HCl solution. As for the anion, this wave may be diffusion-controlled or involve the dehydration kinetics of the undissociated acid (right-hand side of scheme (1)). Rate constants, $k_{3,2}$ and $k_{2,3}$, can replace k_1 and k_2 in scheme (2).

Pyruvic acid

For experiments of type (i) and (ii) the compositions of the solutions used are given in Table 1 (all concentrations being total concentrations). Besides phosphate

buffers, one acetate buffer has been used (0.149 M CH_3COONa + 0.040 M CH_3COOH + 0.151 M KCl, ionic strength, $I = 0.30$, pH = 5.24), in which case the analytical concentration of pyruvic acid was $0.546 \cdot 10^{-3}$ M.

(i) *Total wave.* Since undissociated pyruvic acid is not present at the pH-values of the measurements and since the relaxation time of the anionic dehydration process is estimated to be about 7 sec (as we shall show at the end of this paper) we must expect that the diffusion-current eqn. (4) adequately describes the limiting current if we substitute for ω^* the bulk concentration of non-hydrated anion. NMR[9,11] gives evidence of about 5% of anionic hydrate, although in rather concentrated solutions. Adopting a value of 95% for the non-hydrated species, we calculated values of $D^{\frac{1}{2}}$ for four pulse times, t, for each solution listed in Table 1. Results of $10^3 \cdot D^{\frac{1}{2}}$ cm $sec^{-\frac{1}{2}}$ obtained with two representative solutions are given as follows in parentheses after the values of t (in sec) for which they were found ($t_1 = 2$ sec, $m \approx 1.5$ mg sec^{-1}). For solution 1A these data are: 0.036 (3.10), 0.09 (3.17), 0.54 (3.30), 1.08 (3.26) and for solution 3A the

TABLE 1

PYRUVIC ACID, 25°C

Solution index	NaH_2PO_4 *concn./M*	Na_2HPO_4 *concn./M*	*KCl concn./M*	*Pyruvic acid concn.* $\cdot 10^3$*/M*	*Ionic strength, I*	*pH*	$D^{1/2} \cdot 10^3$*/cm* $sec^{-1/2}$	$\frac{k_{1,2}}{K_{2,1}} \cdot 10^{-12}$*/* $l^2 mole^{-2}$ sec^{-1}*
1A	0.182	0.0227	0.050	0.880	0.30	5.70	3.14	0.593
1B	0.091	0.0113	0.175	0.879	0.30	5.70	3.27	0.570
1C	0.048	0.0060	0.234	0.477	0.30	5.71	3.11	0.589
2A(1)	0.180	0.0226	—	0.495	0.25	5.78	3.14	0.579
2A(2)	0.180	0.0226	—	0.990	0.25	5.78	3.14	0.552
2A(3)	0.180	0.0226	—	1.98	0.25	5.77	3.41	0.565
2B	0.090	0.0113	—	0.495	0.124	5.86	2.80	0.577
2C	0.045	0.0056	—	0.496	0.062	5.94	2.62	0.639
3A	0.142	0.0471	0.017	0.546	0.30	6.19	3.08	0.567
3B	0.071	0.0236	0.158	0.546	0.30	6.18	2.97	0.568
3C	0.035	0.0118	0.230	0.546	0.30	6.17	3.07	0.571

* Each value is calcd. from eqn. (7b) with the D-value of the corresponding soln.

corresponding set runs: 0.036 (3.13), 0.09 (3.02), 0.54 (3.12), 1.08 (3.24). Generally, values at $t = 0.54$ and 1.08 sec are a little higher than those at $t = 0.036$ and 0.09 sec, which indicates that the dehydration process becomes active at the higher pulse times. Hence, the values of $D^{\frac{1}{2}}$ (25.0 ± 0.1°C) entered in Table 1 are those averaged for $t =$ 0.036 and 0.09 sec. The corresponding mean value for the acetate solution is $D^{\frac{1}{2}} = 2.93 \cdot 10^{-3}$ cm $sec^{-\frac{1}{2}}$. Because of the close proximity of the hydrogen wave the systematic error may be high, but it is certainly less than 5%.

(ii) For the *first wave* in the buffered solutions, scheme (2) obviously applies as given by the top line of scheme (1): HA, the reducible acid, can be formed from the non-hydrated anion, A^-, only. There is no significant concentration of HA in the bulk of the solution, while the anion-dehydration process is too slow (see (i), the bulk concentration of non-hydrated anion is taken as 95% of the total pyruvic acid concentration).

However, the decay rate of HA must also be considered. The rate of hydration

of HA ($k_{2,3}$) may appear as one term of a factor in the limiting current, *viz*, $(k_{2,1}+k_{2,3})^{-\frac{1}{2}}$ according to the approximation of reaction-volume theory [12,13]. Now, $k_{2,1}$ is of the order of 10^8 sec^{-1} (refs. 9 and 3) and $k_{2,3}$ is of the order of 1 sec^{-1} (refs. 3, 7 and 8), and hydration of HA is therefore irrelevant.

As $k_1 = k_{1,2}a_{H^+}\gamma_A \gg t^{-1}$ (*cf.* condition (5a)) we must use eqn. (3b). The extensive χ_1–F, f-tables, mentioned in the Introduction, give us the correct χ_1-value for each measurement of the limiting current. Equations (6) substituted in the definition of χ_1 yield

$$\chi_1 = (2a_{H^+}\gamma_A/K_{2,1}\gamma_{HA})t_1^{\frac{1}{2}}(k_{1,2}a_{H^+}\gamma_A + k_{2,1}\gamma_{HA})^{\frac{1}{2}} \quad (7a)$$

Since $K_{2,1} = k_{2,1}/k_{1,2}$ is of the order of 10^{-2} (refs. 9 and 3) and the pH of the solutions varies from 5.2 to 6.2, $k_{1,2}\,a_{H^+} \ll k_{2,1}$ and eqn. (7a) may be simplified to:

$$\chi_1 = 2a_{H^+}\, t_1^{\frac{1}{2}}(\gamma_A/\gamma_{HA}^{\frac{1}{2}})(k_{1,2}/K_{2,1})^{\frac{1}{2}} \quad (7b)$$

We have dropped activity coefficients at this stage and calculated $k_{1,2}/K_{2,1}$-values from the χ_1-data. A representative sample of the results is presented in Table 2. $k_{1,2}/K_{2,1}$-values were constant for short pulse times only, except for solutions 3A, 3B and 3C where, apparently, constancy was achieved for all pulse times used. A possible explanation for the inconstancy at higher pulse times is found by an inspection of eqn. (3b). For large values of $\chi_1\vartheta^{\frac{1}{2}}$, the factor before the square brackets in the summation can become very large. Since in the expansions within these brackets terms with powers of ϑ greater than 2 were omitted, our χ_1–F tables may have produced χ_1-values that were too high (*cf.* F_{exact} and F_{approx} of Table 3.1, ref. 1c). The results of solution 2A(1) may be an illustration of this. However, the set of solutions numbered 3, of which the results of only 3A are given, show less of this upward trend, but there χ_1 is relatively small.

This can in fact only be a part of the explanation. The very pronounced increase in $k_{1,2}/K_{2,1}$ for each of the two higher t-values in the series 2A(1), (2) and (3) (*i.e.*, with increasing pyruvate concentration) cannot be explained on this basis. This behaviour suggests that a further decay mechanism of the non-hydrated acid, HA, becomes operative at higher pulse times. This process must have a relaxation time, τ, which is dependent on concentration, *i.e.* it cannot be first-order. Neither can it be pseudo-first order, which suggests that association of HA must take place, *e.g.* into a hydrogen-bonded dimer (in that case τ decreases as c_{HA} increases). Pyruvic acid would thus get time to stabilize with respect to the anion—stated differently: $k_{2,1}$ is decreased—without losing the possibility of electron transfer with the electrode.

In acetate buffer, the $k_{1,2}/K_{2,1}$-values (Table 2) are also too high for the shortest pulse times, even if it is considered that the precision of these values is small because the current approaches that of the total wave rather closely. Here again, we can offer an explanation on the basis of the mechanism suggested in the preceding paragraph. Hydrogen-bonded structures of pyruvic acid with excess acetic acid may now be formed in the reaction layer (the τ of such a pseudo first-order process is constant).

In the last column of Table 1 we have listed the mean values of $k_{1,2}/K_{2,1}$ obtained with pulse times, $t = 0.036$ and 0.09 sec, again without relevant activity coefficients. From these results it can be concluded that there are no indications for a direct proton transfer from the buffer to the anion. An explanation of the higher results in acetate buffer on this basis is probably incorrect since linear free-energy relationships

TABLE 2

THE FIRST WAVE OF PYRUVIC ACID IN BUFFERED SOLUTIONS, $t_1 = 2$ SEC, $25.0 \pm 0.1°C$

Solution index (cf. Table 1)	*m/mg sec*$^{-1}$	*Pyruvate concn.*$\cdot 10^3$/ *M*	*pH*	*t/sec*	*i/μA*	χ_1*(eqn. (3b))*	$\frac{k_{1,2}}{K_{2,1}} \cdot 10^{-12}$/ *l*^{2} *mole*$^{-2}$ *sec*$^{-1}$
				0.036	10.25	4.34	0.588
1A	1.488	0.880	5.70	0.09	9.05	4.37	0.597
				0.54	7.17	5.57	0.630
				1.08	6.85	7.50	1.758
				0.036	5.20	3.53	0.569
2A(1)	1.566	0.495	5.78	0.09	4.72	3.60	0.588
				0.54	3.75	3.85	0.672
				1.08	3.55	4.05	0.745
				0.036	10.5	3.52	0.563
2A(2)	1.566	0.990	5.78	0.09	9.30	3.45	0.540
				0.54	7.80	4.12	0.750
				1.08	7.95	6.18	1.737
				0.036	20.9	3.56	0.549
2A(3)	1.566	1.98	5.77	0.09	19.1	3.66	0.581
				0.54	17.6	6.40	1.772
				1.08	17.7	>10	>4
				0.036	2.63	1.40	0.581
3A	1.603	0.546	6.19	0.09	2.46	1.36	0.552
				0.54	2.34	1.37	0.561
				1.08	2.44	1.41	0.599
				0.036	12.4	14.7	0.837
Acetate (see text)	1.587	0.546	5.24	0.09	9.15	13.9	0.749
				0.54	5.40	>14	>1
				1.08	4.70	—	—

(*cf.* Brönsted's catalysis law) would then predict an even greater effect for the acidic phosphate buffer components. No such effect can be discerned from Table 1. The influence of ionic strength and pH on $k_{1,2}/K_{2,1}$ must also be relatively small (except perhaps for solution 2C). The average value of $k_{1,2}/K_{2,1}$ (omitting solution 2C) is $\langle k_{1,2}/K_{2,1} \rangle = (0.573 \pm 0.006)\ 10^{12}\ l^2\ \text{mole}^{-2}\ \text{sec}^{-1}$. The standard error is given.

The value of $K_{2,1}$ may be found from the relationship:

$$K_{2,1} = K_i(K_{2,3} + 1)/(K_{1,4} + 1) \tag{8}$$

where K_i, the overall-dissociation constant of pyruvic acid, is given by Pedersen[14] as a function of the ionic strength, I. For $I = 0.30$, $K_i = 6.36 \cdot 10^{-3}$ moles l^{-1} (25°C). Further, the value of $K_{2,3} = 2.09$ (25°C) is found from the pulse-polarographic work in 0.30 *M* HCl, described below under (iii). Finally, $K_{1,4} = 0.054$ (ref. 9), and thus eqn. (8) gives $K_{2,1} = 1.86 \cdot 10^{-2}$ moles l^{-1} (25°C, $I = 0.30$). Using this non-thermodynamic value of $K_{2,1}$, we find $k_{2,1} = 1.06 \cdot 10^{10}$ l mole^{-1}sec^{-1}, which is approximately what would be expected for a diffusion-controlled proton-transfer reaction. The value of $k_{1,2}/K_{2,1}$ found should be multiplied by $\gamma_A{}^2/\gamma_{HA}$ (eqn. (7b)), but if $K_{2,1}$ is transformed

to the non-thermodynamic dissociation constant, the activity factor cancels out if it is assumed that $\gamma_A = \gamma_H = \gamma_\pm$.

A rather serious error may have been incurred by calculating $K_{2,1}$ from eqn. (8). If association of undissociated acid, HA, takes place in the reaction layer as we have supposed, this value of $K_{2,1}$ refers to the equilibrium of A^- with all non-hydrated species, HA, put together, since this is also true for K_i and $K_{2,3}$. But the $k_{1,2}/K_{2,1}$-values given in Table 1 were obtained at pulse times short enough to prevent association. Hence a (much) larger value of $K_{2,1}$, referring to monomer HA only, should have been substituted. This means that the value $k_{1,2} = 1.06 \cdot 10^{10}$ l mole^{-1} sec^{-1} must be considered to be a minimum value. We intend to consider this problem more closely in the future.

(iii) *The wave in* 0.30 *M HCl* was studied with a solution $1.016 \cdot 10^{-3}$ *M* in pyruvic acid. Anion is not present to a significant extent, so the right-hand side of scheme (1) has to be considered. Previous studies, in particular refs. 7,8, suggest a relaxation time for the hydration equilibrium of undissociated pyruvic acid, HA, of about 2 sec, so at the shortest pulse times possible the hydration process behaves as though frozen and the limiting current must be diffusion-controlled. For this purpose we have fitted a pulse time of 0.018 sec to our pulse polarograph and the limiting current was studied with eqn. (4) for $t = 0.018$ and 0.036 sec (replacing ω^* by the as yet unknown bulk concentration of non-hydrated HA). Using the mean value of the diffusion coefficient of the anion at $I = 0.30$ (Table 1, $D^{\frac{1}{2}} = 3.11 \cdot 10^{-3}$ cm sec$^{-\frac{1}{2}}$) we calculated the equilibrium concentration to be $0.328 \cdot 10^{-3}$ moles l^{-1}, so that $K_{2,3} = 2.09$ (67.7% of HA is hydrated), which is not much different from the value given in other references[3,9,10], which use non-polarographic techniques.

With increasing pulse times the limiting current becomes more and more kinetic. To attain any accuracy at all for the rate constants, we have used pulse times $t = 0.54$, 1.08 and 1.80 sec. As $k_{3,2}$ proves to be about 0.7 sec^{-1} (see below) we may not expect condition (5a): $k_{3,2} \ll t^{-1}$, which is a rather stringent one, to apply.

With condition (3a): $k_{3,2} + k_{2,3} \gg t^{-1}$, we do not fare too well either, but it is certainly better. So we use eqn. (3b) and find again $\chi_1 = 2(k_{3,2} + k_{2,3})^{\frac{1}{2}} t_1^{\frac{1}{2}} K_{2,3}^{-\frac{1}{2}}$ with our extended $\chi_1 - F, f$ tables. Results are given in Table 3. The accuracy cannot be high but even so the average value of $k_{3,2} = 0.68$ sec^{-1} (25°C, $I = 0.30$) agrees fairly well with Strehlow's value obtained with the pressure-jump method[8]: $k_{3,2} = 0.22 + 1.25\, C_{H^+} = 0.60$ sec^{-1} (25°C, extrapolated to $I = 0$). For $k_{2,3}$ we find $k_{2,3} = 2.09 \cdot 0.68 = 1.42$ sec^{-1} as an average.

TABLE 3

RATE-CONTROLLED LIMITING CURRENTS OF $1.016 \cdot 10^{-3}$ *M* PYRUVIC ACID IN 0.3 *M* HCl
$t_1 = 2$ sec, $m = 1.645$ mg sec^{-1}, $D^{1/2} = 3.11 \cdot 10^{-3}$ cm sec$^{-1/2}$, $\chi_1 = 2(k_{2,3} + k_{3,2})^{1/2} t_1^{1/2} K_{2,3}^{-\frac{1}{2}}$.

t/sec	$i/\mu A$	χ_1	$k_{2,3}$/sec^{-1}	$k_{3,2}$/sec^{-1}
0.54	5.68	1.90	1.31	0.63
1.08	5.74	1.97	1.40	0.68
1.8	5.94	2.05	1.52	0.73

Glyoxylic acid

For experiments of type (i) and (ii) the composition of the solutions of calcium

glyoxylate in citrate buffer are given in Table 4 (all concentrations being total concentrations).

(i) *Total wave.* Undissociated acid is not present in the bulk of the solution to any significant extent, so scheme (2) is represented by the left-hand side of scheme (1), non-hydrated glyoxylate, A^-, being the reducible species. Previous studies[2,5] suggest a relaxation time for the hydration equilibrium of glyoxylate of $(k_{4,1}+k_{1,4})^{-1} \approx (0.023+1.42)^{-1}=0.70$ sec; therefore at the shortest pulse times, $t=0.018$ and 0.036 sec, the hydration process appears as almost frozen and the limiting current must be nearly diffusion-controlled. On the other hand, condition (5a): $k_{4,1} \approx 0.023 \text{ sec} \ll t^{-1}$, seems to be fulfilled for pulse times up to 2 sec and eqn. (5b) should be valid for all pulse times used ($0.018 < t < 1.80$). As set out in the Introduction, this equation can be split into a diffusion ($i_d : j=0$, corresponding to eqn. (4) with ω^* replaced by c_A^*-) and a kinetic ($i_k : j=1,2\ldots$) part. At short pulse times, the diffusion part dominates, giving us c_A^* and thus $K_{1,4}$, whereas at the larger t-values the rate constants, $k_{1,4}$ and $k_{4,1}$, can be deduced. The following iteration procedure was applied: First, i_k was neglected for pulse times 0.018 and 0.036 sec, and a tentative value of $K_{1,4}$ calculated with eqn.

TABLE 4

GLYOXYLIC ACID, 25°C

Solution index	*Citric acid concn./ M*	*Sodium citrate concn./ M*	*KCl concn./ M*	*Glyoxylate concn.·10³/ M*	*Ionic strength, I*	*pH*	$K_{1,4}$	$k_{4,1}\cdot 10^3/\text{sec}^{-1}$	$k_{1,4}/\text{sec}^{-1}$
1A	0.0125	0.0375	0.1092	8.02	0.3	5.27	68.5	6.99	0.479
1B	0.0125	0.0375	0.3092	8.02	0.5	5.17	71.4	7.04	0.503
1C	0.0250	0.0750	0.1184	8.02	0.5	5.21	73.8	9.38	0.692
2	0.0150	0.0750	0.0928	8.04	0.5	5.57	72.7	8.17	0.594
3	0.00873	0.0750	0.0756	8.00	0.5	5.89	73.8	7.20	0.531

(4) using a diffusion coefficient equal to the average found for pyruvate anion ($I=0.30$; Table 1): $D^{\frac{1}{2}}=3.1\cdot 10^{-3}$ cm $\text{sec}^{-\frac{1}{2}}$ (which is also the value found from conductance measurements[2]). Next, from this value of $K_{1,4}$ the values of i_d were calculated for the pulse times 0.54, 1.08 and 1.80 sec. From the resulting values of $i_k=i-i_d$, the kinetic parameter, $\chi_2=k_{1,4}t_1$, was obtained from the Tables mentioned in the Introduction. Using this value of χ_2, we applied a small corrective i_k to the currents at short pulse times, including $t=0.09$ sec, which resulted in a better mean value of $K_{1,4}$. Thereafter, the whole procedure was repeated until no significant changes in the values of $K_{1,4}$ and χ_2 were found. Table 5 presents a typical set of final values for one of the solutions. Mean values of $K_{1,4}$, $k_{1,4}$ and $k_{4,1}$ for all solutions studied are given in Table 4. The differences between the velocity data are clearly due to general acid–base catalysis.

(ii) For the *first wave* in the citrate buffer solutions, as in the pyruvic acid case, the top line of scheme (1) is all we should have to deal with. There may be up to 1% of hydrated acid present in the bulk of the solution but its specific rate of dehydration can be shown from the published data[2,5] to be about 10^7 times slower than the pseudo first-order specific rate of proton transfer to A^-, the non-hydrated anion. Of much greater concern to us is the short relaxation time of the anion hydration process which may be as short as 1.4 sec (solution 1C, Table 4). An idea of the error made

TABLE 5

GLYOXYLIC ACID IN CITRATE BUFFER, SOLUTION #2 (*cf.* TABLE 4)
$D^{1/2} = 3.1 \cdot 10^{-3}$ cm sec$^{-1/2}$, $t_1 = 2$ sec, $m = 1.67$ mg sec^{-1}.

t/sec	$i/\mu A$	$i_d/\mu A$	$i_k/\mu A$	$K_{1,4}$	$\chi_2 = k_{1,4}t_1$
0.018	5.26	5.21	0.05	72.0	
0.036	3.72	3.65	0.08	74.1	
0.09	2.58	2.46	0.12	72.0	
0.54	1.61	1.27	0.34		1.21
1.08	1.60	1.10	0.50		1.19
1.80	1.73	1.04	0.69		1.18

by considering the dehydration process as frozen can be obtained from the ratio, i_k/i_d, of Table 5, from which we presume that the longest pulse time to be used is 0.09 sec at the most (as the accuracy of our results is not very good in this case anyway).

In section (iii) below we shall see that $k_{2,3} \ll k_{2,1}$, so the decay of non-hydrated acid HA into anything else than A^- is not to be considered at this stage, although stabilization of HA with citric acid is a possibility (see below).

For the same reasons as given for pyruvic acid (ii), we can use eqns. (3b) and (7b) and determine the kinetic parameter, $k_{1,2}\,\gamma_A^2/(\gamma_{HA}\,K_{2,1})$ from the limiting current of the first wave with $t = 0.018$, 0.036 and 0.09 sec. The results are given in Table 6, where activity coefficients in the last column have again been omitted.

TABLE 6

FIRST WAVE OF GLYOXYLIC ACID IN CITRATE BUFFERS
$t_1 = 2$ sec, $D^{1/2} = 3.08 \cdot 10^{-3}$ cm sec$^{-1/2}$, 25.0 ± 0.1°C. The equilibrium concentration of non-hydrated anion is denoted by c_A^*.

Solution index	$c_A^* \cdot 10^3$/ *moles* l^{-1}	m/*mg* sec^{-1}	t/sec	$i/\mu A$	χ_1	$\frac{k_{1,2}}{K_{2,1}} \cdot 10^{-12}$/ $l^2 moles^{-2}\ sec^{-1}$	
1A	0.115	1.603	0.018	3.39	13.7	0.820	0.76
			0.036	2.73	12.7	0.701	
			0.09	2.21	16.5	1.183	
1B	0.111	1.598	0.018	3.62	17.4	0.825	0.78
			0.036	2.88	16.4	0.731	
			0.09	2.13	17.0	0.794	
1C	0.107	1.629	0.018	3.51	17.0	0.944	0.96
			0.036	2.87	17.2	0.976	
			0.09	2.13	19.0	1.189	
2	0.109	1.634	0.018	2.08	6.65	0.765	0.83
			0.036	1.91	6.89	0.821	
			0.09	1.61	7.20	0.896	
3	0.106	1.617	0.018	1.11	3.09	0.719	0.71
			0.036	1.03	3.01	0.682	
			0.09	0.96	3.09	0.716	

The considerable variation of $k_{1,2}/K_{2,1}$ with t may be due in part to a systematic error incurred when determining i. Although the height of the first wave generally has been reckoned from the point of inflection between both waves, this procedure has not been applied consistently. Rather, in any set of waves with different t, this inflection was considered to occur at one and the same potential. Now, a closer inspection of the waves reveals that this is probably not the case. This error in i returns in χ_1 considerably amplified because of the high values of χ_1 that we are finding here: the larger χ_1, the larger the relative error in χ_1 and, even more so, in $k_{1,2}/K_{2,1}$. The great scatter found with pyruvic acid in acetate buffer (Table 2) may have been due to the same cause. Also, high pulse times increase the relative error in $k_{1,2}/K_{2,1}$ since then the first wave approaches i_d. Finally, as we have discussed under pyruvic acid (ii), for obtaining high accuracy in large χ_1-values, eqn. (3b) should have been used with powers of ϑ greater than 2 if higher ϑ-values are used. All these are reasons for not using pulse times greater than $t=0.09$ sec. Consequently, in Table 6 we have given average of $k_{1,2}/K_{2,1}$ over $t=0.018$ and 0.036 sec only, if $\chi_1 > 10$, but over all three pulse times otherwise.

There is a considerable trend in these $k_{1,2}/K_{2,1}$-values, clearly as a function of the concentrations of buffer components, in particular the acidic buffers. This can be demonstrated by plotting $K_{2,1}/k_{1,2}=k_{2,1}/k_{1,2}^2$ against the total citric acid concentration for solutions 1C and 1B. The straight line through these points has an intercept which corresponds with $k_{1,2}/K_{2,1}=0.66\cdot 10^{12}$ l^2 mole^{-2}sec^{-1}. If we next plot the values of $K_{2,1}/k_{1,2}$ of solutions 1C, 2 and 3 against the total citric acid concentration, we find the same straight line to be a reasonably good fit for these points as well. This way of plotting was followed on the assumption that HA decays in two directions: into A^- and into associates with citric acid species, H_iX_l, so that the true decay constant which has actually been determined is $k_{2,1}+k'c_{H_iX}$. This procedure does not prove that the underlying assumption is correct, but from our experience with pyruvic acid we consider the alternative less probable: proton transfer from acidic buffer components to A^- (extrapolation on the basis of this assumption gives $k_{1,2}/K_{2,1}=0.61\cdot 10^{12}$).

To calculate $k_{1,2}$, the value of $K_{2,1}$ is required. According to eqn. (8), we need values of K_i, $K_{2,3}$ and $K_{1,4}$ at 25°C and $I=0.30$. Only $K_{1,4}$ is available under the conditions stated. From Table 4, solution 1A, we take $K_{1,4}=68.5$. Kuta and Valenta[5] found with cyclic voltammetry $K_{2,3}=1.7\cdot 10^3$ at 22°C and in 1 M H_2SO_4. Unfortunately, no accurate value of K_i is available. The value measured by Öjelund and Wadsö[11] is probably the most accurate: $K_i=3.5\cdot 10^{-4}$ moles l^{-1} at 25°C, but at a very low ionic strength. However, the same authors give a corresponding value for pyruvic acid: $K_i=2.5\cdot 10^{-3}$, whereas the value of Pederson at $I=0.30$—which we have used—was $K_i=6.36\cdot 10^{-3}$, which is about 2.5 times larger. It seems reasonable to multiply Öjelund and Wadsö's value for the K_i of glyoxylic acid by the same factor 2.5, which yields $K_i=8.8\cdot 10^{-4}$. Then eqn. (8) gives $K_{2,1}=2.1\cdot 10^{-2}$ moles l^{-1} and $k_{1,2}=1.4\cdot 10^{10}$ l mole^{-1} sec^{-1}. Again this value, approximate as it already is, may have to be considered as a minimum value for the same reason as given for pyruvic acid (ii).

(iii) The wave in 0.30 M HCl was studied with a solution of rather concentrated glyoxylic acid (0.0400 M) in order to achieve currents of 2–3 μA. No anion is present, so the right-hand side of scheme (1) should apply.

Previous data[2,5] suggest that $k_{2,3} \gg t^{-1}$ and $k_{3,2} \ll t^{-1}$ hold fairly well in this

TABLE 7

0.0400 M GLYOXYLIC ACID IN 0.3 M HCl
$m = 1.584$ mg sec^{-1}, $t_1 = 2$ sec, $D^{1/2} = 3.08 \cdot 10^{-3}$ cm sec$^{-1/2}$, 25.0 ± 0.1°C.

t/sec	$i/\mu A$	$\frac{k_{3,2}}{K_{2,3}} \cdot 10^4$/sec^{-1}	
		eqn. (3*b*)	*eqn.* (25) *ref.* 1*d*
0.036	2.05	0.216	0.216
0.09	2.055	0.211	0.210
0.54	2.335	0.211	0.209
1.08	2.69	0.216	0.214

instance, so that conditions (3a) and (5a) are fulfilled simultaneously. Hence, eqns. (3b) and (5b) can both be used. Results obtained with eqn. (3b) are given in Table 7 (3rd column). Equation (5b) has a significant diffusion part at $t = 0.036$ sec, but this is too small in the present case to evaluate an accurate value of $K_{2,3}$ and further work will be necessary. Instead, we have used eqn. (25) from ref. 1d which is an approximation valid if $k_2 t \to \infty$. Nevertheless, the results, given in column 4 of Table 7, agree quite well with those obtained from eqn. (3b).

For the present, we shall adopt for $K_{2,3}$ the value of Kůta and Valenta[5] mentioned under (ii) ($K_{2,3} = 1.7 \cdot 10^3$) in order to calculate the individual rate constants. This gives $k_{2,3} = 61$ sec^{-1} and $k_{3,2} = 3.6 \cdot 10^{-2}$ sec^{-1} from the average values of $k_{3,2}/K_{2,3}$ in Table 7.

The hydration of pyruvate anion

So far we have been able to derive all relevant rate constants of hydration for pyruvic and glyoxylic acids except those for pyruvate anion. We can make a rough estimate of the latter if we assume that the shift in energy levels (including that of the transition state) relevant to the hydration process of the *acid* and which occurs when R = H is replaced by R = CH_3 (scheme (1)), is the same for the process of *anion* hydration. In terms of rate constants this means that the ratios, $k_{2,3}(\mathrm{p})/k_{2,3}(\mathrm{g}) = 1.42/60 = 0.024$ and $k_{3,2}(\mathrm{p})/k_{3,2}(\mathrm{g}) = 0.68/0.036 = 19$ (where p = pyruvic acid, g = glyoxylic acid) which apply to the acids in 0.3 M HCl, are the same for the ratios, $k_{1,4}(\mathrm{p})/k_{1,4}(\mathrm{g})$ and $k_{4,1}(\mathrm{p})/k_{4,1}(\mathrm{g})$, respectively, in any of the buffers used for the measurements on the glyoxylate anion. If we choose the citrate buffer 1B of Table 4 with $k_{1,4}(\mathrm{g}) = 0.503$ sec^{-1} and $k_{4,1}(\mathrm{g}) = 704 \cdot 10^{-3}$ sec^{-1}, we obtain for the hydration constants of pyruvate anion, $k_{1,4}(\mathrm{p}) = 0.012$ sec^{-1} and $k_{4,1}(\mathrm{p}) = 0.134$ sec^{-1}. The ratio $k_{1,4}(\mathrm{p})/k_{4,1}(\mathrm{p})$ which should be about 0.054 (ref. 9), is actually somewhat high: 0.09.

ACKNOWLEDGEMENT

The award of a fellowship to one of us (A.W.F.) by the Netherlands Foundation for Chemical Research (SON) with financial aid from the Netherlands Organization for the Advancement of Pure Research (Z.W.O.) is gratefully acknowledged.

SUMMARY

We have shown that for pyruvic and glyoxylic acids (which in aqueous solution are assumed to behave as indicated by scheme (1)) the method of pulse polarography enables more relevant kinetic and equilibrium constants to be determined than by any other single method so far applied to the study of these acids, including ordinary polarography.

A number of the equations for *instantaneous* currents previously derived for tackling simple kinetic and diffusion problems in pulse polarography[1a-d] could be applied and tested with success. The possibility of varying the pulse time, in this case from 0.018 to 1.80 sec, was especially of value in providing a new insight into the validity of the reaction scheme.

There are strong indications that scheme (1) is not complete. Pyruvic acid reduction in phosphate buffer showed a kinetic behaviour which could be explained only if association of this acid, probably into a reducible hydrogen-bonded dimer, was assumed.

REFERENCES

1a A. A. A. M. BRINKMAN AND J. M. LOS, *J. Electroanal. Chem.*, 7 (1964) 171; 1b, with A. W. FONDS, *ibid.*, 14 (1967) 43; 1c, *ibid.*, 14 (1967) 269; 1d, *ibid.*, 14 (1967) 285.
2 J. KŮTA, *Collection Czech. Chem. Commun.*, 24 (1959) 2532.
3 M. BECKER AND H. STREHLOW, *Z. Elektrochem.*, 64 (1960) 129, 813.
4 M. TAKAGI, *Bull. Univ. Osaka Prefect. Ser. B*, 11 (1961) 177.
5 J. KŮTA AND P. VALENTA, *Collection Czech. Chem. Commun.*, 28 (1963) 1593.
6 YA. I. TUR'YAN, *Soviet Electrochem.*, 1 (1965) 426.
7 M. EIGEN, K. KUSTIN AND H. STREHLOW, *Z. Physik. Chem. N.F.*, 31 (1962) 140.
8 H. STREHLOW, *Z. Elektrochem.*, 66 (1962) 392.
9 M. BECKER, *Ber. Bunsenges. Phys. Chem.*, 68 (1964) 669.
10 V. GOLD, G. SOCRATES AND M. R. CRAMPTON, *J. Chem. Soc.*, (1964) 5888.
11 G. ÖJELUND AND I. WADSÖ, *Acta Chem. Scand.*, 21 (1967) 1408.
12 J. M. LOS AND K. WIESNER, *J. Am. Chem. Soc.*, 75 (1953) 6346; J. M. LOS, L. B. SIMPSON AND K. WIESNER, *ibid.*, 78 (1956) 1564.
13 J. PALDUS AND J. KOUTECKÝ, *Collection Czech. Chem. Commun.*, 23 (1958) 376.
14 K. J. PEDERSEN, *Acta Chem. Scand.*, 6 (1952) 243.

ELECTROANALYTICAL CHEMISTRY AND INTERFACIAL ELECTROCHEMISTRY
Elsevier Sequoia S.A., Lausanne – Printed in The Netherlands

LOGARITHMIC ANALYSIS OF TWO OVERLAPPING D.C. POLAROGRAPHIC WAVES

I. REVERSIBLE AND TOTALLY IRREVERSIBLE PROCESSES

IVICA RUŽIĆ AND MARKO BRANICA
Department of Physical Chemistry, Institute "Ruder Bošković", Zagreb, Croatia (Yugoslavia)
(Received February 15th, 1969)

INTRODUCTION

When two d.c. polarographic waves are close to each other so that the first wave attains its limiting current in the potential region where the second wave begins, it is not possible to obtain by an ordinary logarithmic analysis the limiting current, the half-wave potential ($E_{\frac{1}{2}}$) and the slope of the logarithmic plot (αn) for each wave. Therefore, a mathematical analysis which would enable evaluation of these parameters is desirable. For such an analysis the linear additivity of the currents should be fulfilled at each point analysed.

The polarographic analysis of a mixture of two, or several, reducible compounds the half-wave potentials of which are in close proximity to each other* has been described by several authors[1-4] who, however, determined only diffusion currents, *i.e.*, the concentration of components in a mixture. They determined the experimental values for half-wave potentials and the number of electrons involved in the reaction for each of the components separately. In this paper, we present the analyses of two overlapping reversible or totally irreversible d.c. polarographic waves for the case where the values of half-wave potentials, limiting currents, and the number of electrons involved in the reaction for each of the components are not known. From the recorded polarogram only the sum of the currents at given potential can be found. Several examples of composite polarograms are given in Fig. 1.

PROCEDURE

For the polarogram composed of two overlapping waves, the logarithmic curve should be drawn. The resulting curve has an inflection point and two linear parts. The linear parts should be extrapolated and if these straight lines intersect in the range of $\log[i/(i_d - i)]$between $+2$ and -2, the slope of the steeper straight line must be corrected. In all other cases the slopes of these straight lines already correspond to the real $\alpha_1 n_1$ and $\alpha_2 n_2$. The ratio of diffusion currents (m) is evaluated from the inflection point. In the simplest case, the value of m is equal to that of the inflection

* "Ordinarily we may consider two waves to be well enough separated for practical work if their half-wave potentials differ by 0.3 V or more"[5].

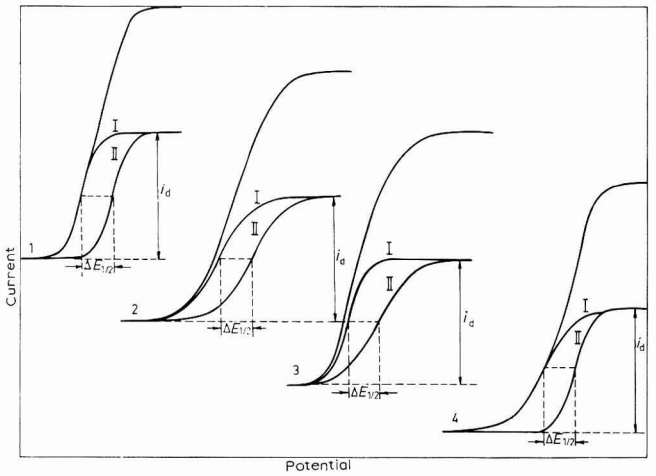

Fig. 1. Polarograms of two overlapping waves of equal height: (1), $1/a'_1 = 30$ mV and $1/a'_2 = 30$ mV; (2), $1/a'_1 = 60$ mV, $1/a'_2 = 60$ mV; (3), $1/a'_1 = 30$ mV, $1/a'_2 = 60$ mV; (4), $1/a'_1 = 60$ mV, $1/a'_2 = 30$ mV.

point. In other cases, some expressions using iteration should be used. Using the true value of the diffusion current ratio, m, the shifts of the linear parts of the logarithmic curve of the composite wave are calculated; from these the half-wave potentials of the separate waves can be obtained.

A logarithmic analysis of a single diffusion-controlled polarographic wave can be made by plotting the value of $\log[i/(i_d - i)]$ against the potential (E)[6]. This can be written:

$$\log x = -a'E + \log A \tag{1}$$

where $x = i/(i_d - i)$, $a' = a \log e = (nF/RT) \log e$ and $A = e^{aE_{1/2}} = 10^{a'E_{1/2}}$ (for details see Appendix I). The analysis of two overlapping waves is performed analogously (for details see Appendices I, II and III). The total currents, $(i_1 + i_2)$ and $(i_{d1} + i_{d2})$, are introduced instead of i and i_d, respectively. The sum of two overlapping waves can be expressed as follows:

$$x = [mx_1(1 + x_2) + x_2(1 + x_1)]/[m(1 + x_2) + 1 + x_1] \tag{2}$$

The ratio, $i/(i_d - i)$, for each component separately is $x_1 = A_1 e^{-a_1 E}$ and $x_2 = A_2 e^{-a_2 E}$, respectively, where $A_1 = e^{a_1 (E_{1/2})_1}$ and $A_2 = e^{a_2 (E_{1/2})_2}$. When the waves are very close to each other the composite polarogram resembles that of a single wave; however, the logarithmic analysis of the composite polarogram gives a curve with an inflection point and two linear parts (Fig. 2). At the foot of the wave, *i.e.*, at sufficiently positive potentials, the conditions $x_1 \ll 1$ and $x_2 \ll 1$ are fulfilled, and eqn. (2) becomes:

$$x = x_1^* = (mx_1 + x_2)/(m + 1) \tag{3}$$

At the top of the composite wave, *i.e.*, at sufficiently negative potentials, it can be supposed that $x_1 \gg 1$ and $x_2 \gg 1$, and thus eqn. (2) becomes:

$$x = x_2^* = (m + 1)x_1 x_2/(mx_2 + x_1) \tag{4}$$

Equations (3) and (4) correspond to the linear parts of the logarithmic curve.

If the condition $x_1 \gg x_2$ is fulfilled for all potentials, eqns. (3) and (4) yield:

$$x_1^* = mx_1/(m+1) = mA_1 e^{-a_1 E}/(m+1) = A_1^* e^{-a_1 E} \quad (5)$$

and

$$x_2^* = (m+1)x_2 = (m+1)A_2 e^{-a_2 E} = A_2^* e^{-a_2 E} \quad (6)$$

The potentials where x_1^* and x_2^* are equal to 1, are denoted as E_1 and E_2, respectively. As shown in Fig. 2, the potentials E_1 and E_2 were obtained experimentally from the intersection point of the potential axis with the extrapolated linear parts of the logarithmic plot. At these potentials the relations, $A_1^* = e^{a_1 E_1}$ and $A_2^* = e^{a_2 E_2}$, are valid.

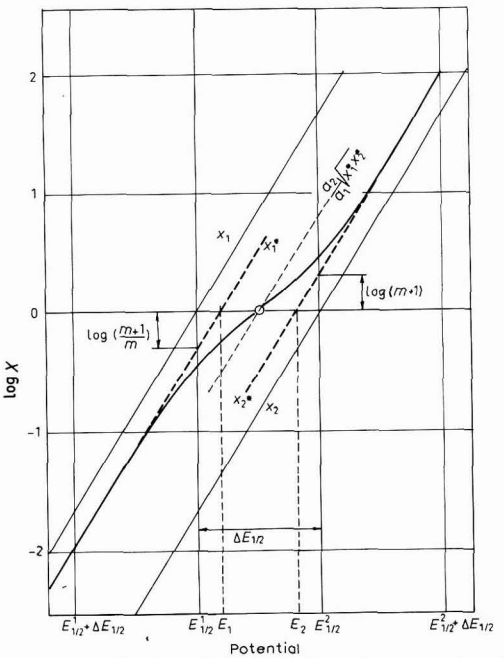

Fig. 2. Logarithmic analysis of the first polarogram given in Fig. 1. The intersection of log x and log $(x_1^* x_2^*)^{\frac{1}{2}}$ gives the inflection point as indicated in Appendix II, eqn. (26).

From eqns. (5) and (6) it follows that:

$$A_1 = (m+1)A_1^*/m \text{ and } A_2 = A_2^*/(m+1)$$

i.e.,

$$(E_{\frac{1}{2}})_1 = E_1 + (1/a_1') \log[(m+1)/m]$$

and

$$(E_{\frac{1}{2}})_2 = E_2 + (1/a_2') \log (m+1)$$

At the inflection point, x is equal to the current ratio, m ($m = x_i$, see Appendix II). When the condition $x_1 \gg x_2$ is not fulfilled for all potentials, more elaborate procedures depending on the ratio of the slopes, a_1 and a_2, should be chosen. There are three cases: (i) the slopes are equal, $a_1 = a_2$; (ii) the slope of the first wave is steeper, $a_1 > a_2$, and (iii) the slope of the second wave is steeper, $a_1 < a_2$.

(*i*) $a_1 = a_2$

In the case of two overlapping waves of equal slope, the half-wave potentials $(E_{\frac{1}{2}})_1$ and $(E_{\frac{1}{2}})_2$, can be evaluated (starting from eqns. (3) and (4)) from the following relations:

$$A_1^* = (mA_1 + A_2)/(m+1), \quad A_2^* = (m+1)A_1A_2/(mA_2 + A_1) \tag{7}$$

and

$$(E_{\frac{1}{2}})_1 = (1/a')\log A_1, \quad (E_{\frac{1}{2}})_2 = (1/a')\log A_2$$

(illustrated graphically in Fig. 3).

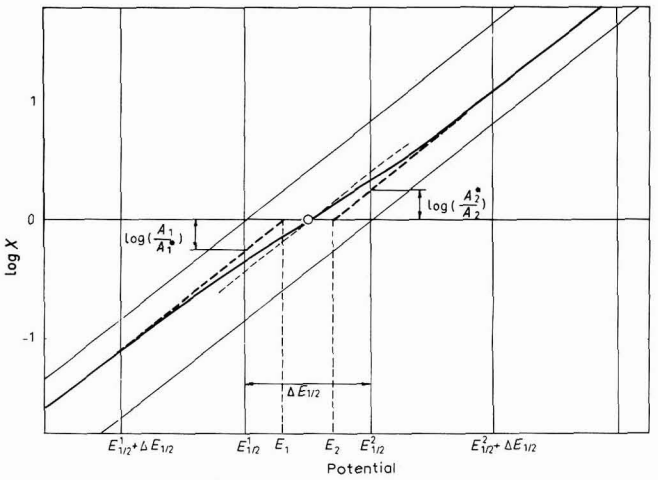

Fig. 3. Logarithmic analysis of the second polarogram given in Fig. 1.

(*ii*) $a_1 > a_2$

When the potentials are more negative than the second half-wave potential, eqn. (6) is valid and the following expression can be used:

$$A_2 = A_2^*/(m+1) \quad i.e., \quad (E_{\frac{1}{2}})_2 = E_2 - (1/a_2')\log(m+1) \tag{8}$$

However, when the potentials are more positive than the first half-wave potential, eqn. (5) is not valid. Therefore, the potential, $\overline{E_1}$, at which the condition, $x = x_1^* = x_2$, is fulfilled, should be found. At this potential the slope $\bar{a}_1$ can be derived from eqn. (2) as:

$$\bar{a}_1 = a_2 + \{(m(m+2)a_1 - ma_2)/(m+1+2A_2^* e^{a_2\overline{E_1}})\}/(m+1) \tag{9}$$

When $A_2^* e^{a_2\overline{E_1}} \ll 1$, eqn. (9) can be simplified:

$$\bar{a}_1 = a_1 + (a_2 - a_1)/(m+1)^2 \tag{10}$$

The slope, a_1, can be evaluated from the experimentally obtained slopes, a_2 and $\bar{a}_1$, using relation (9) or (10). The half-wave potential, $(E_{\frac{1}{2}})_1$, can be calculated using relations (7) and (8):

$$(E_{\frac{1}{2}})_1 = (1/a_1')\log[\{(m+1)^2A_1^* - A_2^*\}/m(m+1)]$$

The corresponding analysis is shown in Fig. 4.

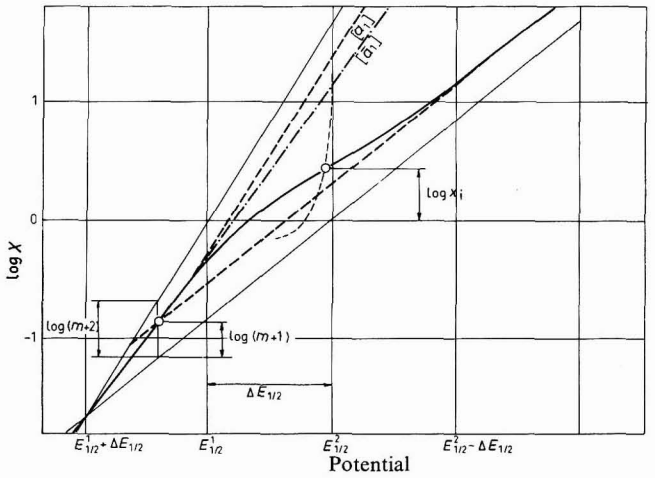

Fig. 4. Logarithmic analysis of the third polarogram from Fig. 1. The inflection point was obtained by successive iteration (see Appendix II).

(*iii*) $a_1 < a_2$

When the potentials are more positive than the first half-wave potential, eqn. (5) is valid and the following expressions can be written:

$$A_1 = (m+1)A_1^*/m \quad i.e., \quad (E_{\frac{1}{2}})_1 = E_1 + (1/a_1')\log[(m+1)/m] \tag{11}$$

When the potentials are more negative than the second half-wave potential, eqn. (6) is not valid. Therefore, the potential, $\bar{E}_2$, at which the condition, $x = x_1^* = x_2$, is fulfilled should be defined. At this potential the slope, $\bar{a}_1$, can be expressed using eqn. (2) as follows:

$$\bar{a}_2 = \frac{\{m(2m+1)a_1 + ma_2 + [(2m+1)a_2 + m^2 a_1]A_1^* e^{a_1\bar{E}_2}\}}{(m+1)[(m+1)A_1^* e^{a_1\bar{E}_2} + 2]} \tag{12}$$

When $A_1^* e^{a_1\bar{E}_2} \gg 1$, eqn. (12) becomes:

$$\bar{a}_2 = a_2 + m^2(a_1 - a_2)/(m+1)^2 \tag{13}$$

The slope, a_2, can be calculated from experimentally obtained slopes, a_1 and $\bar{a}_2$, using eqns. (12) or (13). The half-wave potential, $(E_{\frac{1}{2}})_2$, can be calculated combining relations (7) and (11):

$$(E_{\frac{1}{2}})_2 = (1/a_2')\log[(m+1)A_1^* A_2^*/\{(m+1)^2 A_1^* - m^2 A_2^*\}]$$

The analysis of two overlapping d.c. polarographic waves where $a_1 < a_2$ is shown in Fig. 5.

Determination of the diffusion current ratio from the inflection point

Generally, the inflection point of the plot, log x *vs.* potential, can be expressed by relation (25) (Appendix II). In order to obtain a simpler relation some approximations depending on the values of a_1 and a_2 should be made. When the slope of the first wave is steeper than that of the second wave ($a_1 > a_2$), the third term in the nume-

rator as well as in the denominator (eqn. 25) is often neglected. A simpler relation for the inflection point is:

$$x_i^2 = [x_1^* + (a_1^2 - a_2^2)x_2^*/a_2^2(m+1)^2]/(a_1^2/a_2^2 x_2^*) \tag{14}$$

When the slope of the first wave is smaller than that of the second wave ($a_1 < a_2$), eqn. (25) can be simplified in the following manner:

$$x_i^2 = \frac{a_2^2 x_1^* - (a_1^2 - a_2^2)x_1^* x_2^*/[(m+1)^2 x_1^* - m^2 x_2^*]}{[a_1^2(m+1)^2 x_1^* - m^2(a_1^2 - a_2^2)x_2^*]/(m+1)^2 x_1^* x_2^*} \tag{15}$$

When $(m+1)^2 x_1^* \gg m^2 x_2^*$ at the potential range close to the inflection point, eqn. (15) yields eqn. (14), and if, moreover, $x_1^* \gg (a_1^2 - a_2^2)x_2^*/a_2^2(m+1)^2$, eqn. (14) yields eqn. (28) (see Appendix II). The values of x_1^*, x_2^*, $a_1$and a_2 are known, while the m-value should be appraised approximately.

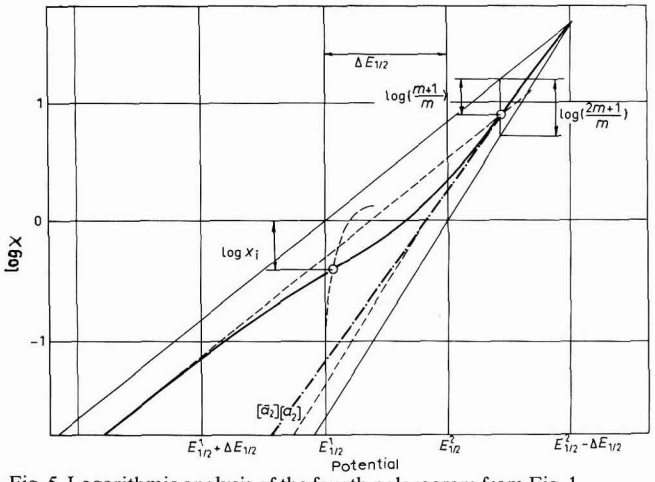

Fig. 5. Logarithmic analysis of the fourth polarogram from Fig. 1.

The current ratio is obtained with sufficient accuracy by application of successive iteration in eqns. (25), (15) or (14). The slopes, a_1 and a_2, required for these equations can be calculated using relations (9) and (12) or (10) and (13). The iteration is performed by applying the following equation:

$$x_1 x_2 = x_2^*(x_1^* - x_i)/(x_i - x_2^*) \tag{16}$$

in combination with eqns. (3) and (4). If eqns. (5) and (6) can be used instead of eqns. (3) and (4), expression (16) yields:

$$m = (x_i - x_2^*)x_1^*/(x_1^* - x_i) \tag{17}$$

When $x_1^* \gg x_i \gg x_2^*$, m becomes x_i. The inflection point should be estimated; from this the first approximate value of m can be calculated. Using eqns. (25), (15) or (14), respectively, a new, more precise, value for the inflection point is obtained. After several successive iterations, an m-value of satisfactory accuracy is obtained.

DISCUSSION

By logarithmic analysis of a composite polarogram it is possible to determine the position of the inflection point; from this the ratio of limiting currents, i_{d1}/i_{d2}, can be calculated. From the linear parts of the logarithmic plot of the composite wave, the half-wave potentials and the number of electrons (n) involved in the reversible electrode reaction, or αn in totally irreversible electrode reactions, can be found. When the difference between the potentials E_1 and E_2 is larger than 20 mV, and when the slopes of the waves correspond to $(F/RT)\alpha n = 60$ mV, it is possible to analyse two waves with satisfactory accuracy. The limitation for the procedure described is given in Fig. 6. Two waves can be separated well enough by classical analysis if the difference between their half-wave potentials exceeds $(\alpha_1 n_1 + \alpha_2 n_2)2F/RT$ (*i.e.*, between 120 and 480 mV). Using the d.c. polarographic method in the case of overlapping waves it is not possible to recognize whether one or both waves are quasi-reversible and another independent method should be used.

The procedure proposed was tested experimentally on polarograms of indium and cadmium solutions. D.c. polarograms of 10^{-4} M cadmium, 10^{-4}–$3 \cdot 10^{-4}$ M indium, and of their mixture in 10^{-2}–$3 \cdot 10^{-2}$ M NaCl, 10^{-3} M $HClO_4$ and 0.49 M $NaClO_4$ ($E_{\frac{1}{2}} = 46$–53 mV) have been recorded on a Radiometer PO-4. The current ratio, i_{d1}/i_{d2}, slopes n_1 and n_2, and the half-wave potentials, $(E_{\frac{1}{2}})_1$ and $(E_{\frac{1}{2}})_2$, were found to be within the limits of error of the technique used.

The method described was successfully applied also in the analysis of two overlapping waves of the reduction of Ni(II)aquo and Ni(II)mono-acetylacetonato complex[7].

APPENDIX

I. The equation for the reversible or totally irreversible single wave can be written as:

$$E = E_{\frac{1}{2}} + (RT/\alpha nF)\ln\{(i_d - i)/i\} = E_{\frac{1}{2}} - (1/a)\ln x \qquad (18)$$

where $a = \alpha nF/RT$ (taking $\alpha = 1$ for the reversible wave) and $x = i/(i_d - i)$. For each of the two overlapping waves, eqn. (18) is valid if the additivity of the currents is fulfilled. Therefore

$$i_1 = x_1 i_{d1}/(1 + x_1) \qquad \text{and} \qquad i_2 = x_2 i_{d2}/(1 + x_2)$$

The sum of the currents, $i = i_1 + i_2$ and $i_d = i_{d1} + i_{d2}$, becomes:

$$x = i/(i_d - i) = \{i_{d1}x_1(1 + x_2) + i_{d2}x_2(1 + x_1)\}/\{i_{d1}(1 + x_2) + i_{d2}(1 + x_1)\} \qquad (19)$$

If the limiting current ratio, i_{d1}/i_{d2}, is denoted as m, eqn. (17) yields:

$$x = \frac{mx_1(1 + x_2) + x_2(1 + x_1)}{m(1 + x_2) + 1 + x_1} = \frac{mx_1 + x_2 + (m + 1)x_1x_2}{mx_2 + x_1 + m + 1} \qquad (20)$$

II. Equation (20) can be written as:

$$x = \frac{(mx_1 + x_2)/(m + 1) + x_1x_2}{(mx_2 + x_1)/(m + 1) + 1} = \frac{x_1^* + x_1x_2}{x_1x_2/x_2^* + 1} \qquad (21)$$

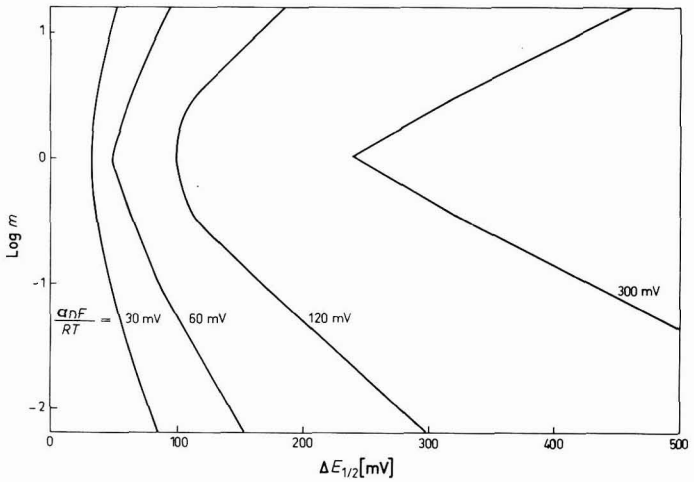

Fig. 6. Limitations to the separation of two overlapping waves of the same slope. The separation is possible when $\Delta E_{\frac{1}{4}}$ is above the plotted limit. Waves with $\Delta E_{\frac{1}{4}}$ greater than $(\alpha_1 n_1 + \alpha_2 n_2)(2\,F/RT)$ are already separated for all m than can be used experimentally $(-2 < \log m < +1)$.

For a logarithmic plot, the following relation can be written:

$$y = \log x = \log(u/v) \tag{22}$$

At the inflection point, $\mathrm{d}^2y/\mathrm{d}E^2 = 0$, and consequently

$$[u\mathrm{d}^2u/\mathrm{d}E^2 - (\mathrm{d}u/\mathrm{d}E)^2]/u^2 - [v\mathrm{d}^2v/\mathrm{d}E^2 - (\mathrm{d}v/\mathrm{d}E)^2]/v^2 = 0 \tag{23}$$

Therefore,

$$x_i^2 = 10^{2y_i} = \frac{u \cdot \mathrm{d}^2u/\mathrm{d}E^2 - (\mathrm{d}u/\mathrm{d}E)^2}{v \cdot \mathrm{d}^2v/\mathrm{d}E^2 - (\mathrm{d}v/\mathrm{d}E)^2} = (u/v)^2 \tag{24}$$

Introducing u and v in eqn. (24) gives:

$$x_i^2 = \frac{x_1^* + (a_1^2 - a_2^2)x_2/a_2^2(m+1) + m(a_1 - a_2)^2/a_2^2(m+1)^2}{1/x_2^* + (a_1^2 - a_2^2)/x_2 a_2^2(m+1) + m(a_1 - a_2)^2/a_2^2(m+1)^2} \tag{25}$$

If $x_1 \gg x_2$ in the whole potential range, then eqn. (25) yields:

$$x_i^2 = \left(\frac{a_2^2 x_1^* x_2^*}{a_1^2}\right)_i = \left(\frac{x_1^* + x_1 x_2}{1 + x_1 x_2/x_2^*}\right)_i^2 \tag{26}$$

Therefore,

$$(x_1 x_2)_i = \sqrt{x_1^* x_2^*} \cdot \frac{a_1\sqrt{x_1^*} - a_2\sqrt{x_2^*}}{a_2\sqrt{x_1^*} - a_1\sqrt{x_2^*}} \approx a_1/a_2 \cdot \sqrt{x_1^* x_2^*} \tag{27}$$

Introducing x_1 and x_2 from eqns. (6) and (7), eqn. (27) yields:

$$m = a_2\sqrt{x_1^* x_2^*}/a_1 = x_i \tag{28}$$

III. When $a_1 > a_2$ and $x_2^* = x$, eqn. (21) becomes:

$$x_2^* = (x_1^* + x_1 x_2)/(1 + x_1 x_2/x_2^*) \quad i.e., \; x_1^* = x_2^* \tag{29}$$

Combining eqns. (4), (7) and (29), it follows that:

$$(mx_1+x_2)/(m+1)=(m+1)x_2 \quad i.e.,\ x_1=(m+2)x_2 \tag{30}$$

The slope, $\bar{a}_1$, at potential, $\bar{E}_1$, can be calculated from eqn. (2):

$$\bar{a}_1=(\mathrm{d}y/\mathrm{d}E)_{\bar{E}_1}/\log \mathrm{e}=\left(\frac{\mathrm{d}x/\mathrm{d}E}{x}\right)_{\bar{E}_1}=\left(\frac{\mathrm{d}u/\mathrm{d}E}{u}-\frac{\mathrm{d}v/\mathrm{d}E}{v}\right)_{\bar{E}_1} \tag{31}$$

Therefore,

$$\bar{a}_1=\frac{m(m+2)a_1+a_2+(a_1+a_2)(m+2)A_2^*\,\mathrm{e}^{a_2\bar{E}_1}}{(m+1)^2+(m+2)A_2^*\,\mathrm{e}^{a_2\bar{E}_1}}-\frac{ma_2+(m+2)a_1A_2^*\mathrm{e}^{a_2\bar{E}_1}}{(m+1)^2+2(m+1)A_2^*\mathrm{e}^{a_2\bar{E}_1}}$$

$$\approx a_2+\frac{m(m+2)a_1-ma_2}{m+1+2A_2^*\,\mathrm{e}^{a_2\bar{E}_1}}\Big/(m+1) \tag{32}$$

When $A_2^*\,\mathrm{e}^{a_2\bar{E}_1}\ll 1$, $\bar{a}_1$ becomes:

$$\bar{a}_1=a_1+(a_2-a_1)/(m+1)^2 \tag{10}$$

IV. When $a_1<a_2$ and $x_1^*=x$, eqn. (21) becomes:

$$x_1^*=(x_1^*+x_1x_2)/(1+x_1x_2^*) \quad i.e.,\ x_1^*=x_2^* \tag{33}$$

Equations (5), (6) and (3) yield:

$$mx_1/(m+1)=(m+1)x_1x_2/(mx_2+x_1) \quad i.e.,\ mx_1=(2m+1)x_2 \tag{34}$$

The slope, $\bar{a}_2$, at the potential, $\bar{E}_2$, can be calculated from eqn. (2):

$$\bar{a}_2=(\mathrm{d}y/\mathrm{d}E)_{\bar{E}_2}\cdot\ln 10=\left(\frac{\mathrm{d}x/\mathrm{d}E}{x}\right)_{\bar{E}_2}=\left(\frac{\mathrm{d}u/\mathrm{d}E}{u}-\frac{\mathrm{d}v/\mathrm{d}E}{v}\right)_{\bar{E}_2} \tag{35}$$

Therefore,

$$\bar{a}_2=\frac{m(2m+1)a_1+ma_2+(m+1)^2(a_1+a_2)A_1^*\,\mathrm{e}^{a_2\bar{E}_2}}{2m(m+1)+(m+1)^2\,A_1^*\,\mathrm{e}^{a_1\bar{E}_2}}-\frac{m^2a_2+(2m+1)a_1A_1^*\,\mathrm{e}^{a_1\bar{E}_2}}{m(2m+1)+(m+1)^2A_1^*\,\mathrm{e}^{a_1\bar{E}_2}}$$

$$\approx\frac{m(2m+1)a_1+ma_2+[(2m+1)a_2+m^2a_1]A_1^*\,\mathrm{e}^{a_1\bar{E}_2}}{(m+1)\,[(m+1)\,A_1^*\,\mathrm{e}^{a_1\bar{E}_2}+2]} \tag{36}$$

When $A_1^*\,\mathrm{e}^{a_1\bar{E}_2}\gg 1$, $\bar{a}_2$ becomes:

$$\bar{a}_2=a_2+m^2(a_1-a_2)/(m+1)^2 \tag{13}$$

NOTATION

a slope of the logarithmic plot (nF/RT) or $(\alpha nF/RT)$;
$\bar{a}$ slope of the composite logarithmic curve at the intersection point of its linear parts;
A exponential function of $E_{\frac{1}{2}}$ $(A=\mathrm{e}^{aE_{\frac{1}{2}}})$;
α transfer coefficient;
E potential;

E_j potential at the intersection point between the linear part of composite logarithmic curve and potential axis;
$\overline{E_j}$ potential at the intersection point of linear parts of the composite logarithmic curve;
$E_{\frac{1}{2}}$ half-wave potential;
i mean current of the composite wave at any potential;
i_d mean diffusion current of the composite wave;
i_j mean current of separated single wave;
i_{dj} diffusion current of separated single wave;
m $= i_{d1}/i_{d2}$, ratio of diffusion currents;
x currents ratio of the composite wave $[i/(i_d - i)]$;
x_j currents ratio of separated single wave, $[i_j/(i_{dj} - i_j)]$;
x_j^* antilogarithm of the linear part of the composite logarithmic curve.

ACKNOWLEDGEMENT

The authors are grateful to Dr. Božena Ćosović whose suggestions and experimental results initiated this work.

SUMMARY

Logarithmic analysis of a composite d.c. polarographic wave, which includes two overlapping waves, gives a composite curve with one inflection point and two linear parts. The ratio of diffusion currents, real half-wave potentials and the slopes of each separate wave can be calculated using the general equations evaluated and the experimental data of inflection point, and intersection points of the extrapolated linear parts with the abscissa. The analysis should be performed first by graphical estimation of the inflection point, and then by applying several iterations. Depending on the condition fulfilled, the appropriate simpler relation is used. The possibilities of application of logarithmic analysis of two overlapping d.c. polarographic waves are discussed with respect to the ratio of diffusion currents and to the difference between the half-wave potentials.

REFERENCES

1 I. M. KOLTHOFF AND E. F. ORLEMAN, *Anal. Chem.*, 19 (1947) 161.
2 L. MEITES, *Anal. Chem.*, 27 (1955) 1114.
3 Y. IZRAEL, *Talanta*, 13 (1966) 1113.
4 A. FRISQUE, V. W. MELOCHE AND I. SHAIN, *Anal. Chem.*, 26 (1954) 471.
5 L. MEITES, *Polarographic Techniques*, John Wiley and Sons, New York, 2nd ed., 1965, pp. 345.
6 J. HEYROVSKÝ AND J. KŮTA, *Principles of Polarography*, NČSAV, Praha, 1965, pp. 129.
7 B. ĆOSOVIĆ, M. VERŽI AND M. BRANICA, to be published.

ELECTROANALYTICAL CHEMISTRY AND INTERFACIAL ELECTROCHEMISTRY
Elsevier Sequoia S.A., Lausanne – Printed in The Netherlands

SOLVATATION D'IONS ET STABILITÉ DES COMPLEXES MERCURI–THIOCYANATES DANS LE N-MÉTHYLACÉTAMIDE ET SES MÉLANGES AVEC LE N,N-DIMÉTHYLFORMAMIDE*

ADAN E. PUCCI**, JACQUES VEDEL ET BERNARD TREMILLON

Faculté des Sciences de Paris, Laboratoire de Recherches de Chimie Analytique (associé au C.N.R.S.), E.N.S.C.P., Paris (France)

(Reçu le 20 février, 1969)

INTRODUCTION

L'influence du solvant sur un équilibre chimique fait intervenir à la fois la modification des forces électrostatiques qui s'exercent entre les espèces ioniques et les différences d'action exercées par les molécules de solvant sur toutes les espèces chimiques en solution participant à cet équilibre. Cette action, la solvatation, dépend de la nature du solvant et de celle du soluté; elle en est spécifique. En revanche, l'action électrostatique doit entraîner—comme l'indique l'équation de Born—une variation approximativement linéaire du logarithme de la constante d'équilibre en fonction de l'inverse de la constante diélectrique du milieu[1]. Mais cette relation a été souvent infirmée par les résultats expérimentaux globaux, ce qui peut provenir du fait que la distinction entre l'action de la constante diélectrique et celle de la solvatation n'a pu être effectuée, sinon d'une manière hypothétique[2]. En particulier, lorsqu'on réalise des mélanges en proportions variables d'eau et d'un solvant organique miscible, la constante diélectrique et la solvatation spécifique varient toutes deux en même temps.

Cependant, une étude récente[3], portant sur la comparaison de forces d'acides dans deux solvants possédant sensiblement la même constante diélectrique—l'eau et l'acétamide à 98°C—, a permis de mettre en évidence le rôle très important des différences de solvatation des espèces chimiques dans les deux milieux. Nous avons pensé que le N-méthylacétamide (NMA) et le N,N-diméthylformamide (DMF), qui sont isomères, pourraient à l'opposé donner une solvatation sensiblement analogue et permettraient ainsi de réaliser une étude où la seule influence de la constante diélectrique interviendrait, le mélange de ces deux solvants permettant de faire varier cette dernière de 165 à 35 (à 40°C). L'étude décrite ici a eu pour objet les constantes de stabilité des complexes mercuri–thiocyanates, aisément déterminées électrochimiquement. Elle nous a fait apparaître l'influence d'un facteur caractéristique sur la solvatation de certains ions: la structure des solvants moléculaires, qui semble être responsable de l'existence d'un minimum de stabilité des complexes étudiés pour un mélange intermédiaire.

* Cet article est extrait de la thèse de Doctorat d'Université soutenu par A.E. Pucci le 14-10-1968 à la Faculté des Sciences de Paris.

** Adresse actuelle: Departamento de Química, Universidad Nacional del Sur, Bahía Blanca (Rep. Argentina).

Il est à remarquer que les études d'équilibre effectuées dans les mélanges de solvants ayant des constantes diélectriques supérieures à celle de l'eau sont actuellement peu nombreuses; Reynaud[4] a récemment déterminé les constantes pK_A de quelques couples acide–base dans les mélanges eau–NMA à 25°C et constaté également que la stabilité des acides de type HA (acides benzoïque et acétique) passe par un minimum pour un mélange intermédiaire.

Coefficients de solvatation d'ions

Le coefficient de solvatation (ou coefficient de partage) Γ_i d'un ion i, traduisant le changement de propriétés thermodynamiques de cet ion lorsqu'il est transféré d'une solution aqueuse à une solution dans un autre solvant S, est défini par la relation:

$$RT \log \Gamma_i = (\mu_i^0)_s - (\mu_i^0)_{eau}$$

L'évaluation expérimentale de ce coefficient nécessite l'adoption d'une hypothèse extra-thermodynamique concernant les solvatations des constituants d'un couple de référence. Nous avons récemment exposé les résultats d'une étude de ce genre, dans laquelle nous avons exploité une méthode préconisée par Strehlow et coll.[5] pour la comparaison des échelles de potentiel dans des solvants différents, consistant à utiliser comme référence le couple oxydo–réducteur ferrocène–cation ferricinium. En déterminant par rapport à ce couple les potentiels normaux E^0_{eau} et E^0_S d'un couple M/M^{n+} dans l'eau et dans le solvant S, on peut définir une grandeur

$$R^0_O(M) = (nF/2.3\ RT)(E^0_{eau} - E^0_s)$$

dont la valeur est égale à $-\log \Gamma_{M^{n+}}$ si l'on admet que le potentiel du couple ferrocène–ferricinium est invariable lorsqu'on change de solvant, ce qui implique seulement que les solvatations des deux constituants de ce couple varient de la même manière. Nous avons appliqué cette méthode au cation Ag^+ dans divers mélanges hydro–organiques[7], ainsi qu'au proton grâce à la grandeur $R^0_O(H)$ déduite de mesures à l'électrode à hydrogène[6] ou à l'électrode de verre[7].

En outre, si un anion X^- forme avec le cation M^{n+} un sel peu soluble, MX_n, dont le produit de solubilité est désigné par K_s, son coefficient de solvatation, Γ_{X^-}, est calculé au moyen de l'expression:

$$n \log \Gamma_{X^-} = R^0_O(M) - \log [(K_s)_{eau}/(K_s)_S]$$

Nous avons ainsi évalué des coefficients de solvatation pour les anions halogénures et thiocyanate dans divers mélanges hydro–organiques grâce à la détermination des produits de solubilité des sels d'argent correspondants[7].

C'est également cette méthode que nous avons utilisée pour la comparaison des échelles de pH dans l'acétamide fondu et dans l'eau à 98°C[3], en déterminant $R^0_O(H)$ pour ces deux milieux.

Dans la présente étude, nous avons à nouveau expérimenté la même méthode dans le but essentiel de tester l'hypothèse de départ concernant la faible variation de solvatation des ions concernés dans les mélanges NMA–DMF.

RESULTATS EXPERIMENTAUX

1. Comme dans nos études précédentes [3,6,7], nous avons adopté comme potentiel de référence dans les différents milieux le potentiel de demi-vague de la courbe

intensité–potentiel d'oxydation "réversible" du ferrocène en ferricinium (ferrocène $-e \rightarrow$ ferricinium$^+$) à une micro-électrode tournante de platine (courbe stationnaire, en régime de diffusion convective). En appelant i_l la valeur de l'intensité-limite de diffusion du ferrocène, il faut vérifier pour la vague que la variation de $E=f \log [i/i_l-i)]$ est une droite dont la pente est égale à 2.3 $RT/F=62$ mV par unité de logarithme à la température des expériences, 40°C ($\pm$0.2°C).

Dans le NMA, cette condition de réversibilité n'a été vérifiée que pour une vitesse de rotation de l'électrode égale à 45–50 t/min; à vitesse plus élevée, la pente de la droite approximative est plus grande que la valeur théorique précédente, indiquant que l'oxydation ne s'effectue pas dans les conditions où l'on peut appliquer l'équation des vagues réversibles. En revanche, dans les mélanges avec le DMF, nous avons obtenu une vague réversible à des vitesses de rotation plus élevées; dans le DMF pur, la vague est encore réversible à 700 t/min.

Si les coefficients de diffusion du ferrocène et de l'ion ferricinium sont peu différents l'un de l'autre, le potentiel de demi-vague ainsi obtenu est peu différent du potentiel normal du couple et peut être assimilé à la valeur de ce dernier, comme cela a déjà été admis[4,8].

2. Nous avons ensuite déterminé les potentiels normaux, dans les différents mélanges NMA–DMF étudiés, des couples Hg/Hg^{2+}, Ag/Ag^+ et H_2/H^+. Pour cela, il a d'abord été prouvé que les ions mercureux sont pratiquement quantitativement dismutés dans tous les mélanges à 40°C. Les ions mercuriques ont ainsi pu être produits par oxydation coulométrique à intensité constante d'une nappe de mercure; mais, si le rendement de l'oxydation a été très voisin de 100% dans le NMA pur, il a été assez nettement inférieur, de l'ordre de 80% seulement, dans les mélanges avec le DMF. Les ions Ag^+ ont également été produits par oxydation coulométrique d'une électrode d'argent; à partir de la concentration 10^{-2} M, une coloration brunâtre de la solution apparaît, puis une fine poudre grisâtre. La concentration des ions Ag^+ diminue lentement au cours du temps. Ces phénomènes correspondraient à une réduction lente des ions Ag^+ par le DMF[9].

Les potentiels d'équilibre ont été mesurés à une électrode à gouttes de mercure pour le couple Hg/Hg^{2+}, à une micro-électrode d'argent pour le couple Ag/Ag^+, et à une micro-électrode de platine platiné pour le couple H_2/H^+. Dans ce dernier cas, l'acide fort utilisé a été l'acide *p*-toluènesulfonique anhydre; la détermination n'a cependant pas été possible dans le DMF pur. La validité de la formule de Nernst a été vérifiée dans les trois cas.

Dans tous les mélanges, l'électrode de comparaison utilisée a été l'électrode argent/chlorure d'argent saturé/chlorure de potassium saturé. Pour les déterminations effectuées en solution aqueuse à 40°C, nous avons utilisé l'électrode au calomel et au chlorure de potassium saturé, dont le potentiel par rapport à l'électrode normale à hydrogène est +0.230 V à 40°C.

L'ensemble des résultats observés lors de ces déterminations est reporté dans le Tableau 1.

3. Pour atteindre les coefficients de solvatation de l'anion thiocyanate, nous avons cherché à déterminer les valeurs du produit de solubilité du thiocyanate d'argent dans les mélanges NMA–DMF. Nous avons opéré par titrage potentiométrique d'ions Ag^+ (introduits coulométriquement) par du thiocyanate de potassium. Mais, nous n'avons observé la précipitation de AgSCN, comme en solution aqueuse, que

J. Electroanal. Chem., 22 (1969) 253–263

TABLEAU 1

RÉSULTATS DES DÉTERMINATIONS POTENTIOMÉTRIQUES EFFECTUÉES DANS LES MÉLANGES NMA–DMF ET EN SOLUTION AQUEUSE À 40(±0.2) °C

Force ionique $\mu = 0.1$ (Et_4NClO_4, 0.1 *M*). Les valeurs de potentiel sont données par rapport au potentiel de l'électrode de comparaison: Ag/AgCl/KCl saturés, pour les mélanges NMA–DMF; Hg/Hg_2Cl_2/KCl saturés pour l'eau. Les intervalles d'incertitude correspondent à un taux de confiance de 95%

Mélanges (% *en poids*)		*Couple ferrocène–ferricinium* $E = E_{\frac{1}{2}} + a \log \{i/(i_1 - i)\}$		*Couple* H_2 (1*atm*)/H^+ $E_{eq} = E^0_H + b \log \lvert H^+ \rvert$		*Couple* Hg/Hg^{2+} $E_{eq} = E^0_{Hg} + c \log \lvert Hg^{2+} \rvert$		*Couple* Ag/Ag^+ $E_{eq} = E^0_{Ag} + d \log \lvert Ag^+ \rvert$	
NMA	*DMF*	$E_{\frac{1}{2}}$/*mV*	*a*/*mV*	E^0_H/*mV*	*b*/*mV*	E^0_{Hg}/*mV*	*c*/*mV*	E^0_{Ag}/*mV*	*d*/*mV*
100	0	504±1	62±2	−291±6	62±2	554±5	31±3	556±4	62±2
80	20	516±1	62±2	−256±5	61±2	578±3	31±2	587±3	62±1
60	40	537±1	62±1	−235±8	61±3	596±5	32±2	601±3	62±1
40	60	552±1	62±2	−204±6	64±3	615±2	33±1	628±9	62±4
20	80	550±1	62±1	−198±5	60±2	626±3	31±1	647±3	62±1
0	100	540±1	61±2			635±3	31±1	664±4	61±1
eau		223±2	62±2	(−230)		558±1	30±2	552±2	61±1

dans le cas du NMA pur. En outre, le précipité est ensuite redissous dans un excès de thiocyanate par formation de complexe anionique.

L'interprétation de la courbe potentiométrique nous a conduit aux valeurs suivantes des constantes d'équilibre dans le NMA à 40°C et $\mu = 0.1$:

$$Ag(SCN)_3^{2-} \rightleftharpoons Ag^+ + 3\ SCN^- \qquad \log(\beta_3/\text{mole}^{-3}l^3) = 10.7(\pm 0.3)$$

$$AgSCN\downarrow \rightleftharpoons Ag^+ + SCN^- \qquad -\log(K_s/\text{mole}^2l^{-2}) = 13.7(\pm 0.2)$$

En solution aqueuse et dans les mêmes conditions de température et de force ionique, nous avons obtenu :

$$-\log(K_s/\text{mole}^2l^{-2}) = 11.2(\pm 0.1)$$

4. Pour l'étude des complexes mercuri–thiocyanates, différentes méthodes électrochimiques ont été exploitées : détermination de courbes polarographiques, titrages potentiométriques et ampérométriques.

(a) Les courbes de titrages potentiométriques et ampérométriques (avec une électrode indicatrice à gouttes de mercure, potentiel imposé +0.40 V par rapport à l'électrode de comparaison) ont montré dans tous les cas l'apparition d'un point équivalent net correspondant à l'addition de deux ions SCN^- pour un cation Hg^{2+}, c'est-à-dire à la réaction de formation du complexe $Hg(SCN)_2$. Il n'apparaît pas, dans les mélanges NMA–DMF comme dans l'eau, d'autre point équivalent correspondant à la formation d'un complexe supérieur anionique. Deux courbes de titrage caractéristiques obtenues dans le NMA pur sont représentées Fig. 1 ; l'allure est identique dans le DMF pur et dans tous les mélanges.

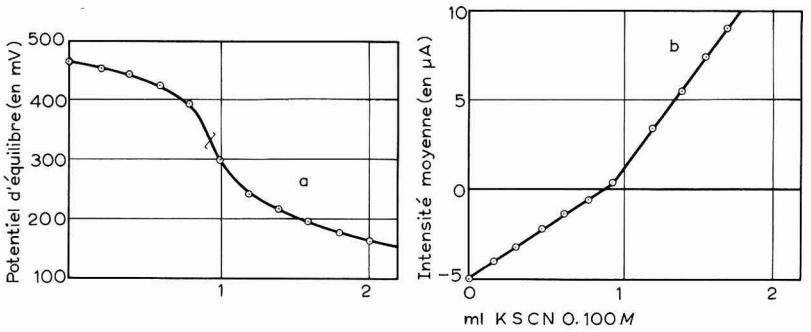

Fig. 1. Courbes de titrages : (a), potentiométrique ; (b), ampérométrique (à $E = 0.40$ V), de 25 ml de solution de Hg^{2+} $1.9 \cdot 10^{-3}$ M dans le NMA, par du thiocyanate de potassium. $T = 40°C$, $\mu = 0.1$ (Et_4NClO_4, 0.1 M).

(b) L'oxydation d'une électrode à gouttes de mercure en présence de solutions de thiocyanate de potassium conduit à des vagues polarographiques caractéristiques, telles que celles représentées Fig. 2, obtenues dans le NMA pur ; l'allure est identique dans tous les mélanges et dans le DMF. Le palier de ces vagues est caractéristique de la formation du complexe $Hg(SCN)_2$ et sa hauteur a été vérifée proportionnelle à la concentration des ions SCN^-, de 10^{-4}–$5 \cdot 10^{-3}$ M au moins.

(c) Les variations du potentiel d'équilibre d'une électrode de mercure dans une solution contenant des ions mercuriques dilués (environ $2 \cdot 10^{-4}$ M, produits coulométriquement) + Et_4NClO_4, 0.1 M + SCN^-, 10^{-4}–10^{-2} M ont permis d'identifier les

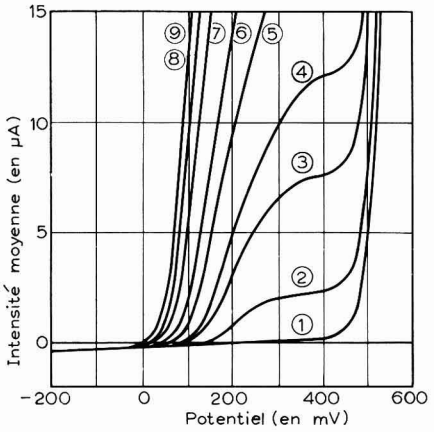

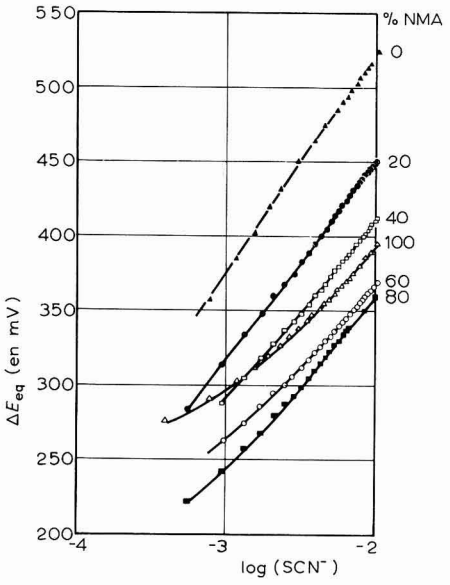

Fig. 2. Courbes polarographiques anodiques d'oxydation du mercure dans le NMA ($+Et_4NClO_4$, 0.1 *M*) à 40°C, en présence de thiocyanate de potassium à différentes concentrations: (1), 0; (2), $7.9\cdot10^{-4}$; (3), $2.34\cdot10^{-3}$; (4), $3.84\cdot10^{-3}$; (5) $6.00\cdot10^{-3}$; (6), $1.00\cdot10^{-2}$; (7), $1.66\cdot10^{-2}$; (8), $2.00\cdot10^{-2}$; (9), $2.50\cdot10^{-2}$ *M*.

Fig. 3. Variations du potentiel d'équilibre d'une électrode de mercure en présence de Hg(II) $2\cdot10^{-4}$ *M*, dans les mélanges NMA–DMF à 40°C ($\mu=0.1$), en fonction de la concentration de thiocyanate.

complexes supérieurs, $[Hg(SCN)_3]^-$ et $[Hg(SCN)_4]^{2-}$, et de déterminer les valeurs de leurs constantes de stabilité dans les différents milieux utilisés. Une vingtaine de mesures ont été effectuées dans chaque milieu (Fig. 3), conduisant aux valeurs de constantes et aux incertitudes reportées dans le Tableau 2.

TABLEAU 2

CONSTANTES GLOBALES DE FORMATION DES COMPLEXES MERCURI–THIOCYANATES DANS LES MÉLANGES NMA–DMF ET DANS L'EAU, À 40 (±0.2) °C

Force ionique $\mu=0.1$. Les intervalles d'incertitude correspondent à un taux de confiance de 95%

Mélanges (% *en poids*) *NMA*	*DMF*	$Hg(SCN)_2$ $log\ (\beta_2/mole^{-2}\ l^2)$	$Hg(SCN)_3^-$ $log\ (\beta_3/mole^{-3}\ l^3)$	$Hg(SCN)_4^{2-}$ $log\ (\beta_4/mole^{-4}\ l^4)$
100	0	14.6±0.3	18.45±0.30 18.30±0.50*	20.54±0.33 20.13±0.25*
80	20	14.4±0.3	17.26±0.64	19.52±0.12
60	40	14.7±0.2	17.70±0.54	19.65±0.30
40	60	15.0±0.3	non déterminable	21.13±0.06
20	80	16.2±0.3	non déterminable	22.71±0.25
0	100	17.7±0.2	non déterminable	25.20±0.20 25.13±0.17*
eau		15.2±0.3	18.0±0.3	20.0±0.2

* Résultats obtenus par polarographie anodique; les autres sont déduits des mesures potentiométriques.

(d) Les constantes de formation du complexe $Hg(SCN)_2$ ont été ensuite déduites des courbes de titrages potentiométriques, en tenant compte, pour l'interprétation de la partie située au-delà du point équivalent, de l'existence simultanée des trois complexes. La constante de formation β_4 de $[Hg(SCN)_4]^{2-}$, et dans certains cas celle β_3 de $[Hg(SCN)_3]^-$, ayant été déterminées précédemment, il devient facile d'obtenir la constante de formation β_2 de $Hg(SCN)_2$. β_2 et β_3 peuvent aussi être déduites simultanément de la courbe de titrage par résolution mathématique (au moyen d'un calculateur EMD-848) d'une équation du 4ème degré, par itération.

L'ensemble des valeurs obtenues pour les constantes globales de formation des complexes, $Hg(SCN)_2$ (β_2), $[Hg(SCN)_3]^-$ (β_3) et $[Hg(SCN)_4]^{2-}$ (β_4), est reporté dans le Tableau 2. Le calcul des diagrammes de répartition de ces différents complexes en fonction de log $|SCN^-|$, à partir de ces valeurs, montre que le complexe intermédiaire, $[Hg(SCN)_3]^-$, n'existe jamais seul et ne prédomine que dans un domaine restreint de $|SCN^-|$, à la fois dans le NMA et en solution aqueuse; il disparaît, même, pratiquement, dans les mélanges NMA–DMF à partir d'une proportion suffisante de DMF.

Technique expérimentale

1. *Purification des solvants.* Les impuretés présentes dans le N-méthylacétamide commercial sont la méthylamine, l'acide acétique et l'eau. La purification consiste à neutraliser successivement chacune d'elles, respectivement, par l'acide sulfurique (1%), le carbonate de potassium (2%) et l'oxyde de calcium (1%). Chacune de ces neutralisations est suivie d'une distillation sous vide (point d'ébullition du NMA sous une pression de 3 mm de mercure: 74°C). La température du bouilleur ne doit pas dépasser 130°C pour éviter toute décomposition du produit. Le réfrigérant et le ballon dans lequel est recueilli le distillat sont maintenus à une température légèrement supérieure à 30°C, ce qui évite la cristallisation du NMA au cours des opérations. Le solvant ainsi purifié a été conservé dans des flacons opaques contenant 10 g de tamis moléculaire par litre de solvant.

La pureté et la qualité du produit au moment de son utilisation ont été contrôlées:

(a) Par une détermination de la variation du courant résiduel en fonction du potentiel de l'électrode à gouttes de mercure. Ceci indique la présence ou l'absence de méthylamine ou d'acide acétique. Dans les conditions des essais, l'absence de vague d'oxydation (méthylamine) ou de réduction (acide acétique) correspond à une concentration d'impuretés inférieure a 10^{-4} *M*.

(b) Par un titrage de l'eau par la méthode de Karl–Fischer, le réactif (iode) étant introduit par coulométrie à intensité constante. La teneur en eau du solvant distillé utilisé a toujours été inférieure à $5 \cdot 10^{-3}$ *M*.

Le N,N-diméthylformamide, produit Merck "pour synthèse" (teneur en eau inférieure à 0.1%) a été purifié par simple distillation. Après cette opération, le produit ne présentait plus qu'une teneur en eau inférieure à $5 \cdot 10^{-3}$ *M*. La pureté a été contrôlée comme celle du NMA.

2. *Instrumentation.* Pour le tracé des courbes intensité–potentiel, nous avons utilisé un polarographe Tacussel, modèle PR 61 (montage potentiostatique à trois électrodes).

L'électrode de comparaison a été constituée d'un fil d'argent en spirale, recou-

vert d'un film de chlorure d'argent par anodisation dans une solution de chlorure, ce fil plongeant dans un solvant identique à celui étudié, saturé de chlorure d'argent et de chlorure de potassium. Le compartiment de cette électrode a été relié à la cellule principale par l'intermédiaire d'un autre compartiment contenant une solution de Et_4NClO_4 0.1 *M*, afin d'éviter toute diffusion ou migration de chlorure dans la cellule principale.

DISCUSSION ET CONCLUSIONS

La première conclusion à tirer concerne la validité de l'hypothèse initiale sur une éventuelle invariabilité de la solvatation dans les mélanges NMA–DMF. Les valeurs de la grandeur R_O^0 pour les cations Ag^+, Hg^{2+} et H^+, tirées des déterminations de potentiels normaux reportés Tableau 1, sont données dans le Tableau 3. Dans la mesure où est valable l'hypothèse que la molécule de ferrocène et le cation ferricinium sont eux-mêmes solvatés de façon identique, ces valeurs sont voisines de $-\log \Gamma$ et donnent une évaluation approximative des coefficients de solvatation des cations envisagés. Il apparaît ainsi que ces trois cations sont nettement plus fortement solvatés par les mélanges NMA–DMF que par l'eau (dans l'ordre, $Hg^{2+} > H^+ > Ag^+$) et que notre hypothèse est vérifiée d'une façon assez satisfaisante, surtout pour les mélanges intermédiaires, de 40–80% de NMA.

TABLEAU 3

COEFFICIENTS DE SOLVATATION DES CATIONS Ag^+, Hg^{2+} ET H^+ DANS LES MÉLANGES NMA–DMF ($+Et_4NClO_4$ 0.1 *M*) À 40°C

Valeurs de $R_O^0 \simeq -\log \Gamma$ *pour*:	*% en poids de NMA*:					
	100	80	60	40	20	0
Ag^+	4.47	4.16	4.27	4.08	3.74	3.31
Hg^{2+}	9.20	8.80	8.95	8.78	8.36	7.74
H^+	5.51	5.14	5.14	4.89	4.76	

Dans le cas du proton, ce résultat signifie que les mélanges NMA–DMF sont plus basiques que l'eau et de basicités à peu près identiques quelles que soient les proportions des deux amides. Le décalage d'échelles de pH des solutions aqueuses aux solutions dans les mélanges est approximativement de 5 unités (*cf.* ref. 3 pour le cas de l'acétamide à 98°C).

Pour l'anion SCN^-, nous ne pouvons calculer qu'une seule valeur de $R_O^0(SCN^-)$, dans le NMA pur, le seul des milieux envisagés où le produit de solubilité de AgSCN a pu être déterminé. On obtient $R_O^0(SCN) = -6.97 \simeq -\log \Gamma_{SCN^-}$. L'anion SCN^- serait ainsi, au contraire des cations, beaucoup moins solvaté par les amides que par l'eau ; c'est un fait qui a déjà été observé, notamment pour d'autres anions comme les halogènures[7,10]. C'est à cet effet contraire de solvatation pour cation et anion que l'on peut principalement attribuer le fait que les stabilités des complexes mercuri–thiocyanates ne sont pas très différentes en solution dans les mélanges NMA–DMF (surtout ceux de constantes diélectriques voisines de celle de l'eau) et en solution aqueuse.

Les variations du logarithme des constantes de formation que nous avons pu déterminer, en fonction de l'inverse de la constante diélectrique du solvant, sont reproduites Fig. 4. On peut constater que cette variation n'est sensiblement linéaire que pour les mélanges riches en DMF, et l'on observe un minimum de stabilité dans un mélange contenant approximativement 25% de DMF. Remarquons au passage que β_4 présente la même valeur qu'en solution aqueuse pour un mélange ayant sensiblement la même constante diélectrique que l'eau, mais il ne peut s'agir que d'une coïncidence fortuite.

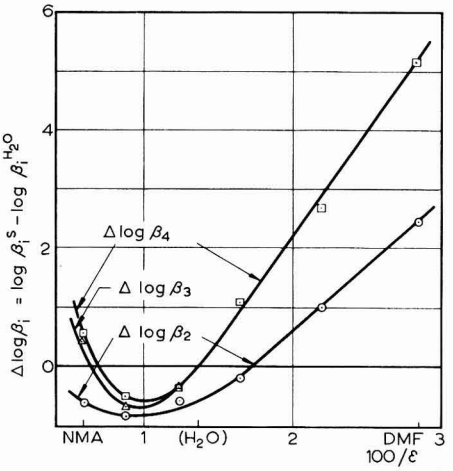

Fig. 4. Variations en fonction de l'inverse de la constante diélectrique, ε, de la différence de stabilité des complexes mercuri–thiocyanates dans les mélanges NMA–DMF(S) et en solution aqueuse. Force ionique $\mu = 0.1$ et temp. 40°C.

L'existence du minimum de stabilité peut certainement être interprêtée par l'influence de la variation, avec les proportions des constituants du solvant, de la solvatation de l'anion SCN^-, que l'on peut expliquer de la façon suivante. Il est établi [11,12] que la valeur élevée de la constante diélectrique du NMA est due à la formation de liaisons hydrogène associant les molécules de solvant en polymère linéaire liquide; les deux groupements méthyle se trouvent alors en position *trans*. Au contraire, le DMF, dont les atomes d'hydrogène ne peuvent donner naissance à de telles associations, reste monomère et présente de ce fait une constante diélectrique beaucoup plus faible. Les résultats de Dawson et Wharton[13] montrent qu'il suffit de peu de DMF ajouté au NMA pour provoquer une importante diminution de la constante diélectrique, ce qui est l'indication d'une rupture des chaînes de polymère par l'insertion des molécules monomères de DMF. Or, on peut admettre avec Parker[14] que, dans les solvants protoniques comme le NMA, la solvatation des anions comporte une importante contribution de la liaison hydrogène entre les molécules de solvant et l'anion dissous. On peut alors supposer que l'effet "déstructurant" du DMF ajouté au NMA renforce le pouvoir de liaison hydrogène de ce dernier et augmente par conséquent la solvatation de l'anion SCN^-. D'où la diminution de stabilité des complexes mercuri–thiocyanates, par rapport au NMA pur, lorsque le pourcentage de DMF augmente. Le minimum de stabilité correspond à l'effet, en sens opposé, de la diminution de cons-

tante diélectrique qui provoque une stabilisation des complexes. Lorsque la proportion de DMF est suffisamment grande, la solvatation de SCN^- doit devenir sensiblement invariable et les modifications de log β ne correspondent plus alors qu'à l'influence des variations de constante diélectrique ε; c'est pourquoi, semble-t-il, nous avons pu observer les variations linéaires de log β en fonction de $1/\varepsilon$.

En conclusion, l'hypothèse effectuée sur la possibilité d'obtention d'une solvatation invariable en utilisant des mélanges de deux amides isomères s'est avérée convenablement vérifiée pour les cations mais non pour les anions. Dans le cas de ces derniers, l'intervention des liaisons hydrogène dans la solvatation apporte une influence importante de la structure même du solvant. Cet effet est vraisemblablement responsable d'autres minimums ou maximums de constantes d'équilibre, notamment de couples acide–base, qui ont pu être observés à plusieurs reprises, dans les mélanges NMA–eau[4] et aussi dans divers mélanges hydro–organiques. Il est indubitable qu'une meilleure compréhension de l'influence du solvant sur la stabilité des composés dissous, acides ou complexes, sera atteinte grâce à l'étude de l'influence de la structure du solvant sur la solvatation des ions.

REMERCIEMENTS

A. E. Pucci tient à exprimer ses remerciements à la Commission Spéciale des Sciences Agricoles de l'Université du Sud de Bahia Blanca, République Argentine, qui lui a donné la possibilité d'effectuer ce travail.

RÉSUMÉ

Les coefficients de solvatation des cations Ag^+, Hg^{2+}, H^+, dans les mélanges N-méthylacétamide + N,N-diméthylformamide ont été évalués à partir de mesures de potentiels normaux et en supposant l'invariabilité du potentiel du couple ferrocène–cation ferricinium. Il a été montré que la solvatation de ces cations, plus énergique qu'en solution aqueuse, reste à peu près inchangée quand la proportion des deux amides isomères varie. Les constantes de formation des complexes mercuri–thiocyanates dans ces mélanges ont été également déterminées par mesures potentiométriques et par polarographie anodique. La stabilité de ces complexes $Hg(SCN)_2$, $[Hg(SCN)_3]^-$ et $[Hg(SCN)_4]^{2-}$ passe par un minimum pour un mélange voisin de NMA 75% × DMF 25% (en poids). Ce minimum est interprêté par l'effet d'une augmentation de la solvatation de l'anion thiocyanate lorsque du DMF est ajouté au NMA, brisant la structure de polymère linéaire par liaisons hydrogène de ce dernier. Dans les mélanges riches en DMF, le logarithme des constantes de formation augmente sensiblement linéairement en fonction de l'inverse de la constante diélectrique.

SUMMARY

The solvation coefficients of Ag^+, Hg^{2+} and H^+ in NMA–DMF mixtures were determined by formal potential measurements, the potential of the ferrocene–ferricinium couple being assumed constant. The solvation of these cations, stronger than in aqueous solutions, has been found to remain approximately unchanged as the proportion of the two isomeric amides is varied. The formation constants of the

mercury(II)–thiocyanate complexes in these mixtures have been determined by potentiometric measurements and also by anodic polarography. The stability of the complexes is minimum for a mixture of approximately 75% NMA and 25% (by weight) DMF. This minimum is interpreted by the effect of an increase in the solvation of the thiocyanate anion when DMF is added to NMA, so breaking the structure of the linear polymer (due to hydrogen bonds) of the latter. In mixtures of high DMF content, the logarithm of the formation constants is approximately directly proportional to the inverse of the dielectric constant.

RÉFÉRENCES

1 I. M. KOLTHOFF ET S. BRUCKENSTEIN, *Acid–Base Equilibria in Non-Aqueous Solutions*, dans *Treatise on Analytical Chemistry*, I. M. KOLTHOFF ET P. J. ELVING éd., Part I, Vol. 1, Interscience Publ. Inc., New-York, 1959, chap. 13.
2 J. C. TOULLER, M. GRALL, M. BIGOIS ET B. TRÉMILLON, *Bull. Soc. Chim. France*, (1965) 1853.
3 S. GUIOT ET B. TRÉMILLON, *J. Electroanal. Chem.*, 18 (1968) 261.
4 R. REYNAUD, *Bull. Soc. Chim. France*, (1968) 3945.
5 H. M. KOEPP, H. WENDT ET H. STREHLOW, *Z. Elektrochem.*, 64 (1960) 483.
6 J. VEDEL, *Ann. Chim. Paris*, (1967) 335.
7 C. BARRAQUÉ, J. VEDEL ET B. TRÉMILLON, *Bull. Soc. Chim. France*, (1968) 3421.
8 I. M. KOLTHOFF ET F. G. THOMAS, *J. Phys. Chem.*, 69 (1965) 3049.
9 J. K. GORMAN, Thèse, Univ. Micr. 58–7254; *Dissertation Abstr.*, 19 (1959) 1930.
10 S. GUIOT, *Ann. Chim. Paris*, (1969), à paraître.
11 S. MIZUSHIMA, *J. Am. Chem. Soc.*, 72 (1950) 3490.
12 G. R. LEADER ET J. F. GORMLEY, *J. Am. Chem. Soc.*, 73 (1951) 573.
13 L. R. DAWSON ET W. W. WHARTON, *J. Electrochem. Soc.*, 107 (1960) 710.
14 A. J. PARKER, *Quart. Rev. (London)*, 16 (1962) 163.

ELECTROANALYTICAL CHEMISTRY AND INTERFACIAL ELECTROCHEMISTRY
Elsevier Sequoia S.A., Lausanne Printed in The Netherlands

ELECTROCHEMICAL BEHAVIOUR OF BROMATE IN PERCHLORIC ACID SOLUTIONS

PIER GIORGIO DESIDERI AND LUCIANO LEPRI
Institute of Analytical Chemistry, University of Florence (Italy)
(Received March 3rd, 1969)

INTRODUCTION

The electroreduction of bromate in alkaline, neutral, and weakly acid media has been investigated by several authors[1-10]. A thesis on work in mineral acid media by Yonan[11] and the work in acid sulphuric medium of Rozhdestvenskaya and Songina[12,13] should also be cited. The three waves recorded in H_2SO_4 solutions using a rotating platinum electrode were attributed by these authors to the reduction of interaction products between bromate and H_2SO_4, and not to the direct reduction of bromate.

This study continues the investigation on the electrochemical behaviour of strong oxidants in acid medium[14], especially of oxyhalogens[15,16], by means of a platinum microelectrode with periodical renewal of the diffusion layer[17] and has been undertaken in order to elucidate the reduction mechanism of bromate in $HClO_4$. Polarographic, chronopotentiometric and voltammetric methods at constant potential have been used in this investigation.

EXPERIMENTAL

Reagents and apparatus

A Metrohm Polarecord E 261 polarograph was used for polarographic measurements. The current–time curves were recorded with a Tektronix type 502 B DB cathode-ray oscillograph with a photographic camera incorporated. The circuit is that described by Mark and Reilley[18]. The chronopotentiograms were obtained with a Beckman Electroscan 30. Polarographic and chronopotentiometric potentials are referred to SCE. A spherical microelectrode of smooth platinum was used; before every recording it was polished with very fine Cr_2O_3 obtained by thermal decomposition of $(NH_4)_2Cr_2O_7$ and, whenever necessary, was pre-oxidized electrolytically for 5 min with a current density of 300 mA/cm^2. The $KBrO_3$ solution was prepared by dissolving accurately weighed portions of pure salt in water twice distilled from alkaline permanganate. The Br_2 and $HClO_4$ solutions, obtained by dilution, were standardized by the usual titrimetric procedures.

RESULTS AND DISCUSSION

The polarographic characteristics of $KBrO_3$

The reduction of $KBrO_3$ in $HClO_4$ solution, on a smooth platinum micro-

electrode with periodical renewal of the diffusion layer, shows characteristics different from those observed for iodate reduction in the same medium. The curves of Fig. 1, obtained from a 1 m*M* $KBrO_3$ solution in 1 *M* $HClO_4$ in the potential range, +1.4 to −0.41 V/SCE, show the following characteristics:

(1) the presence of a weak cathodic current just before the hydrogen evolution on a smooth platinum microelectrode (curve a);

(2) a distinct cathodic current on a pre-oxidized platinum microelectrode (curve b);

(3) the presence of a current maximum in the potential range where platinum oxide reduction occurs.

It follows from the curves of Fig. 1 that an electrode pre-oxidation is required in order to take advantage of current increase and to record the start of a limiting current before hydrogen evolution. Consequently, unless otherwise specified, the following data are related to an electrolytically pre-oxidized electrode.

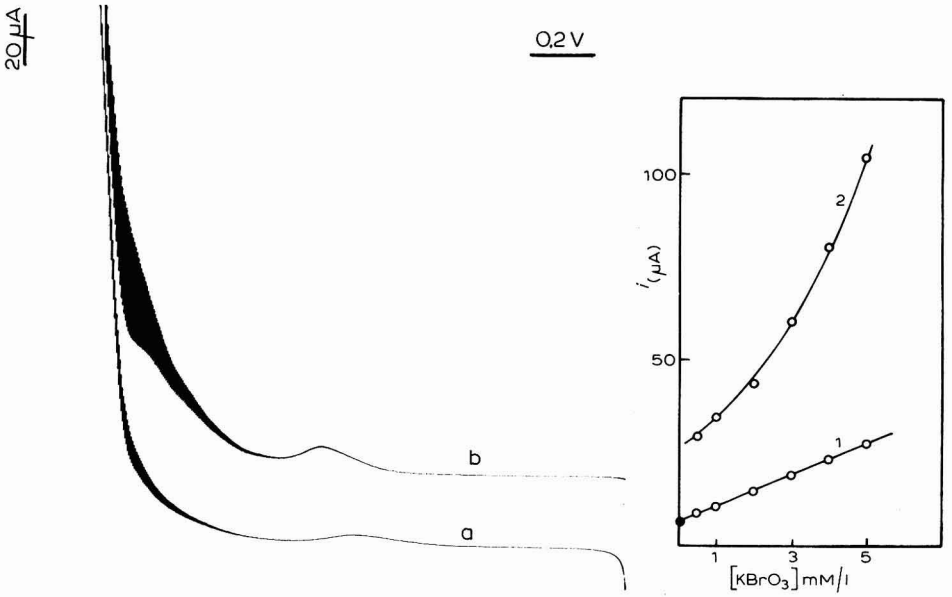

Fig. 1. 1 m*M* $KBrO_3$ in 1 *M* $HClO_4$ on: (a), smooth; (b), pre-oxidized platinum electrode. Starting potential, +1.4 V/SCE.

Fig. 2. Values of the peak current, i_p, (1) and of the current measured at −0.280 V/SCE (2) as the $KBrO_3$ concn. changes. Supporting electrolyte: 1 *M* $HClO_4$.

Characteristics of current maximum

The current maximum is obtained only with a superficially oxidized electrode recording the curve from 1.4 V to −0.41 V/SCE. No current maximum is observed when recording the curve in the opposite direction with the electrode superficially reduced. Such a maximum occurs in the potential range where platinum oxide reduction occurs.

Figure 2 (curve 1) shows the currents measured at the maximum potential, for different bromate concentrations. The value of the maximum current corresponding

to zero bromate concentration, is that related to the supporting electrolyte alone. Curve 2, in the same Figure, represents the behaviour of the current, measured at −0.280 V/SCE corresponding to the potential of inflexion preceding the discharge of the supporting electrolyte.

The shape of curve 1 shows that the current maximum is due not only to the reduction of the platinum oxide film but is the sum of two processes: the reduction of oxide and the partial reduction of bromate. When the oxide film on the electrode surface is absent (as in the case of recording the curve towards less positive potentials) reduction phenomena are not observed in the potential range where the oxide reduction occurs. Therefore, the existence of a catalytic effect by platinum oxide on the bromate reduction, in the above mentioned potential range, is evident. The reduction of bromate could be attributed to the catalytic properties of the freshly reduced products of platinum oxide. The catalytic activity of such products, as observed by means

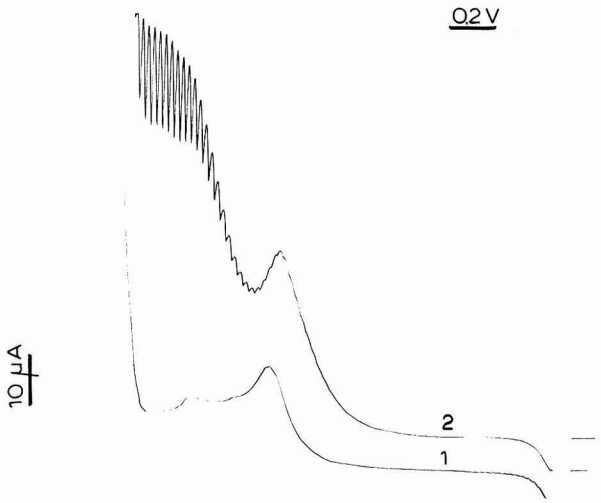

Fig. 3. Polarograms of: (1), 1 *M* $HClO_4$; (2), 1 *M* $HClO_4$ + 1 m*M* $KBrO_3$, recorded with a scanning rate of 5.5 mV/sec. Starting potential, +1.4 V/SCE.

of chronopotentiometric measurements[19], markedly decreases with time. It should be possible, therefore, by decreasing the total time of electrolysis, to increase the catalytic effect of freshly reduced platinum oxide.

Curves 1 and 2 of Fig. 3 (obtained with a potential scanning rate six times higher than that of curve 1 of Fig. 1) show, in fact, a notable increase of peak current and, especially, an advance of the reduction potential of bromate in the range following the peak. Therefore, it is possible to reach a well defined limiting current. The fact that the current decreases until it almost completely disappears when the potential scanning is stopped at the peak potential (*cf.* Fig. 4), confirms that the reduction products of platinum oxide exert an increased catalytic power, but this activity is of short duration.

Nature of electrode process

By applying the usual diagnostic criteria to the reduction curve of bromate,

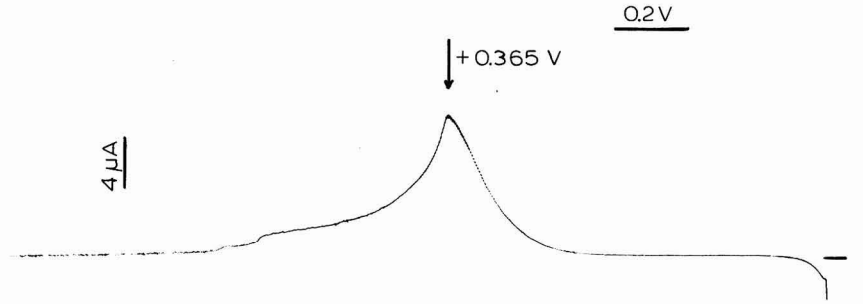

Fig. 4. Behaviour of the current when the potential scanning is stopped at the peak potential. Starting potential, +1.4 V/SCE.

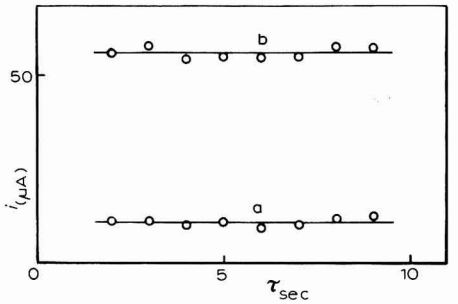

Fig. 5. i_p- and i_l-values at −0.280 V/SCE as the renewal time of the diffusion layer increases.

we have the following results:

The current, i_p, in the potential region of current maximum appears to have a catalytic character as shown by its behaviour as the renewal time of the diffusion layer increases (Fig. 5, curve a). The current values are referred to the peak potential. The behaviour of current i_l, measured at the inflexion potential (−0.280 V/SCE) preceding the supporting electrolyte discharge (curve b), confirms that also in this potential region, the current maintains its catalytic characteristics. This is confirmed by the amount of the current increase as the temperature increases (*cf.* Table 1). The temperature coefficient is greater than 3%/degree for peak current and about 5%/degree for the current at the inflexion potential. The data in Table 1 show also that the peak potential (E_p) shifts towards more positive values as the temperature increases. The average shift is 3.7 mV/degree.

The effect of acid concentration

Curves a, b, c and d of Fig. 6, related to 1 m*M* $KBrO_3$ solutions in $HClO_4$ of variable acid concentration, show that bromate reduction is markedly influenced by increase in acid concentration. As the acid concentration increases there is (i) a net increase of the intensity of the peak current, (ii) a shift of the polarographic curve towards more positive potentials, (iii) a notable increase of single current oscillations and (iv) a radical change in the shape of the curve. The reduction process is not, however, the same for the whole potential–current curve: curves f, g and h show that there is a reduction process different from that occurring in the remaining portion of

TABLE 1

i_p- AND i_l-VALUES AT -0.280 V/SCE AND E_p-VALUES AT DIFFERENT TEMPERATURES
1 m*M* $KBrO_3$ in 1 *M* $HClO_4$; $t = 4.5$ sec.

T (°C)	i_p (μA)	i_l (μA)	E_p (V/SCE)
10	4.50	18.5	+0.293
15	5.20	24.0	+0.307
20	6.70	30.3	+0.330
25	8.04	35.5	+0.338
30	8.07	45.2	+0.354
35	11.00	52.0	+0.378
40	12.60	57.2	+0.400
45	14.00	66.3	+0.412
50	17.50	77.2	+0.445
55	20.00	86.0	+0.451
60	25.00	106.0	+0.472

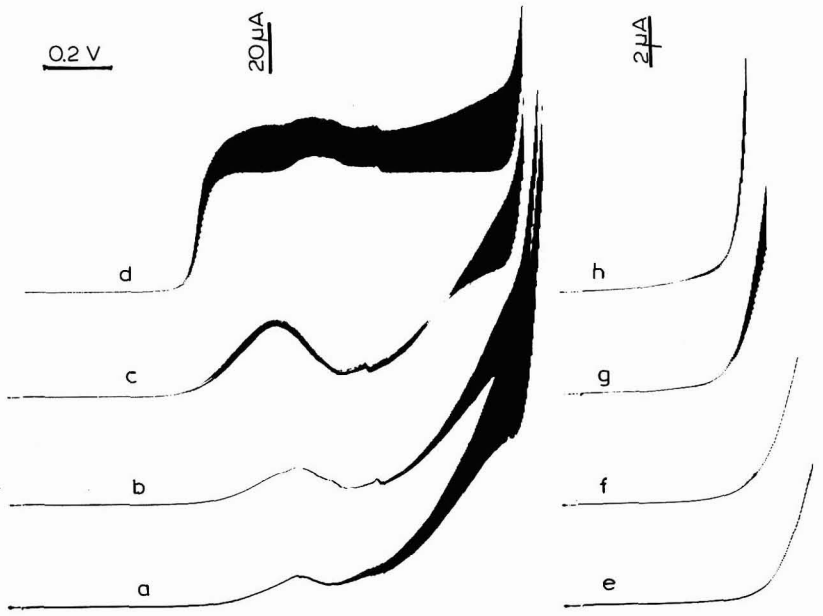

Fig. 6. 1 m*M* $KBrO_3$ plus: (a), 1 *M* $HClO_4$; (b), 3 *M* $HClO_4$; (c), 5 *M* $HClO_4$; (d), 6 *M* $HClO_4$. Curves (e), (f), (g) and (h) are, respectively, the initial part of curves (a), (b), (c) and (d) recorded at ten times the sensitivity. Starting potential, +1.2 V/SCE.

the polarographic curve. Curves f, g and h are the initial portions of the corresponding curves, b, c and d, but obtained with a ten-fold increase of instrumental sensitivity. The different reduction process is shown by inversion of current oscillations.

In 5 *M* $HClO_4$ (curve c) a second inversion is also recorded in the potential region near that of reduction of hydrogen ions.

Table 2 shows that the peak current increases as the acid concentration increases. The intensity of the current in 7 M $HClO_4$ solution (61 μA) is little different from that (62.5 μA) measured for 1 mM $KBrO_3$ solution in 1 M $HClO_4$ at the inflexion potential (−0.280 V/SCE) which precedes the hydrogen ions discharge. Table 2 also gives the values of peak current as C_{HClO_4} increases, in medium of constant ionic strength ($\mu = 6$), using $HClO_4$ and $NaClO_4$ mixtures.

TABLE 2

VALUES OF THE PEAK CURRENT AT DIFFERENT $HClO_4$ CONCENTRATIONS

$(i_p)_1$ relates to 1 mM $KBrO_3$ solutions with variable ionic strength; $(i_p)_2$ relates to 1 mM $KBrO_3$ solutions at constant ionic strength ($\mu = 6$).

C_{HClO_4} (M)	$(i_p)_1$ ($\mu = var.$)	$(i_p)_2$ ($\mu = 6$)
1	8.05	6.00
2	14.50	10.00
3	17.50	15.50
4	21.50	30.50
5	35.30	53.00
6	57.00	57.00
7	61.00	—

Chronopotentiometric measurements

The chronopotentiometric behaviour of bromate in perchloric solutions is similar to that observed polarographically with regard to the presence of catalytic complications in the reduction process on the pre-oxidized electrode. In $HClO_4$ solutions $\leqslant 3$ M bromate gives a chronopotentiogram with two steps (curves b and c in Fig. 7). The first is similar to that given by the supporting electrolyte alone (curve a) due to platinum oxide reduction and occurs in the same potential region. For $C_{HClO_4} = 6$ M (curve d) a distinct change in the shape of the chronopotentiogram is observed: a characteristic peak, corresponding to the inversion of electrode potential direction, and a step, characterized by constancy of potential with time, appear. A plot of $i_0\tau^{\frac{1}{2}}$-values *vs.* the current density (i_0), imposed at $KBrO_3$ in 3 M and 6 M $HClO_4$ solutions, shows opposite behaviour for the two steps: one increases, the other decreases. Such a behaviour is indicated from lines 1, 2, 3 and 4 in Fig. 8. Lines 1 and 2 represent the behaviour of $i_0\tau^{\frac{1}{2}}$ for the chronopotentiogram c in Fig. 7 with regard to the step at potentials between +0.1 and −0.2 V/SCE. Lines 3 and 4 represent the behaviour of $i_0\tau^{\frac{1}{2}}$ for the step characterized by invariance of potential (0.7 V/SCE) with time and for the other step that occurs at potentials between +0.65 and +0.3 V/SCE in the chronopotentiogram d of the same Figure.

The decrease of the product, $i_0\tau^{\frac{1}{2}}$, as the current density increases (curves 2 and 4) is characteristic of electrode processes with kinetic complications. The increase in the product $i_0\tau^{\frac{1}{2}}$ (lines 1 and 3) depends on the reduction of platinum oxide. This behaviour, in fact, is like that observed when the supporting electrolyte alone is used (line 5) and is related to the reduction of the pre-oxidized platinum electrode. The chronopotentiogram characterized by invariance of the potential with time (curve d in Fig. 7) is similar to that observed for iodate solutions[15,16] in which a catalytic cycle

(where iodine is the electroactive species) has been revealed. In the case of bromate, a chronopotentiogram similar to the iodate chronopotentiogram is recorded only for $C_{HClO_4} > 3$ *M* owing to the lower rate of the bromate–bromide reaction compared with the iodate–iodide reaction. Only for $HClO_4$ concentrations above 3 *M* is the presence of a catalytic cycle (where the bromine is the electroactive species) observed. In fact, by adding increasing amounts of bromine to 1 m*M* $KBrO_3$ in $HClO_4 > 3$ *M*, a gradual decrease of the peak potential is observed. This justifies the use of strong mineral acid solutions (hydrogen ion concentration about 3–4 *M*) in redox titrations where bromate is used as oxidant.

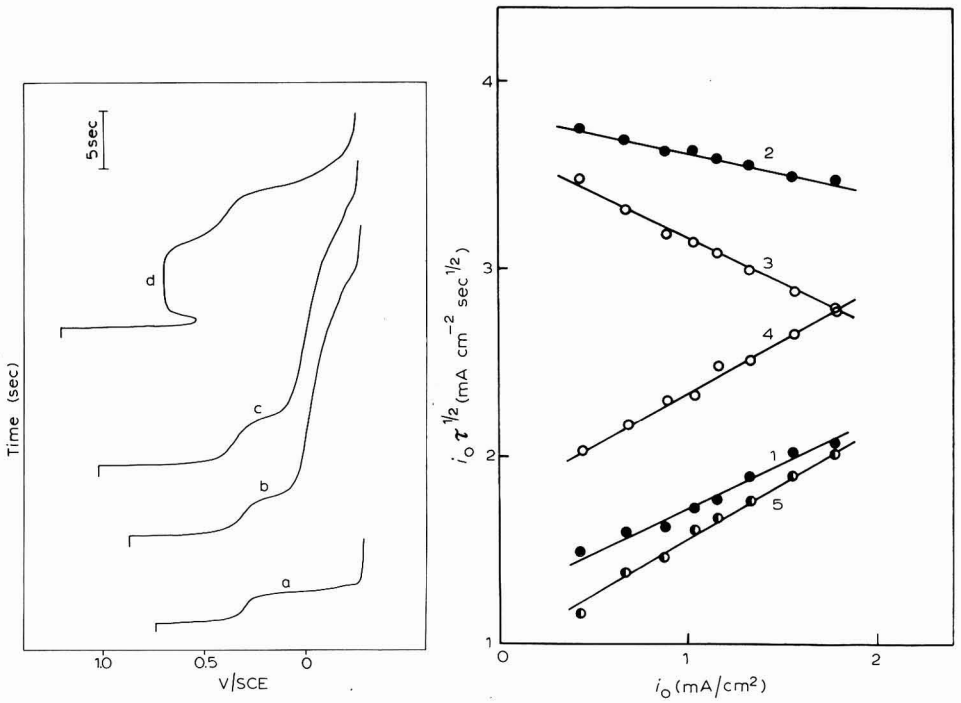

Fig. 7. Chronopotentiograms of: (a), 1 *M* $HClO_4$; (b), 1 m*M* $KBrO_3$ in 1 *M* $HClO_4$; (c), 1 m*M* $KBrO_3$ in 3 *M* $HClO_4$; (d), 1 m*M* $KBrO_3$ in 6 *M* $HClO_4$.

Fig. 8. $i_0\tau^{\frac{1}{2}}$ *vs.* current density (i_0): (1), $i_0\tau_1^{\frac{1}{2}}$; (2), $i_0\tau_2^{\frac{1}{2}}$ are referred to the chronopotentiogram (c) of Fig. 7; (3), $i_0\tau_1^{\frac{1}{2}}$ and (4), $i_0\tau_2^{\frac{1}{2}}$ are referred to the chronopotentiogram (d) of the same Figure. (5), $i_0\tau^{\frac{1}{2}}$ of the chronopotentiogram (a).

Voltammetry at constant potential

To complete the investigation of the bromate reduction process, voltammetry at constant potential was used with bromate in 1–7 *M* $HClO_4$ solutions, at variable and constant ionic strength. The current–time curves given in Fig. 9 and 10 refer to bromate in 3 *M* and 5 *M* $HClO_4$ solutions, respectively. These curves have been selected because they are indicative of the electrode reduction process. Differences were not noted in experiments on solutions at constant ionic strength ($\mu = 5$). The oscillograms have been recorded at the potentials corresponding (on polarograms b and c in Fig. 6)

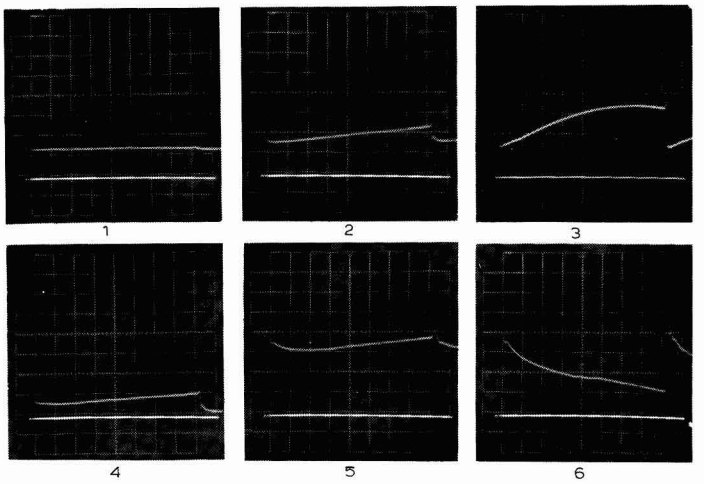

Fig. 9. Oscillograms related to curve (b) of Fig. 6 and recorded at the following potentials: (1), +0.760; (2), +0.600; (3), +0.360; (4), +0.200; (5), −0.360; (6), −0.500 V/SCE. Abscissa, 0.5 sec/major division. Ordinate, 10 μA/major division.

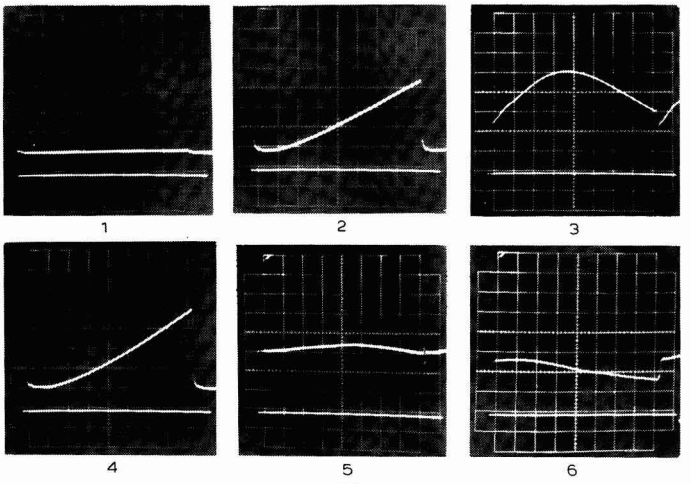

Fig. 10. Oscillograms related to curve (c) of Fig. 6 and recorded at the following potentials: (1), +0.760; (2), +0.560; (3), +0.360; (4), +0.260; (5), −0.260; (6), −0.500 V/SCE. Abscissa, 0.5 sec/major division. Ordinate, 10 μA/major division.

to (1) the first point of inversion (see curves f and g in Fig. 6); (2) about half the peak height; (3) the peak; (4) a point of the polarographic curve intermediate between the peak and the second point of inversion; (5) the potential region in which hydrogen ion reduction is prevailing. The unusual shape of oscillograms 2 and 4 (observed once in a previous work[16]) is characteristic of an autocatalytic electrode process where an electroactive intermediate is restored through a redox reaction in the solution. The shape of curve 3 indicates the presence of a mixed process to which contribute (besides the

autocatalytic reduction of bromate) a reduction stage in which platinum oxides are concerned and a limiting stage due to the slowness of the diffusion process in the second half of the electrolysis time. The last stage, observable in 3 *M* $HClO_4$ (Fig. 9), becomes predominant in 5 *M* $HClO_4$ solution (Fig. 10).

In both Figures, curve 4, recorded at potentials at which platinum oxides are completely reduced, is obvious confirmation for the catalytic power of the reduction products of platinum oxide. The appearance of catalytic properties on freshly-reduced platinum electrodes was reported by Anson and King[19] in work on the reduction of vanadate and iodate. They attributed this catalytic activity to the formation of a particularly active film (similar to that obtained when the electrode is lightly platinized) on the electrode surface after platinum oxide reduction. The electrochemical behaviour of bromate on a platinized platinum electrode is therefore being investigated.

REDUCTION MECHANISM OF BROMATE IN $HClO_4$

From polarographic, chronopotentiometric and voltammetric data at constant potential the following conclusion can be drawn.

In $HClO_4$ solutions more concentrated than 3 *M*, bromate is reduced principally through an autocatalytic cycle involving bromine as the only species electrochemically reduced.

The electrode process is given by the scheme:

$$Br_2 + 2\,e^- \rightleftharpoons 2\,Br^-$$

$$Br^- + \tfrac{1}{5}\,HBrO_3 + H^+ \rightleftharpoons \tfrac{3}{5}\,Br_2 + \tfrac{3}{5}\,H_2O$$

For $C_{HClO_4} \leqslant 3$ *M* bromate is reduced predominantly through heterogeneous catalysis by the freshly formed reduction products of platinum oxide; the contribution due to the autocatalytic cycle is small.

ACKNOWLEDGEMENT

This work was performed with the financial support of C.N.R.

SUMMARY

The reduction of bromate in $HClO_4 > 3$ *M* on a smooth pre-oxidized platinum microelectrode with periodical renewal of the diffusion layer shows that the reduction process occurs through an autocatalytic cycle where bromine acts as electroactive intermediate. In $HClO_4 \leqslant 3$ *M*, the reduction is markedly influenced by the freshly formed reduction products of platinum oxide.

REFERENCES

1 A. Rylich, *Collection Czech. Chem. Commun.*, 7 (1935) 288.
2 I. M. Kolthoff and J. J. Lingane, *Chem. Rev.*, 24 (1939) 1–94.
3 J. J. Lingane and I. M. Kolthoff, *J. Am. Chem. Soc.*, 61 (1939) 825.
4 E. F. Orlemann and I. M. Kolthoff, *J. Am. Chem. Soc.*, 64 (1942) 1970.
5 R. Curti and S. Locchi, *Anal. Chem.*, 29 (1957) 534–7.
6 V. I. Zykov and S. I. Zhdanov, *Zh. Fiz. Khim.*, 32 (1958) 644–53.

7 S. I. ZHDANOV, V. I. ZYKOV AND T. V. KALISH, *Trudy Chetvertogo Soveshchaniya po Elektrokhimii, Moscow, 1956*, 164–9 (Pub. 1959).
8 W. KEMULA AND E. RAKOWSKA, *Z. Physik. Chem. (Frankfurt)*, (1958) 33–45.
9 V. I. ZYKOV, *Zh. Fiz. Khim.*, 33 (1959) 2156–63.
10 R. TAKAHASHI AND I. TACHI, *Rev. Polarog. Kyoto*, 9 (1961) 76–83.
11 Y. A. YONAN, *Dissertation Abstr.*, B 27 (1967) 3010.
12 Z. B. ROZHDESTVENSKAYA AND O. A. SONGINA, *Zh. Analit. Khim.*, 15 (1960) 138–46.
13 Z. B. ROZHDESTVENSKAYA, V. P. GLADISHEV AND O. A. SONGINA, *Izv. Akad. Nauk Kaz. SSR, Ser. Tekhn. i Khim. Nauk*, 2 (1963) 8–14.
14 P. G. DESIDERI, *J. Electroanal. Chem.*, 2 (1961) 39; 4 (1962) 359; 6 (1963) 344.
15 P. G. DESIDERI, *J. Electroanal. Chem.*, 9 (1965) 318.
16 P. G. DESIDERI, *J. Electroanal. Chem.*, 17 (1968) 129.
17 D. COZZI, G. RASPI AND L. NUCCI, *J. Electroanal. Chem.*, 12 (1966) 36.
18 H. B. MARK, JR. AND C. N. REILLEY, *J. Electroanal. Chem.*, 3 (1962) 54.
19 F. C. ANSON AND D. M. KING, *Anal. Chem.*, 34 (1962) 362.

Elsevier Sequoia S.A., Lausanne – Printed in The Netherlands

BOOK REVIEWS

Advances in Electrochemistry and Electrochemical Engineering, Vol. 6, *Electrochemistry*, edited by Paul Delahay, Interscience Publishers, New York, 1967, 482 pages, price 155 s.

This new volume of this well-known series contains five contributions, of interest and value to electrochemists.

In the first chapter, C. A. Barlow Jr. and J. Ross Macdonald outline current knowledge in the *Theory of Discreteness of Charge Effects in the Electrolyte Compact Double Layer*. The discussion is wisely split up into two parts—qualitative and quantitative, followed by calculations on examples of different types of imaging, cases of non-polarizable and polarizable anions, etc. The authors have succeeded in showing how much there is still to be known about the double layer, and this review will be a useful starting point for further studies.

Although a review of the vast amount of literature on the oxygen electrode would seem to be an arduous task, H. P. Hoare presents a very successful chapter on *The Oxygen Electrode on Noble Metals*, including platinum, gold, palladium and iridium, and some alloy electrodes. The treatment is well-balanced and contains many experimental data as well as critical discussion on theories concerning such topics as the rest potential, the mechanisms of evolution and reduction of oxygen, and reactions of peroxide at the electrodes mentioned.

Electrochemical Kinetics of Metal Complexes are discussed by J. Koryta. A generalized theory is given of the d.c. polarographic current and the exchange current density in the case where a complex is the reacting species, when a number of other complexes are present in the solution. Possible control by slow dissociation or association is dealt with as well as double-layer effects. Some attention is given to adsorption of electroactive complexes, although, in this respect, theoretical work other than that of Laitinen and Randles could have been mentioned. The chapter contains numerous experimental examples, to show that there are still many interesting problems to be solved in electrochemistry.

In the *Electrochemical Response of Porous and Rough Electrodes*, R. de Levie deals with the effect of surface geometry on electrochemical measurements. The discussion on the effect in porous electrodes should be of special interest to electrochemists working on batteries and fuel cells. The distribution of current and potential is calculated for a one-dimensional single pore in the case of mass transfer and reaction control. Transient responses and impedance measurements are also discussed. The second part is a review on the present state of knowledge of roughness effects on macroscopically flat electrodes. The discussion is largely qualitative because the theory for surface roughness has not yet been fully developed.

In the last chapter, J. M. Hale and W. Mehl discuss *Insulator Electrode Reactions*. The subject is new and the authors have confined themselves to a description of experimental work on anthracene only. This material is drawn chiefly from the work of Mehl and coworkers. The fundamentals of insulator electrodes in

general are discussed in detail and modern charge transfer theories and their application to insulator electrodes are examined.

M. Sluyters-Rehbach, B. Timmer and D. J. Kooyman, Laboratory of Analytical Chemistry, State University, Utrecht.

J. Electroanal. Chem., 22 (1969) 275–276

Classical Electromagnetism via Relativity—an Alternative Approach to Maxwell's Equations, by W. G. V. Rosser, Butterworths, London, 1968, x + 294 pages, 65s.

The study of Maxwell's equations is an essential step towards understanding electromagnetism. They are generally introduced after the student has become familiar with electric and magnetic quantities. This new book emphasizes the unity of electromagnetism by approaching Maxwell's equations through Coulomb's law and the transformations of special relativity. It therefore reverses the historical approach, since the theory of special relativity was hewn by Einstein from optics and electromagnetism.

Chapter 1 presents a useful survey of special relativity. It is followed by calculations of the force between moving charges, showing that the weak magnetic interaction can be interpreted as a second-order relativistic effect. The electric and magnetic fields near a moving charge are used in Chapter 4 to develop Maxwell's equations for systems of point charges moving with uniform velocities; accelerating charges are considered in an Appendix. The scalar and vector potentials are treated in Chapter 5 and relativistic electromagnetism in the final Chapter. Problems are included in most Chapters.

The book has been extremely carefully written and is easy to follow. The author is a thoughtful and helpful guide, but the quick student may find the style too slow and repetitive. The book is recommended to those who have some knowledge of electromagnetic theory — it should help to clarify their understanding of this important subject. The MKSA system of units (S.I.) has been used.

A. D. Buckingham, Department of Theoretical Chemistry, University of Bristol.

J. Electroanal. Chem., 22 (1969) 276

ELECTROANALYTICAL CHEMISTRY AND INTERFACIAL ELECTROCHEMISTRY App. 1
Elsevier Sequoia S.A., Lausanne – Printed in The Netherlands

PRELIMINARY NOTES

THE MECHANISM OF ANODIC ACETAMIDATION. A COMMENT ON A PAPER BY COLEMAN, RICHTOL AND AIKENS

The recent paper by Coleman, Richtol and Aikens[1] alledgedly verifies the two electron oxidation mechanism for acetamidation of hexamethylbenzene (HMB) originally proposed by Eberson and Nyberg[2]. We have found that bibenzyl is a major by-product formed during anodic oxidation of toluene in acetonitrile and can only arise from a one-electron oxidation of the substrate[3]. More recently, bibenzyls have been observed during the anodic acetamidation of several alkyl benzenes and a modification of the original mechanism is necessary to account for these products[4].

The detailed mechanism proposed on the basis of the current function observed during rapid sweep voltammetry is illustrated by equation (1)[1]. This mechanism corresponds to the theoretical case analyzed by Nicholson and Shain[5] in which ΔE° (the

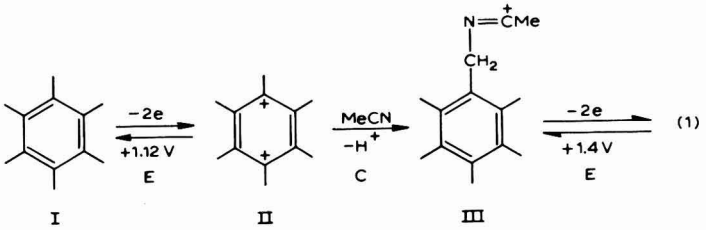

potential separation between charge transfer steps) is large and two distinct oxidation peaks are observed during stationary electrode voltammetry. The current function for the first peak for this mechanism is indistinguishable from that for the case in which ΔE° is zero or small k_f/a is large[5]. In this case the ECE mechanism takes place at the first peak (eqn.2). A mechanism of this type can be written involving one

$$A \underset{E_1}{\overset{-ne}{\rightleftharpoons}} B \xrightarrow[C]{k_f} C \xrightarrow[E_2]{-ne} D \qquad (2)$$

$$\Delta E^\circ = E_2^\circ - E_1^\circ$$

electron oxidation of HMB (eqn. 3). Since the chemical step involves deprotonation, k_f

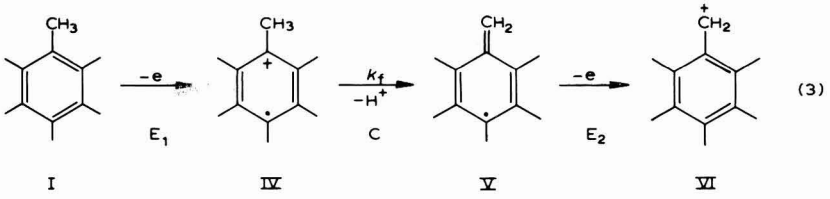

could be very large, making the current function for this mechanism very similar to that of the mechanism previously proposed (eqn. 1)[1]. Furthermore, this mechanism allows for the formation of bibenzyls as a side reaction[3,4]. The extent of bibenzyl formation would be a function of ΔE°, slight changes in ΔE° (referring to ΔE° for different substrates) would be expected to have a profound effect on the benzyl radical lifetime and thus the extent of the coupling reaction.

Thus, voltammetry of HMB does not distinguish between the two mechanisms and the observation of bibenzyl formation, although strong evidence for mechanism (3) does not conclusively prove it. Mechanism (1) does not appear to be energetically favorable since aromatic systems, for example 9,10-diphenylanthracene[6], which are known to form dications, undergo anodic oxidation by two discrete one-electron transfer steps separated by about 500 mV. An exception is the reversible two-electron oxidation of tetra-*p*-anisylethylene, however, this is a special case since charge separation by the olefinic linkage is possible[7]. It does not seem reasonable that HMB dication with only one aromatic ring for charge delocalization should be formed in one two-electron transfer step while the polycyclic aromatic compounds capable of extensive charge delocalization undergo two distinct one-electron transfers with considerable energy separation.

A more convincing argument for mechanism (3) could be derived from a case in which k_f is small (proton loss from the cation-radical is slow) and the observation of an oxidation peak corresponding to the transfer of less than two electrons. The structurally similar hexaethylbenzene (HEB) provides such a case. Voltammetric peak currents (for 1.0 m*M* solutions) and n values for several well characterized one- and two-electron oxidations are tabulated in Table 1. 3,6-Dimethoxytetramethylbenzene (DMT) and 3,6-diacetoxytetramethylbenzene (DAT) are included because their structural and molecular weight similarity to HMB and HEB would be expected to result in similar diffusion coefficients[8]. HMB gives a peak current of slightly less than DMT and DAT and verifies that about two electrons are involved in the first oxidation peak. On the other hand, HEB gives a peak current almost identical to that of 1,4-di-methoxybenzene which undergoes quasi-reversible one-electron oxidation in acetonitrile[9]. Thus, the initial step in the oxidation of HEB is formation of the cation-radical. The oxidation peak for HEB (+ 1.58 V *vs.* SCE) is slightly more anodic than that for HMB (+ 1.49 V *vs.* SCE) and it

TABLE 1

Stationary Electrode Peak Currents of Aromatic Compounds

Compound (concn. 1 m*M*)	$i_p/\mu A$ [a]	n	
9,10-Diphenylanthracene	90	1.0	[6]
9,10-Dimethylanthracene	96	1.0	[10]
4,4'-Dimethoxystilbene	93	1.0	[11]
1,4-Dimethoxybenzene	121	1	[9]
3,6-Dimethoxytetramethylbenzene	212	2.0	[8]
3,6-Diacetoxytetramethylbenzene	210	2.0	[8]
Hexamethylbenzene	197	2	
Hexaethylbenzene	120	1	

[a] Measured at 10 V min^{-1} at a Beckman platinum button (No. 39273) in acetonitrile with lithium perchlorate (0.1 *M*) as supporting electrolyte.

seems highly unlikely that two electrons are removed more easily from HMB than a single electron is lost from HEB. Therefore, we feel safe in assigning mechanism (3) for both HEB and HMB. Mechanism (3) also satisfies all the experimental observations reported for other substrates[3,4]. We have recently shown that mechanism (3) is followed during anodic hydroxylation of pentamethylanisole[12].

The author gratefully acknowledges valuable discussions with Dr. Lennart Eberson. This work was supported by a grant from the Swedish Natural Science Research Council.

Division of Organic Chemistry,
University of Lund, Chemical Center,
P.O.B. 740, S-22007 Lund (Sweden)

VERNON D. PARKER

1 A.E. Coleman, H.H. Richtol and D.A. Aikens, *J. Electroanal. Chem.*, 18 (1968) 165.
2 L. Eberson and K. Nyberg, *Tetrahedron Letters,* (1966) 2389.
3 V.D. Parker and B.E. Burgert, *Tetrahedron Letters,* (1968) 2411.
4 L. Eberson and B. Olofsson, *Acta Chem. Scand.*, in press.
5 R.S. Nicholson and I. Shain, *Anal. Chem.*, 37 (1965) 178.
6 M.E. Peover and B.S. White, *J. Electroanal. Chem.*, 13 (1967) 93.
7 V.D. Parker, K. Nyberg and L. Eberson, *J. Electroanal. Chem.*, in press.
8 V.D. Parker, *Chem. Commun.*, in press. Both DMT and DAT undergo quantitative two-electron oxidation accompanied by the generation of duroquinone.
9 A. Zweig, W.G. Hodgson and W.H. Jura, *J. Am. Chem. Soc.*, 86 (1964) 4124.
10 L.S. Marcoux, J.M. Fritsch and R.N. Adams, *J. Am. Chem. Soc.*, 89 (1967) 5766.
11 V.D. Parker and L. Eberson, *Chem. Commun.*, (1969) 340.
12 V.D. Parker and R.N. Adams, *Tetrahedron Letters,* (1969) 1721.

Received June 5th, 1969

App. 4 ELECTROANALYTICAL CHEMISTRY AND INTERFACIAL ELECTROCHEMISTRY
Elsevier Sequoia S.A., Lausanne – Printed in The Netherland

THE ELECTRICAL DOUBLE LAYER ON MERCURY IN PROPYLENE CARBONATE

The advantages of propylene carbonate as a solvent for electrochemical purposes have been discussed[1,2]. Some preliminary measurements[3,4] revealed the presence of a hump in the capacity of a mercury electrode in this solvent. It might be due to re-orientation of the solvent, since propylene carbonate has a relatively high dipole moment and dielectric constant. On the other hand, as it occurred on the positive side of the point of zero charge it could be related to the adsorption of anions. Further measurements made to aid in the elucidation of this point are reported here.

B.D.H. propylene carbonate was purified by two distillations under a pressure of about 80 Nm^{-2}, when the boiling temperature was about 65°C. B.D.H. 'low in chloride' sodium perchlorate was dried at 110°C and 1.3 Nm^{-2} for 24 h and then kept in a vacuum desiccator until used. Mercury was purified as described previously[5]. The reference electrode consisted of a silver wire dipping into a solution containing 0.05 mol l^{-1} $AgClO_4$ and 0.5 mol l^{-1} $NaClO_4$. This electrode and the junction of this solution with the working solution were stable over the period of the experiment. Capacity was measured using the bridge described previously[6]. No significant dispersion with frequency was found. The point of zero charge for each solution was found using a streaming mercury electrode[7]. Attempts to measure electrocapillary curves were completely unsuccessful. The meniscus became completely stuck in the capillary and no treatment was found by which this could be prevented.

Capacity curves for six concentrations of $NaClO_4$ in propylene carbonate were measured at 25°C and these results are shown in Fig.1. Since the interfacial tensions, activity coefficients and transport numbers are unknown, it is not possible to make a complete thermodynamic analysis of these data. However, the fact that the diffuse layer minimum is clearly visible at concentrations as high as 0.1 mol l^{-1} suggests that specific adsorption is weak. Analysis was therefore carried out to test the assumption that specific adsorption is absent. The charge on the mercury electrode was found by computer integration of the capacity curves[8]. The reciprocal of the capacity at constant charge was then plotted against the reciprocal of the diffuse layer capacity at this charge assuming no specific adsorption. Simple diffuse layer theory was assumed with the bulk dielectric constant of propylene carbonate (65.1)[9]. These plots are shown in Fig.2. If specific adsorption is indeed absent the plots should be linear with unit slope. Lines of unit slope are shown in Fig.2 and suggest that within the experimental accuracy specific adsorption is absent.

It is unfortunately impossible to use this test convincingly in the region of the hump where the charge is about + 15 $\mu C\ cm^{-2}$ but the apparent lack of specific adsorption at the lower positive charges makes it seem more probable that the hump is due to solvent re-orientation than to anion adsorption although there may be a combination of the two effects as in water[10]. A full thermodynamic analysis was carried out up to a charge of + 24 $\mu C\ cm^{-2}$ with the aid of the computer programme previously described[11] making the reasonable assumptions that the co-ordinates of the electrocapillary maximum were independent of concentration (against a constant reference electrode with corrections for liquid junction potential). It was also assumed that the activity coefficient of $NaClO_4$ in

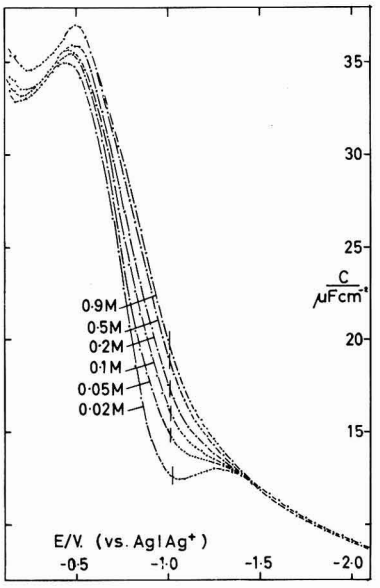

Fig. 1. Capacity of a mercury electrode in contact with anhydrous propylene carbonate at 25°C. Potential with respect to Ag/0.05 mol l^{-1} $AgClO_4$ + 0.5 mol l^{-1} $NaClO_4$.

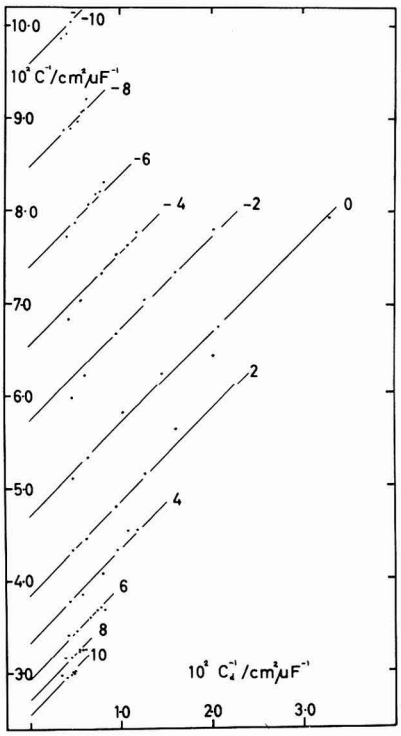

Fig. 2. Plot of the reciprocal of the experimental capacity against the reciprocal of the calculated diffuse layer capacity at constant charge on the electrode.

this solvent is independent of concentration. This is much less reasonable and will lead to semi-quantitative results only. Anionic surface excesses are found with charges approximately equal and opposite to the charge on the electrode at the lower concentrations. Smaller surface excesses are found at the higher concentrations. This tends to support the suggestion that specific adsorption of anions is weak.

On the negative side of the point of zero charge the capacity becomes almost independent of concentration. There is some evidence that it goes through a minimum of about 8.4 μF cm^{-2}, but at this point the series rèsistance begins to increase, so that it is possible that the true minimum is obscured by a pseudo-capacity. Ideal polarizable behaviour is observed over a range of about 2 V.

We should like to thank the Science Research Council for a grant supporting this work.

Department of Physical Chemistry,
The University,
Bristol BS8 1TS

T. BIEGLER*
ROGER PARSONS

1 R.F. Nelson and R.N. Adams, *J. Electroanal. Chem.*, 13 (1967) 184.
2 R. Jasinski, *J. Electroanal. Chem.*, 15 (1967) 89.
3 J. Lawrence, *B.Sc. Thesis*, Bristol, 1964.
4 R. Payne, *J. Phys. Chem.*, 71 (1967) 1548.
5 J.D. Garnish and R. Parsons, *Trans. Faraday Soc.*, 63 (1967) 1754.
6 R. Parsons and P.C. Symons, *Trans. Faraday Soc.*, 64 (1968) 1077.
7 D.C. Grahame, R.P. Larsen and M.A. Poth, *J. Am. Chem. Soc.*, 71 (1949) 2978.
8 R. Parsons and F.G.R. Zobel, *J. Electroanal. Chem.*, 9 (1965) 333.
9 M. Watanabe and R.M. Fuoss, *J. Am. Chem. Soc.*, 78 (1956) 527.
10 E. Schwartz, B.B. Damaskin and A.N. Frumkin, *Zh. Fiz. Khim.*, 36 (1962) 2419.
11 J. Lawrence, R. Parsons and R. Payne, *J. Electroanal. Chem.*, 16 (1968) 193.

Received 7th June, 1969

*Present address: Chemical Research Laboratories, CSIRO, Port Melbourne, Victoria, Australia.

Elsevier Sequoia S.A., Lausanne – Printed in The Netherlands

ANNOUNCEMENT

SEVENTH INTERNATIONAL POWER SOURCES SYMPOSIUM 1970

Following the successful Symposium held in 1968, the Seventh International Power Sources Symposium will be held at Brighton on 15th, 16th and 17th September, 1970, when about thirty-five papers will be presented. As far as possible papers on similar topics will be grouped together and the presentation of each paper will be followed by a discussion.

An audience of about four hundred is expected, representative of research and development work, applications engineering and user experience in the power sources field throughout the world. The Symposium is sponsored by the Joint Services Electrical Power Sources Committee.

Full details of the Symposium will be issued at a later date, but it is essential to prepare the programme of papers considerably in advance. It will be appreciated, therefore, if you could inform me by the end of **June 1969** whether you or your organisation will wish to present a paper or papers, and, if so, to indicate the probable subject of the papers. Papers should be in English on original, unclassified work related to primary or secondary cells, fuel cells, solar cells or other non-mechanical power sources of which this will be the first publication. They should be limited to a maximum of five thousand words, free from advertising matter and in the normal form suitable for publication in scientific or technical journals. Facilities for showing slides etc. will be provided at the Symposium. To allow the maximum time for discussion the time for presentation of the papers will be strictly limited, and authors must prepare an abbreviated form of their papers for presentation at the Symposium.

Pre-prints of the papers will be despatched in advance of the Symposium to delegates who have paid the registration fee. The full text of all papers together with the discussions will be published in book form. A copy will be despatched without further cost to all delegates who have paid the registration fee.

It may not be possible to present all the papers offered, and the Committee reserves the right to accept or reject papers to meet the need to provide an acceptable and attractive programme of papers within the time available.

Further guidance on the form which the papers should take will be forwarded with the notification of the acceptance of papers. The following time table must be adhered to in their preparation:

Notification of intention to offer papers	-	30th June 1969
Synopsis of papers for programme	-	30th November 1969
Notification of acceptance of papers	-	30th December 1969
Full text of papers to be delivered	-	*31st March 1970*
Issue of pre-prints of papers	-	August 1970

Because of the time required for printing, proof reading etc. *this time table is crucial and cannot be extended.*

International Power Sources Symposium,
P.O. Box No. 136
20–26 Wellesley Road
CROYDON CR9 2EG
England

D.H. COLLINS
Chairman
International Power Sources
Symposium Committee

J. Electroanal. Chem., 21 (1969) App. 7–8

Vol. 22 No. 2 JOURNAL OF ELECTROANALYTICAL CHEMISTRY AND INTERFACIAL ELECTROCHEMISTRY AUGUST 1969

CONTENTS